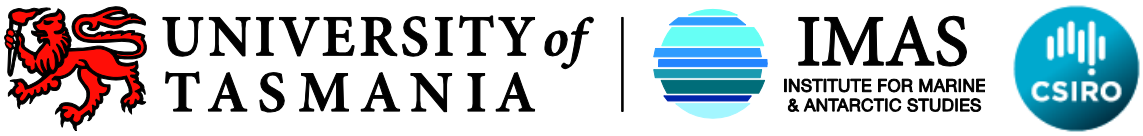

Ocean temperature and salinity responses to 50 year changes in surface conditions

Véronique Lago

B.Sc., Université de Sherbrooke

M.Sc., University of Alberta

Submitted in fulfilment of the requirements for the degree of

Doctor of Philosophy in Quantitative Marine Science

University of Tasmania

February, 2017

Declaration

This thesis contains no material which has been accepted for the award of any other degree or diploma in any tertiary institution, and to the best of my knowledge and belief, contains no material previously published or written by another person, except where due reference is made in the text of the thesis.

Véronique Lago, B.Sc., M.Sc.

10th February 2017

Published work

The publishers of the paper comprising Chapter 2 hold the copyright for that content, and access to the material should be sought from the Journal of Climate. The paper comprising Chapter 3 is prepared for submission to the Journal of Climate. The remaining non published content of the thesis may be made available for loan and limited copying and communication in accordance with the Copyright Act 1968.

Statement of co-authorship

The following people and institutions contributed to the publication of work undertaken as part of this thesis:

Véronique Lago, University of Tasmania, Institute for Marine and Antarctic Studies; Centre for Australian Weather and Climate Research, CSIRO, Oceans and Atmosphere and Centre of Excellence for Climate System Science.

Susan E. Wijffels, Centre for Australian Weather and Climate Research, CSIRO, Oceans and Atmosphere.

Paul J. Durack, Program for Climate Model Diagnosis and Intercomparison, Lawrence Livermore National Laboratory.

John A. Church, Centre for Australian Weather and Climate Research, CSIRO, Oceans and Atmosphere.

Simon J. Marsland, Centre for Australian Weather and Climate Research, CSIRO Oceans and Atmosphere Flagship.

Nathan L. Bindoff, University of Tasmania, Institute for Marine and Antarctic Studies; Centre for Australian Weather and Climate Research, CSIRO, Oceans and Atmosphere; Centre of Excellence for Climate System Science and Antarctic Climate and Ecosystems Cooperative Research Centre.

Publications produced as part of this thesis include:

Chapter 2 (Paper 1):

Lago, V., S.E. Wijffels, P.J. Durack, J.A. Church, N.L. Bindoff and S.J. Marsland (2016): Simulating the role of surface forcing on observed multidecadal upper ocean salinity changes. *Journal of Climate*, **29**, pp. 5575-5588. doi: 10.1175/JCLI-D-15-0519.1

Details of the Authors roles to the publication of the work undertaken in Chapter 2:

Véronique Lago (60%), Susan E. Wijffels (10%), Paul J. Durack (10%), John A. Church (5%), Nathaniel L. Bindoff (5%) and Simon J. Marsland (5%)

Véronique Lago contributed to the conception and design of the project, analysis and interpretation of the research and writing.

Susan E. Wijffels contributed to the conception and design of the project, analysis and interpretation of the research and revising the writing.

Paul J. Durack contributed to the analysis and interpretation of the research and revising the writing.

John A. Church contributed to the analysis and interpretation of the research and revising the writing.

Nathaniel L. Bindoff contributed to the analysis and interpretation of the research.

Simon J. Marsland contributed to the design of the project, interpretation of the research and revising the writing.

To be submitted:

Chapter 3 (Paper 2):

Lago, V., S.E. Wijffels, P.J. Durack, J.A. Church, N.L. Bindoff and S.J. Marsland (in preparation): Subsurface temperature response to surface changes in a 50 year idealized ocean model simulation

Details of the Authors roles to the publication of the work undertaken in Chapter 3:

Véronique Lago (65%), Susan E. Wijffels (9%), Paul J. Durack (9%), John A. Church (7%), Simon J. Marsland (7%) and Nathaniel L. Bindoff (3%)

Véronique Lago contributed to the conception and design of the project, analysis and interpretation of the research and writing.

Susan E. Wijffels contributed to the conception and design of the project, analysis and interpretation of the research and revising the writing.

Paul J. Durack contributed to draft part of the work, the analysis and interpretation of the research and revising the writing.

John A. Church contributed to the analysis and interpretation of the research and revising the writing.

Nathaniel L. Bindoff contributed to the analysis and interpretation of the research.

Simon J. Marsland contributed to the design of the project, interpretation of the research and revising the writing.

Non-published work:

Chapters 1, 4 and 5:

Theses chapters were not written to be submitted for publication. The following authors provided assistance in the research presented in these chapters:

Details of the Authors roles to the publication of the work undertaken in Chapter 1, 4 and 5:

Véronique Lago (75%), John A. Church (8%), Susan E. Wijffels (5%), Paul J. Durack (5%), Simon J. Marsland (5%) and Nathaniel L. Bindoff (2%)

Véronique Lago contributed to the conception and design of the project, analysis and interpretation of the research and writing.

John A. Church contributed to the analysis and interpretation of the research and revising the writing.

Susan E. Wijffels contributed to the design of the project, analysis and interpretation of the research and revising the writing.

Paul J. Durack contributed to the analysis and interpretation of the research and revising the writing.

Simon J. Marsland contributed to the design of the project, interpretation of the research and revising the writing.

Nathaniel L. Bindoff contributed to the analysis and interpretation of the research.

We the undersigned agree with the above stated “proportion of work undertaken” for each of the above published (or submitted) peer-reviewed manuscripts contributing to this thesis:

Signed:	_____	_____
	Professor Nathan L. Bindoff	Professor Craig Johnson
	Supervisor	Head of School
	Institute for Marine and Antarctic Studies	Institute for Marine and Antarctic Studies
	University of Tasmania	University of Tasmania
Date:	10/02/2017	14/02/2017

Abstract

Changes in the global ocean's temperature and salinity in the last decades are evidence of the Earth's warming climate. These interior ocean changes are driven by changes in ocean surface fluxes of heat, freshwater and momentum. The warming atmosphere induces increased Sea Surface Temperature (SST) and amplifies the water cycle (evaporation-minus-precipitation) and in turn the Sea Surface Salinity (SSS) pattern. There is strong evidence of significant changes in the temperature and salinity fields in the ocean interior, but little is known of the relative contribution to these trends from each of the surface forcings. Changing surface winds also impact on ocean circulation and penetration of surface properties into the ocean interior. However, coincident wind changes that have occurred alongside ocean temperature and salinity changes are not well known and available reanalyses that provide our only coherent insight to wind changes are sometimes contradictory. Using a global ocean model, changes from each independent surface forcing is decomposed in idealized experiments. The results show that to reproduce the observed pattern of salinity changes in each major ocean basin using a density space coordinate for the analysis, both the SSS pattern amplification and SST increase need to be taken into consideration. Changes in SSS are transmitted to the subsurface salinity field mainly through subduction while the warming ocean results in migration of isopycnals relative to the mean salinity field creating apparent salinity changes in density space. The SSS pattern amplification results in a subsurface warming in the ventilated gyres and subpolar regions of similar amplitude to that from heat subducted as a result of the increased SST. Warming in the subpolar regions is mainly driven by the reduced convective heat loss as a result of the fresher and less dense surface water which strengthens vertical stratification. To investigate wind changes three different reanalyses datasets are used to compare how imposing the surface forcing due to wind changes affect the subsurface properties. Equatorial cooling between 100 and 300 m across the Pacific and Indian Oceans is consistent across datasets, which is in agreement with a reported strengthening of the trade winds. There is a ~0.5 to ~1^{o}C and ~0.1 PSS-78 changes under the subtropical gyres induced by changes in the surface wind reanalyses but the results are not inconsistent with different reanalyses winds and are inconsistent with the

available observations. This suggests that there are some inconsistencies in the available wind reanalyses which affects the temperature and salinity under the subtropical gyres, where the ocean is most sensitive to small changes in wind stress curl. Each of the three surface forcings acts linearly together in these idealized experiments to produce most of the observed key features of multidecadal subsurface temperature and salinity changes as estimated from a suite of independent temperature and salinity analyses.

Acknowledgments

I would like to thank the people who gave me assistance and support during my Ph.D. My supervisors Dr. Susan Wijffels, Dr. John Church, Dr. Simon Marsland and Prof. Nathan Bindoff have been very supportive and gave me valuable insights, guided me and taught me how to become a better scientist. You are my inspiration for what I hope to become as a physical oceanographer. I would also like to thank Dr. Paul Durack for his highly appreciated help throughout my Ph.D. and for providing some useful observational data.

Of course, I could not have achieved this Ph.D. without the financial help and support from the Quantitative Marine Science program at the Institute for Marine and Antarctic Studies. The QMS program provides some great opportunity for students. The multi-cultural environment at IMAS makes Hobart all the more an amazing place to live. Furthermore, the Centre of Excellence provided some great opportunities with their great annual winter school, writing workshop and their financial support.

I would like to extend my thanks to my friends here in Hobart and overseas for their continual support in good times and harder times. I have met some wonderful people who, I hope, will stay in my life for a long time. I would also like to thank my parents, my brother and my family for their understanding of my decisions. My grand-mother in particular, who shares my love for nature and water, is an inspiration of strength for the many difficulties she overcame in all humility and without looking back.

Table of Contents

List of Figures

List of Tables

Chapter 1

Introduction

1.1 Overview

The oceans have the capacity to influence regional and global climate through variations in global and regional energy storage. The ocean has a heat capacity about a thousand times that of the atmosphere, allowing it to store and redistribute energy (Levitus *et al.*, 2005). Heat storage in the deeper ocean would not be possible without ocean dynamics. Advective and convective processes, which are a response to momentum and density gradients imposed at the surface, allow ocean surface properties to be carried into the ocean interior. The variations in density result from changes in the temperature and salinity fields, which at the surface result from air-sea interactions.

In recent decades, changes have been observed simultaneously in the ocean and in the atmosphere. In the ocean, changes include increases in temperature and changes to salinity both at the surface and ocean interior (e.g. Levitus *et al.*, 2000; Dickson *et al.*, 2002, Curry *et al.*, 2003; Boyer *et al.*, 2005; Levitus *et al.*, 2005; Hosoda *et al.*, 2009; Durack and Wijffels, 2010; Helm *et al.*, 2010; Skliris *et al.*, 2014). These changes are reflected in the atmospheric boundary interaction which has led to an increased ocean heat uptake (Levitus *et al.*, 2000; Ishii *et al.*, 2005; Purkey and Johnson, 2010; Kuhlbrodt and Gregory, 2012; Levitus *et al.*, 2012), an amplification of the hydrological cycle (Bindoff *et al.*, 2007; Durack and Wijffels, 2010; Helm *et al.*, 2010; Durack *et al.*, 2012) and changes to wind patterns (Huang *et al.*, 2006; Seidel *et al.*, 2008).

1.2 Salinity

The changes in the Sea Surface Salinity (SSS) depend on the changes in the pattern and intensity of evaporation minus precipitation (E-P), terrestrial runoff, horizontal and vertical advection and mixing (Curry *et al.*, 2003; Boyer *et al.*, 2005; Hosoda *et al.*, 2009; Schanze *et al.*, 2010; Durack and Wijffels, 2010; Yu, 2011). Changes in the salinity directly affect the density and thus the stability of ocean structure. A decreased surface salinity increases the stratification and so it

requires more energy to mix the surface layer with the denser subsurface water. Alternatively, an increased surface salinity leads to greater vertical mixing by increasing the surface density.

Some regions are particularly sensitive to changes in salinity due to local mixing processes and a surface anomaly can be transferred to large areas of the subsurface ocean. For example, the subpolar North Atlantic has sites of deep water formation through seasonally driven deep convection. The convection is produced when the surface increases in density due to both cooling and brine rejection associated with sea-ice formation (Lazier *et al.*, 2002; Yashayaev *et al.*, 2007; Dickson *et al.*, 2002). The Southern Ocean also has deep convection, mainly in the Weddell and Ross Seas, which is affected by changes in surface salinity (e.g. Marsland and Wolff, 2001; Stammer, 2008; de Lavergne *et al.*, 2014; Kjellsson *et al.*, 2015; Morrison *et al.*, 2015). Water masses formed in both of these regions spread through large parts of the global oceans. The subpolar North Pacific does not have the equivalent processes due to stronger precipitation which maintains a stronger stratification that prevents large scale open-ocean convections (Warren, 1983; Emile-Geay *et al.*, 2003).

Durack and Wijffels (2010) evaluated global salinity changes from 1950 to 2008 by combining historical profiles and the more recent Argo Program data (Gould *et al.* 2004). They presented 50 years linear trends produced with the data from that period. They confirmed the increased salinities within the subsurface subtropical gyres and decreased salinities in the Southern Ocean (Curry *et al.*, 2003; Boyer *et al.*, 2005; Hosoda *et al.*, 2009; Helm *et al.*, 2010; Skliris et al 2014). They also found a freshening of the shallow tropical waters. In the North Atlantic, an augmentation of the outflow from the Mediterranean Sea forced an increase in the deep water salinity (Potter and Lozier, 2004). In every basin, the surface salinity pattern is increased in magnitude and the amplified pattern is subducted to the ocean interior. Durack and Wijffels (2010) suggest that the changes in salinity on isopycnals are likely a combination of the subducted changes in surface salinity and a poleward migration of outcrops due to a warming atmosphere and sea surface temperature (SST).

1.2.1 Evaporation - Precipitation

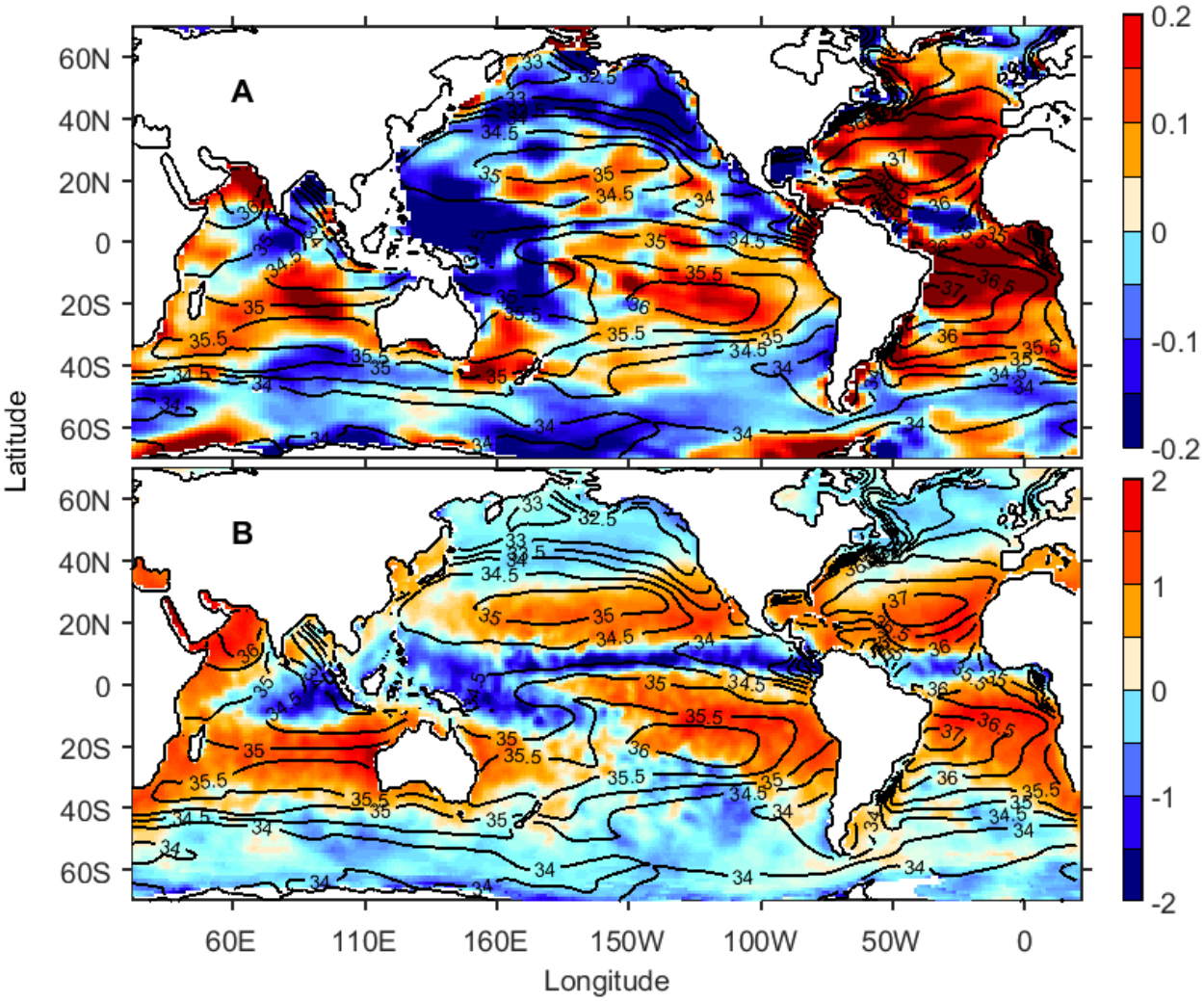

Figure 1.1. a) Surface salinity trend (PSS-78 per 50 years; Durack and Wijffels, 2010) and b) Mean annual evaporation minus precipitation rate (m per year; Josey et al., 1998). In both panels, the black contours are the mean salinity field every 0.5 PSS-78.

The long-term climatological mean surface salinity pattern is closely related to the pattern of E-P (Figure 1.1b; Lagerloef *et al.*, 2010; Durack and Wijffels, 2010. Also, the long-term changes in surface salinity have a strong correspondence to the climatological mean E-P field, which has been shown in models to strengthen (amplify) with warming (Durack *et al.*, 2012). Schanze *et al.* (2010) highlighted the importance of the hydrological cycle as the main component of the freshwater budget in the ocean with an annual mean of about 13 ± 1.3 Sv in evaporation and

12.2 ± 1.2 Sv in precipitation. Terrestrial runoff added to meltwater from snow and glacier accounts for approximately only 1.25 ± 0.1 Sv. Changes in the E-P pattern could destabilize the upper-ocean stratification and lead to changes in salinity in the ocean interior (Skliris *et al.*, 2014).

The water cycle depends on the exchanges between the atmosphere and the ocean through evaporation-precipitation. Approximately 78% of the total rain falls over the ocean and about 86% of the atmospheric water vapour has been evaporated from the ocean (Baumgartner and Reichel, 1975, Adler *et al.*, 2003). Even though estimates of E-P are assessed from the local wind speed, temperature and humidity dependence as well as satellite images (Zhang *et al.*, 2007), the incomplete E-P data over the ocean poses a challenge in quantifying these fields, especially in a time varying point of view. The global evaporation pattern is strongest over the subtropical gyres and the western boundary currents and weaker at higher latitudes and around the equator (Schanze *et al.*, 2010). The pattern of time averaged precipitation rate has higher precipitation in the western boundary currents, the higher latitudes and around the equator, but weaker precipitation in the subtropical gyres.

The atmosphere's capacity to hold water vapour is approximately exponentially dependent on temperature according to the Clausius-Clapeyron relation, that is, for a 1^{o}C increase in temperature, the air can hold a corresponding 7% increased water vapour (Schmitt, 2009). Thus, assuming unchanged physics, the evaporative component of the water cycle is expected to increase. The SST has increased by ~0.5^{o}C over the past 50 years, which suggests an approximately 4% increase in the global water cycle (Trenberth *et al.*, 2007, Durack *et al.*, 2012). However, the corresponding change to SSS has amplified by about 8% (Curry *et al.*, 2003; Boyer *et al.*, 2005; Hosoda *et al.*, 2009; Helm *et al.*, 2010; Skliris *et al.*, 2014; Durack *et al.*, 2012). This amplified SSS pattern drives the observed changes in salinity in the ocean interior (Durack and Wijffels, 2010).

1.3 Temperature

The mean global ocean surface temperature has increased by around 0.5°C per 50 years over the past decades (Figure 1.2; Ishii *et al.*, 2005; Rayner *et al.*, 2006; Smith and Murphy, 2007; Solomon *et al.*, 2007, Ishii and Kimoto, 2009; Durack and Wijffels, 2010; Levitus *et al.*, 2012; Good *et al.*, 2013). The SST increase is more pronounced in the North Atlantic and lesser in the Southern Ocean (Figure 1.2a; Marshall *et al.*, 2014). However, the observed warming in the Southern Ocean is likely underestimated due to the sparse observations (Gille, 2002; Gouretski and Koltermann, 2007; Durack *et al.*, 2014), the mean surface temperature change is significantly smaller south of 55°S (Figure 1.2b).

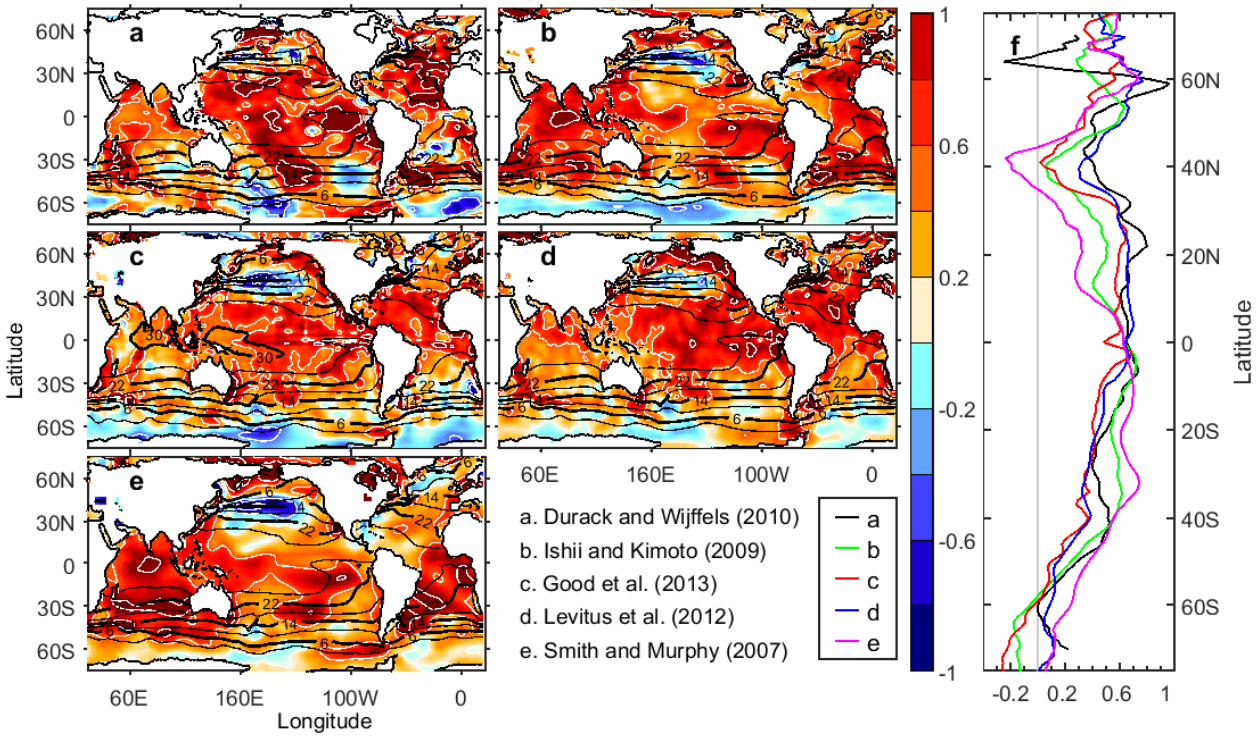

Figure 1.2. Surface temperature change (°C per 50 years) for multiple observational datasets (a to e). The black contours are the mean surface temperature every 4°C. Panel f has the zonally averaged global temperature change for each dataset (°C per 50 years).

The surface density is lower closer to the equator, where the surface temperature is higher, and increases towards the poles. This increase in SST has reduced the surface density and as a result

the broad-scale long-term warming of the global ocean has therefore led to a general poleward migration of isopycnals. The lateral shifts in certain regions are estimated to be at the scale of 50 to 100 km over a 50 years period (Durack and Wijffels, 2010) (Figure 1.3).

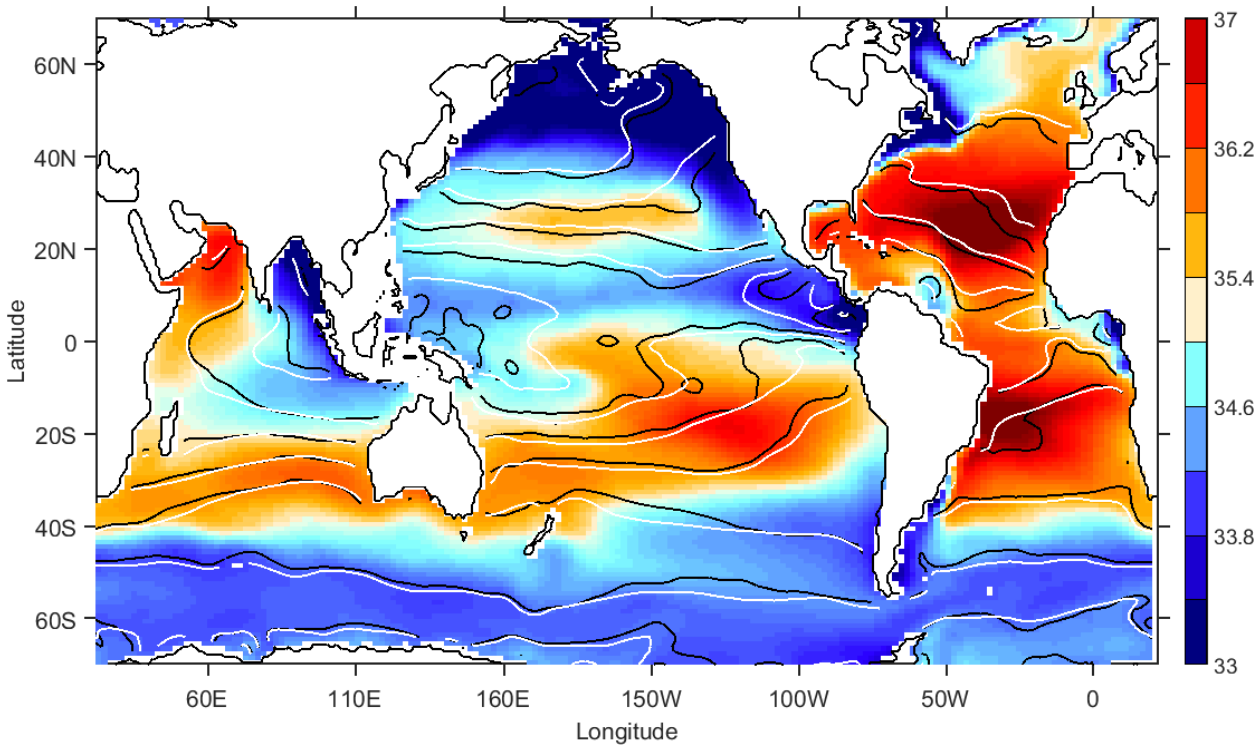

Figure 1.3. Outcrops in 1950 (black lines) and 2000 (white lines). The coloured pattern is the mean salinity between 1950 and 2008. (Durack and Wijffels, 2010).

The increased surface temperature is transmitted to the ocean interior through subduction, convection, advection and mixing and increases the ocean heat content (Meehl *et al.*, 2011; Balmaseda *et al.*, 2013). It also impacts both the circulation by affecting local density gradients and sea level by increasing the steric height (Church *et al.*, 2004; Domingues *et al.*, 2008, Levitus *et al.*, 2012). Levitus *et al.* (2000) showed that the volume mean warming of the world's ocean heat content from the mid 1950s to mid 1990s represents approximately a 0.06°C temperature increase. The upper 75 m of ocean warmed at a rate of 0.11°C per decade between 1971 and 2010 (Rhein *et al.*, 2013). The oceans are estimated to contribute 93% of the increase to the Earth's heat content between 1971 and 2010 (Rhein *et al.*, 2013). Most of the heat is stored in the upper 700 m of the ocean with a larger increase in the Atlantic Ocean (Levitus *et al.*, 2005).

This warming of the upper layers of the oceans is global and roughly similar in each basin at equivalent latitudes. Exceptions include cooling in the South Pacific, due to local decadal variations (Barnett *et al.*, 2005). In the North Atlantic Deep Water cooling is observed after the renewal of deep convection post 1970s (Dickson *et al.*, 2002). Finally, the South Indian Ocean has some subsurface cooling due to variations in the Indonesian Throughflow (ITF) and wind patterns (Alory *et al.*, 2007; Schwarzkopf and Böning, 2011).

1.4 Winds

The atmospheric winds are driven by radiative forces. The surface zonal wind speed over the ocean comprises the trade winds in the equatorial and subtropical regions and the westerlies at high latitude (Figure 1.4a). The surface wind transfers its kinetic energy into both kinetic and potential energy to the ocean surface (Wunsch and Ferrari, 2004). The force applied on the surface of the ocean depends quadratically on the atmospheric surface wind speed (Zhai *et al.*, 2013):

$$\tau = \rho_a c_d |U_{10} - u_0|(U_{10} - u_0)$$

Where τ is the surface wind stress, ρ_a is the sea level air density, c_d is a drag coefficient, u_0 is the surface velocity of the ocean and U_{10} is the wind velocity at 10 m. The surface wind stress affects the ocean mixing and circulation in the Ekman layer (Wunsch and Ferrari, 2004).

The Southern Ocean and equatorial region are sensitive to changes in the wind field (Wunsch, 1998; Meredith *et al.*, 2012; Lai *et al.*, 2015). Over the Southern Ocean, the westerlies have the strongest wind speed and drives the Antarctic Circumpolar Circulation (ACC). The ACC is the biggest current in terms of volume and allows a connection between all of the main ocean basins. The westerlies over the ACC drive Ekman transport northward which results in Ekman pumping at the convergence of the Southern Hemisphere gyres which cools the northern edge of the Southern Ocean. The steep isopycnals at the junction of the ACC and the Southern Hemisphere gyres also drive eddy diffusion which warms the Southern Ocean. The ACC is the main driver of

the ocean dynamics of this region, which explains the importance of the wind stress in the Southern Ocean (Figure 1.4).

At the equator the Hadley atmospheric circulation converge at the surface, where the southward meridional surface wind velocity in the Northern Hemisphere meets the northward meridional surface wind velocity in the Southern Hemisphere (Figure 1.4b). At low latitudes, the trade winds drive the westward equatorial circulation. The trade winds drive meridional Ekman transport at the surface of the ocean. The Ekman transport changes sign at the equator due to the change of hemisphere which change the sign of the Coriolis parameter. This change of sign induces a divergence at the equator which drives equatorial upwelling in the ocean.

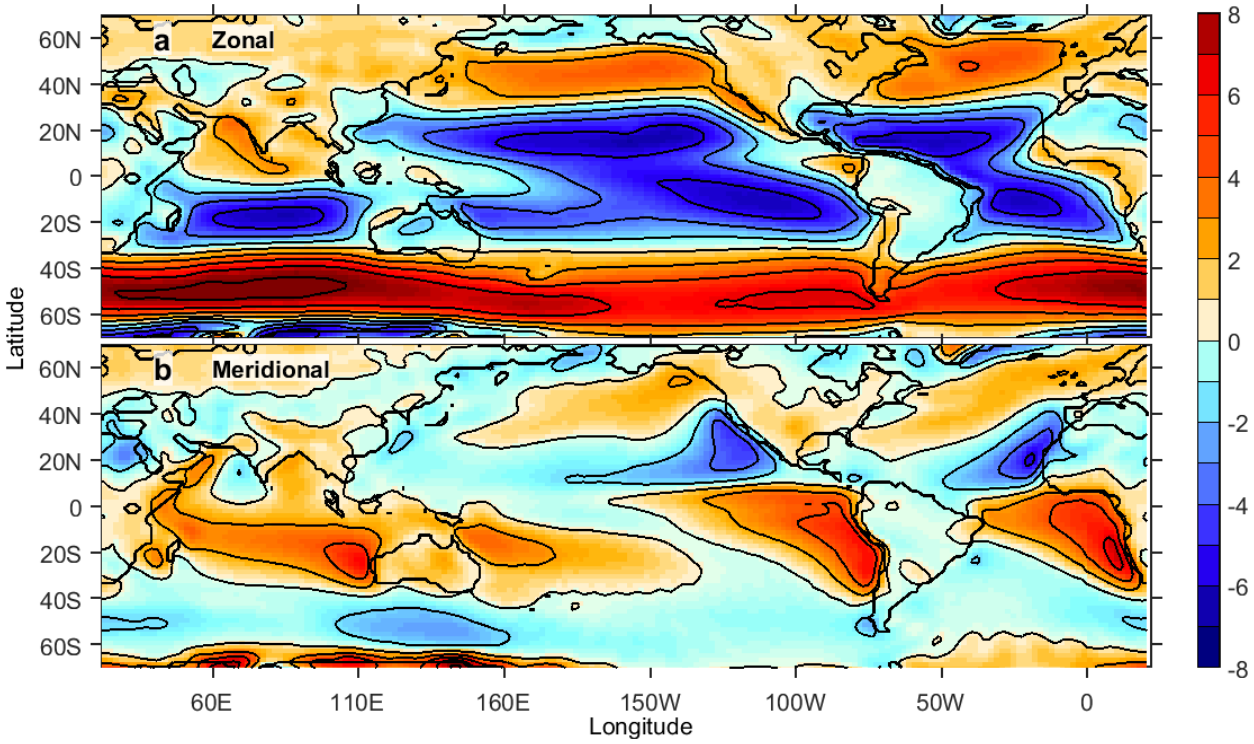

Figure 1.4. Mean zonal (a) and meridional (b) wind speed at 10 m (m/s) between 1950 and 2008 as the average of three data reanalysis: ERA-40 (Uppala et al., 2005), Japanese 55-year Reanalysis (JRA-55; Kobayashi et al., 2015) and National Oceanic and Atmospheric Administration 20th Century Reanalysis (NOAA-20CR; Compo et al., 2011). Positive wind speeds are eastward and northward. The black contours are every 2 m/s.

The wind pattern has changed in the past decades, however, due to sparse and limited observations there are uncertainties in the exact nature of these changes (Wu *et al.*, 2005; Krueger *et al.*, 2013). Data reanalyses point to a strengthening of the westerlies at high latitudes and a possible poleward shift (Swart and Fyfe, 2012). There is also evidence of an increased to the trade winds over the tropical Pacific (Merrifield, 2011). Additionally, there are signs of a poleward extension of the Hadley circulation (Wu *et al.*, 2012).

The effect of wind stress on the ocean circulation and dynamics is well studied and understood. However, because of the sparse wind observations, the nature of the changes in the wind field and its effect on the ocean circulation and mixing is still not fully understood. The strengthened westerlies over the Southern Ocean might drive an increase in eddy diffusivity leading to an increased poleward heat flux (Meredith and Hogg, 2006; Fyfe *et al.*, 2007; Hogg *et al.*, 2008). Additionally, Merrifield (2011) suggests that increased trade winds in the equatorial Pacific drive a sea level height increase on the western side of the Pacific.

1.5 Model

For this study, a model is used to decompose the impact of multidecadal trends of each surface forcing individually, and together. This decomposition aims to identify the contribution of surface warming, salinity pattern amplification and wind pattern change to the observed changes in temperature and salinity in the ocean interior. The model used for this study is the Australian Community Climate and Earth System Simulator Ocean Model (ACCESS-OM; Bi *et al.*, 2013). It combines the Modular Ocean Model version 4.1 (MOM4p1; Griffies, 2009), data atmospheric model (MATM) and Los Alamos National Laboratory Sea Ice Model version 4.1 (CICE4.1; Hunke and Lipscomb, 2010). The OASIS3 coupler controls the information exchange between these submodels (Valcke, 2006). The Coordinated Ocean-ice Reference Experiments version 2 (COREv2; Large and Yeager, 2004; 2009) atmospheric forcing dataset is applied to MOM4p1 through the MATM submodel.

The version of ACCESS-OM used here follows the same physical parameterisations as Bi *et al.* (2013; Table 1) with two exceptions: the explicit convection and the near-equator reduction of vertical diffusion. The advection of tracers uses the multi-dimensional flux limited scheme for conservative temperature, salinity, and age tracers (Sweby 1984, Hundsdorfer and Trompert 1994). The horizontal friction uses Smagorinsky isotropic biharmonic friction as formulated by Griffies and Hallberg (2000). Convection is implicit using vertical diffusivity following Killworth *et al.* (1991). The background vertical mixing in the deep ocean is 1 m^2/s^2. In the upper ocean, the vertical mixing follows the Large *et al.* (1994) k-parametrisation profile (KPP) mixed layer scheme. The neutral physics are parameterised following the scheme described by Gent and McWilliams (1990) in which the diffusion is relaxed by bringing neutral directions toward surfaces of constant generalized vertical coordinate rather than constant geopotential surfaces with baroclinic closure of the thickness diffusivity (Ferrari *et al.* 2010). The isoneutral diffusivity has a background value of 600 m^2/s^2 following Redi (1982). The parameterisation for tidal mixing in the abyssal ocean follows Simmons *et al.* (2004) and the parameterization of barotropic coastal tidal dissipation according to Lee *et al.* (2006). The shelf waters overflow at high latitudes are parameterised using the sigma transport scheme of Beckmann and Doescher (1997) with the downslope mixing scheme from Griffies (2009).

The model was spun-up for 500 years with normal year COREv2 forcing which provided a relatively state for the commencement of the experiments. Like most similar models, ocean adjustment continues after the completion of the spin-up in the deep water masses (Griffies *et al.*, 2009; Bi *et al.*, 2013). To account for this ongoing drift, a control experiment is subtracted from each other experiment in all data presented.

Bi *et al.* (2013) did a thorough evaluation of the ACCESS-OM model performance. The ocean circulation and temperature and salinity fields in ACCESS-OM are realistic (Bi *et al.*, 2013). However, some water masses ventilated at high latitudes do not penetrate as far equatorward as observed and the ITF is not well resolved, which is common for z-grid models (Sloyan and Kamenkovitch, 2007). Additionally, the main thermocline is too deep and thick, but, the wind-driven subduction and subtropical and equatorial circulation system are overall well simulated.

The Atlantic Meridional Overturning Circulation and the Pacific equatorial circulation are closed to observations. The Antarctic Circumpolar Current is too strong, but is within the range of simulated with other CORE models (Bi *et al.*, 2013).

1.5.1 Grid

The ocean and ice models, MOM4 and CICE, are both structured with Arakawa B-grids (Arakawa and Lamb, 1977; Figure 1.5 and Figure 1.6). This spatial discretization defines the location of the horizontal velocity components at the northeast corner of each cell, half distance between the centre of two adjacent cells. The vertical velocity is at the centre of the bottom face of each cell. The tracers, salinity, temperature, density and hydrostatic pressure, are diagnosed at the centre of a cell.

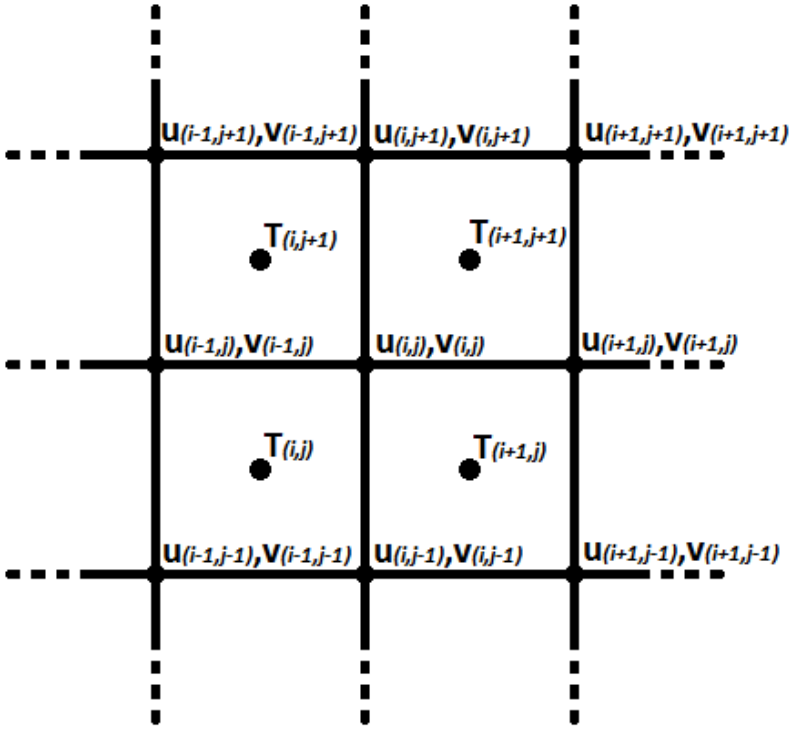

Figure 1.5. Two-dimensional sectional view of the Arakawa B-Grid used in MOM4 and CICE (ACCESS-OM). The indices i and j represent the grid cell number within the grid zonally and meridionally respectively. The tracers, T, are the salinity, temperature and hydrostatic pressure. The u and v components are respectively the eastward and northward velocities.

In the ocean model, MOM4, the equations of state are discretised on a fixed curvilinear grid. The discretization nature of the grid generates differences with the physics of reality. Griffies *et al.* (2000) summarized the strengths and weaknesses of an Arakawa B-grid for an ocean model. This grid type simulates well the gravity waves and geostrophic currents at coarser resolution. B-grids are also superior for boundary currents, fronts and Rossby waves. However, in consideration to smaller-scale processes and finer resolution models, B-grids are not an ideal choice. Generally, B-grids are preferred for coarse resolution models for their superiority in resolving flows at these resolutions. In ACCESS-OM, the Arakawa B-grid model is an appropriate choice for the resolution.

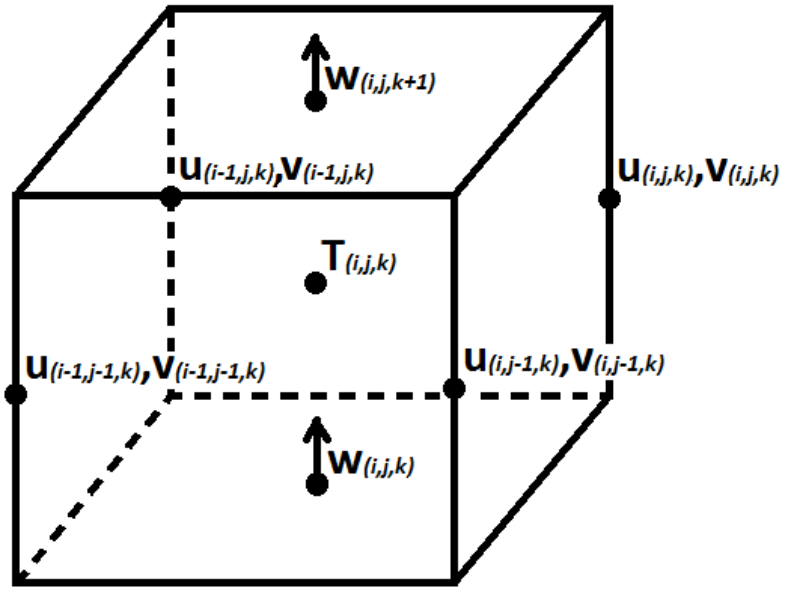

Figure 1.6. Three-dimensional view of an Arakawa B-Grid cell as used in MOM4 and CICE (ACCESS-OM). The indices i, j and k represent the grid cell number within the grid zonally, meridionally and vertically respectively. The tracers, T, are the salinity, temperature and hydrostatic pressure. The u, v and w components are respectively the eastward, northward and upward velocities.

The grid is a tripolar grid to avoid discontinuities at the North Pole (Murray, 1996) (Figure 1.7). This grid follows the geographical coordinates between 78°S and 65°N. The grid is not defined over the interior continent of Antarctica. In the Arctic Ocean, north of 65°N, two poles are selected over land masses. The grid over the Arctic Ocean joins these two poles without the

discontinuity of a pole within the ocean limits. The grid has a 1° resolution in the zonal direction. In the meridional direction, the resolution varies from ¼° at 78°S to 1° at 30°S and refines to ⅓° between 10°S and 10°N.

In the vertical direction, there are 50 levels between 0 and 6000 m. The thickness of the levels varies from finer near the surface, where smaller scale processes occur, to thicker at depth. The variations in the topography are approximated through a partial cell method which has been shown to improve a model's ocean simulation (Adcroft *et al.*, 1997, Myers and Deacu, 2004). The partial cell method keeps the cell rectangular, but allows the deeper cell to vary in thickness according to the local bathymetry.

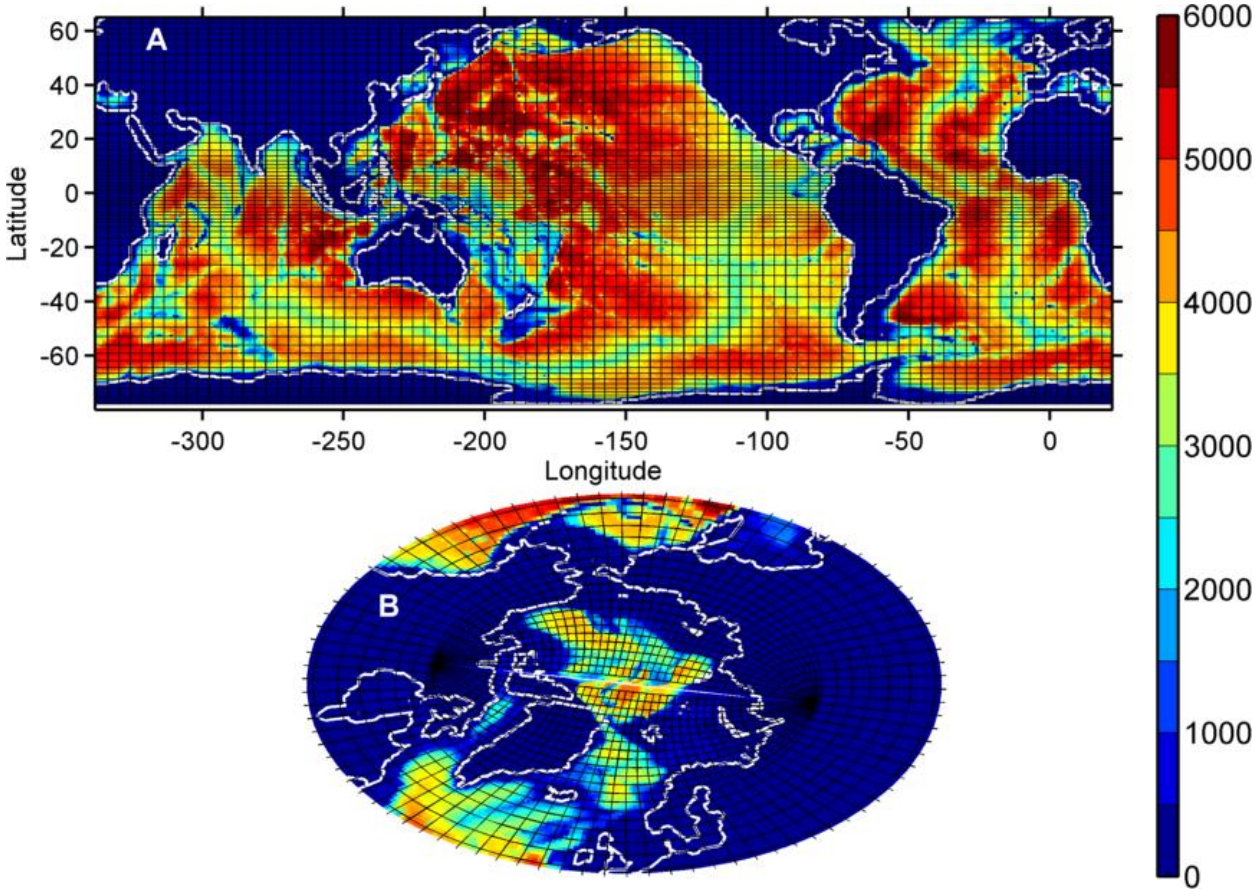

Figure 1.7. ACCESS-OM tripolar grid every four grid cells in each direction between 80°S and 65°N (a) and north of 55°N. The coloumodellr scale corresponds to the depth of the deepest cell. The lines show the grid every four grid cells in each direction.

1.5.2 Forcings

The COREv2 normal year dataset from Large and Yeager (2004) is used in MATM. This dataset acts as a substitute for a complete atmospheric model integrated to an ocean only or ocean-ice model. It prescribes the atmospheric boundary conditions over both the ocean and sea ice.

The COREv2 forcing is on a spherical grid of 192 longitudinal points by 94 latitudinal points. Due to timestep differences, the field is applied to the model with temporal interpolation. The COREv2 precipitation field varies monthly, the shortwave and longwave radiation daily; and temperature, humidity, zonal velocity, meridional velocity and sea level pressure six-hourly.

1.5.3 Restoring

The salinity restoring is applied at the surface of the ocean through virtual salt flux. A virtual salt flux is a modelling strategy used for rigid-lid approximation of the ocean, i.e. fixed volume. The surface salinity is corrected to the restoring condition by this virtual salt flux. The freshwater fluxes at the surface are input by locally changing the surface salinity rather than imposing a volume flux of freshwater. This technique can be summarized as a parameterization of salt flux locally input or output at the surface of the ocean. This technique induces only small errors (Yin *et al.*, 2010) and can be considered as a valid approximation. In our experiments, we also use temperature restoring at the surface to impose a virtual heat flux. The virtual heat flux damps the SST towards a restoring field.

1.6 Experiments

The aim of this project is to decompose the role of each surface boundary flux on the ocean into the spatio-temporal subsurface changes. A set of idealized experiments that impose individual anomalies at the surface boundary, in accordance with observed changes over a 50 years period. The anomalies correspond to an enhanced surface boundary condition while other fluxes are kept annually constant. The subsurface trends in salinity and temperature induced by the changes in each of these surface conditions are then assessed.

Table 1.1. Summary of the surface boundary condition imposed in each idealized experiment.

Experiment name	Temperature uniform increase (°C)	Salinity pattern amplification (%)	Wind change
Control	0	0	-
ΔT	0.5	0	-
ΔS	0	8	-
ΔTΔS	0.5	8	-
Δ*ERA-40*	0	0	ERA-40
Δ*JRA-55*	0	0	JRA-55
Δ*NOAA-20CR*	0	0	NOAA-20CR
Δ*CMIP5*	0	0	CMIP5
ΔMeanTrend	0	0	MeanTrend
ΔTΔSΔMeanTrend	0.5	8	MeanTrend

The surface temperature increase, salinity pattern amplification and wind change are applied individually and together (Table 1.1). A period of 50 years will be the main focus to enable comparisons with the 50 years trends observations of salinity and temperature from 1950 to 2008 compiled by Durack and Wijffels (2010). The temperature is linearly increased by 0.5°C between 55°S and 60°N, which compares well with the observed mean surface temperature increase for the same time period. The observed sea surface temperature has warmed north of 60°N (Figure 1.2). However, because of the experimental setup through surface restoring increasing linearly throughout the year, increasing the sea surface temperature north of 60°N would warm the ocean surface under the sea ice, which is unrealistic. In order to avoid this problem, we impose no warming at high latitudes and concentrate the study mainly to the ventilated gyres area. The sharp change in temperature at the edge of our warming domain creates a gradually amplifying sharp gradient at the surface. However, within the limits of the change in temperature we impose (0.5°C after 50 years), this gradient dissipates locally in the upper ~100 m.

The salinity pattern is amplified by 8% which reflects the hydrological cycle amplification (E-P) for that time period. The 8% amplification of the global mean surface salinity pattern has been evaluated by Durack *et al.* (2012) for a 50 years trend during the period 1950 to 2000. We apply

the 8% amplification by linearly amplifying the difference with the mean salinity over the intra-annual monthly cycle.

Finally, wind speed changes from three data reanalyses are tested; ERA-40 (Uppala *et al.*, 2005), JRA-55 (Japanese 55-year Reanalysis; Kobayashi *et al.*, 2015) and NOAA-20CR (National Oceanic and Atmospheric Administration 20th Century Reanalysis; Compo *et al.*, 2011) along with the wind speed trends in the CMIP5 historical multi-model ensemble (Taylor *et al*., 2012). The wind change experiments impose the 50 years trends per grid cell from each of these datasets. An additional wind trend dataset is created from the average of the trends from all three reanalyses (MeanTrend). The wind trends are imposed in a linear change over the COREv2 normal year intra-annual field to avoid discontinuity from the spin-up. Two additional experiments where surface temperature changes and surface salinity pattern amplification are applied together with fixed wind and with MeanTrend wind change are also performed to identify how these changes act together.

Changes in temperature and salinity are imposed through a strong 6 hourly surface restoring in a thickness of 10 m. In the experiments with no imposed trend in either temperature or salinity, a fixed interannual field is restored at the surface. For the fixed annual fields, we take the surface temperature and salinity of the last year of the spin-up. In experiments with no changes in the wind field, the winds are kept constant with the COREv2 normal year forcing.

References

Adcroft, A., C. Hill, J. Marshall, 1997: Representation of topography by shaved cells in a height coordinate ocean model. *Monthly Weather Review*, **125**, pp. 2293–2315.

Adler, R., G. Huffman, A. Chang, R. Ferraro, P. Xie, J. Janowiak, B. Rudolf, U. Schneider, S. Curtis, D. Bolvin, *et al.*, 2003: The version-2 Global Precipitation Climatology Project (GPCP) monthly precipitation analysis (1979–present). *Journal of Hydrometeorology*, **4**, pp. 1147–1167.

Alory, G., S. Wijffels, and G. Meyers, 2007: Observed temperature trends in the Indian Ocean over 1960–1999 and associated mechanisms. *Geophysical Research Letters*, **34**, L02606. doi:10.1029/2006GL028044

Arakawa, A., and V.R. Lamb, 1977: Computational design and the basic dynamical processes of the UCLA general circulation model. *Methods in Computational Physics,* **17***,* pp. 173–265.

Balmaseda, M.A., K.E. Trenberth and E. Kallen, 2013: Distinctive climate signals in reanalysis of global ocean heat content. *Geophysical Research Letters*, **40**, pp. 1754-1759. doi:10.1002/grl.50382

Barnett, T.P., D. W. Pierce, K. M. AchutaRao, P.J. Gleckler, B. D. Santer, J.M. Gregory, W.M. Washington, 2005: Penetration of Human-Induced Warming into the World's Oceans. *Science*, **309**, pp. 284-287. doi:10.1126/science.1112418

Baumgartner, A. and E. Reichel. 1975: World water balance: mean annual global, continental and maritime precipitation, evaporation and runoff. *Elsevier Scientific*, 182 pp.

Beckmann, A. and R. Döscher, 1997: A method for improved representation of dense water spreading over topography in geopotential-coordinate models. *Journal of Physical Oceanography,* **27**, pp. 581–591.

Bi, D., S.J. Marsland, P. Uotila, S. O'Farrell, R. Fiedler, A. Sullivan, S.M. Griffies, X. Zhou, and A.C. Hirst, 2013: ACCESS-OM: the Ocean and Sea ice Core of the ACCESS Coupled Model. *Australian Meteorology and Oceanography Journal*, **63(1)**, pp. 213-232.

Bindoff, N.L., and T.J. McDougall, 1994: Diagnosing climate change and ocean ventilation using hydrographic data. *Journal of Physical Oceanography*, **24**, pp. 1137–1152.

Boyer, T.P., S. Levitus, J.I. Antonov, R.A. Locarnini, R. and H.E. Garcia (2005) Linear trends in salinity for the World Ocean, 1955-1998. *Geophysical Research Letters*, **32**, L01604. doi:10.1029/2004GL021791

Boyer, T.P., J.I. Antonov, S. Levitus, and R. Locarnini, 2005: Linear trends of salinity for the world ocean, 1955-1998. *Geophysical Research Letters*, **32**, L01604. doi:1029/2004GL021791

Compo, G. P., Whitaker, J. S., Sardeshmukh, P. D., Matsui, N., Allan, R. J., Yin, X., Gleason, B. E., Vose, R. S., Rutledge, G., Bessemoulin, P., Brönnimann, S., Brunet, M., Crouthamel, R. I., Grant, A. N., Groisman, P. Y., Jones, P. D., Kruk, M. C., Kruger, A. C., Marshall, G. J., Maugeri, M., Mok, H. Y., Nordli, Ø., Ross, T. F., Trigo, R. M., Wang, X. L., Woodruff, S. D. and Worley, S. J., 2011: The Twentieth Century Reanalysis Project. *Quaterly Journal of the Royal Meteorological Society*, **137**, pp. 1–28. doi:10.1002/qj.776

Church, J.A., N.J., White, R. Coleman, K. Lambeck and J.X. Mitrovica, 2004: Estimates of the Regional Distribution of Sea Level Rise over the 1950–2000 Period. *Journal of Climate*, **17**, pp. 2609-2625.

Curry, R., R. Dickson and I. Yashayaev, 2003: A change in the freshwater balance of the Atlantic Ocean over the past four decades. *Nature*, **426**, pp. 826-829.

de Lavergne, C., J.B. Palter, E.D. Galbraith, R. Bernardello and I. Marinov, 2014: Cessation of deep convection in the open Southern Ocean under anthropogenic climate change. *Nature Climate Change*, **4**, pp. 278-282.

Dickson, R. R., I. Yashayaev, J. Meincke, W. Turrell, S. Dye and J. Holfort, 2002: Rapid Freshening of the deep North Atlantic over the past four decades. *Nature*, **416**, pp. 832-837.

Domingues, C.M., J.A. Church, N.J. White, P.J. Gleckler, S.E. Wijffels, P.M. Barker and J.R. Dunn, 2008: Improved estimates of upper-ocean warming and multi-decadal sea-level rise. *Nature*, **453**, pp. 1090-1093. doi:10.1038/nature07080

Durack, P.J. and S. E. Wijffels, 2010: Fifty-year trends in the global ocean salinities and their relationship to broad-scale warming. *Journal of Climate*, **23**, pp. 4342-4362.

Durack, P.J., S.E. Wijffels, R.J. Matear, 2012: Ocean salinities reveal strong global water cycle intensification during 1950 to 2000. *Science*, **336**, pp. 455-458.

Durack, P.J., P.J. Gleckler, F.W. Landerer and K. E. Taylor, 2014: Quantifying underestimates of long-term upper-ocean warming. *Nature Climate Change*, **4**, pp. 999-1005. doi:10.1038/NCLIMATE2389

Emile-Geay, J., M.A. Cane, N. Naik, R. Seager, A.C. Clement amd A. can Geen, 2003: Warren revisited: Atmospheric freshwater fluxes and "Why is no deep water formed in the North Pacific". *Journal of Geophysical Research: Oceans*, **108**(C6). doi:10.1029/2001JC001058

Ferrari, R., S.M. Griffies, G. Nurser and G.K. Vallis, 2010: A Boundary Value Problem for the Parameterized Mesoscale Eddy Transport. *Ocean Modelling*, **32**, pp. 143–156.

Fyfe, J.C., O.A. Saenko, K. Zickfeld, M. Eby, and A.J. Weaver, 2007: The Role of Poleward-Intensifying Winds on Southern Ocean Warming. *Journal of Climate*, **20**, pp. 5391–5400. doi:10.1175/2007JCLI1764.1

Gent, P.R. and J.C. McWilliams, 1990: Isopycnal mixing in ocean circulation models. *Journal of Physical Oceanography*, **20**, pp. 150–155.

Gille, S.T., 2002: Warming of the Southern Ocean Since the 1950s. *Science*, **295**, pp. 1275-1277, doi:10.1126/science.1065863

Good, S.A., M.J. Martin and N.A. Rayner, 2013: EN4: Quality controlled ocean temperature and salinity profiles and monthly objective analyses with uncertainty estimates. *Journal of Geophysical Research: Oceans*, **118**, pp. 6704-6716. doi:10.1002/2013JC009067

Gould, J., D. Roemmich, S. Wijffels, H. Freeland, M. Ignaszewsky, X. Jianping, S. Pouliquen, Y. Desaubies, U. Send, K. Radhakrishnan, K. Takeuchi, K. Kim, M. Danchenkov, P. Sutton, B. King, B. Owens and S. Riser, 2004: Argo profiling floats bring new era of in situ ocean observations. *Eos, Transactions American Geophysical Union*, **85** (19). doi:10.1029/2004EO190002

Gouretski, V. and K.P. Koltermann, 2007: How much is the ocean really warming? *Geophysical Research Letters*, **34**, L01610. doi:10.1029/2006GL027834

Griffies, S.M., C. Boning, F.O. Bryan, E.P. Chassignet, R. Gerdes, H. Hasumi, A. Hirst, A.-M. Treguier, D. Webb, 2000: Developments in ocean climate modelling. *Ocean Modelling*, **2**, pp. 123-192.

Griffies, S.M. and R.W. Hallberg, 2000: Biharmonic friction with a Smagorinsky viscosity for use in large-scale eddy-permitting ocean models. *Monthly Weather Rev*iew, **128**, pp. 2935–2946.

Griffies, S.M., 2009: Elements of MOM4p1: GFDL Ocean Group Tech. Rep. 6. NOAA/Geophysical Fluid Dynamics Laboratory, 444 pp.

Helm, K.P., N.L. Bindoff and J.A. Church, 2010: Changes in the global hydrological-cycle inferred from ocean salinity. *Geophysical Research Letters*, **37**, L18701. doi:10.1029/2010GL044222

Hogg, A.M., M.P. Meredith, J.R. Blundell and C. Wilson, 2008: Eddy Heat Flux in the Southern Ocean: Response to Variable Wind Forcing. *Journal of Climate*, **21**, pp. 608–620. doi:10.1175/2007JCLI1925.1

Hosoda, S., T. Suga, N. Shikama and K. Mizuno, 2009: Global Surface Layer Salinity Change Detected by Argo and Its Implication for Hydrological Cycle Intensification. *Journal of Oceanography*, **65**, pp. 579-596. doi:10.1007/s10872-009-0049-1

Huang, R.X., W. Wang, L.L. Liu, 2006: Decadal variability of wind-energy input to the world ocean. *Deep Sea Research II*, **53**, pp. 31-41.

Hunke, E.C. and Lipscomb, W.H., 2010: CICE: the Los Alamos Sea ice Model Documentation and Software 504 User's Manual. LA-CC-06-012 Tech. Rep., 1–76.

Hundsdorfer, W. and R.A. Trompert, 1994: Method of lines and direct discretisation: a comparison for linear advection. *Applied Numerical Mathematics*, **13**, pp. 469–490.

Ishii, M., A. Shouji, S. Sugimoto, and T. Matsumoto, 2005: Objective analyses of sea-surface temperature and marine meteorological variables for the 20th century using icoads and the Kobe collection. *International Journal of Climatolology*, **25**, pp. 865–879.

Ishii, M. and M. Kimoto, 2009: Reevaluation of historical ocean heat content variations with time-varying XBT and MBT depth bias corrections. *Journal of Oceanography*, **65**, pp. 287-299.

Josey, S. A., E. C. Kent, and P. K. Taylor, 1998: The Southampton Oceanography Centre (SOC) ocean–atmosphere heat, momentum, and freshwater flux atlas. Southampton Oceanography Centre Rep. 6, 30 pp.

Killworth, P. D., D. Stainforth, D. J. Webb, and S. M. Paterson, 1991: The development of a free-surface Bryan-Cox-Semtner ocean mode. *Journal of Physical Oceanography*, **21**, pp. 1333–1348.

Kjellsson, J., P.R. Holland, G.J. Marshall, P. Mathiot, Y. Aksenov, A.C. Coward, S. Bacon, A.P. Megann and J. Ridley, 2015: Model sensitivity of the Weddell and Ross seas, Antarctica, to vertical mixing and freshwater forcing. *Ocean Modelling*, **94**, pp. 141-152.

Kobayashi, S., Y. Ota, Y. Harada, A. Ebita, M. Moriya, H. Onoda, K. Onogi, H. Kamahori, C. Kobayashi, H. Endo, K. Miyaoka and K. Takahashi, 2015: The JRA-55 Reanalysis: General Specifications and Basic Characteristics. *Journal of the Meteorological Society of Japan*, **93**, No. 1, pp. 5−48. doi:10.2151/jmsj.2015-001

Krueger, O., F. Schenk, F. Feser, and R. Weisse, 2013: Inconsistencies between long-term trends in storminess derived from the 20CR reanalysis and observations. Journal of Climate, **26**, pp. 868–874.

Kuhlbrodt, T. and J.M. Gregory, 2012: Ocean heat uptake and its consequences for the magnitude of sea level rise and climate change. *Geophysical Research Letters*, **39**, L18608. doi:10.1029/2012GL052952

Lagerloef, G., R. Schmitt, J. Schanze, and H.-Y. Kao. 2010. The ocean and the global water cycle. *Oceanography,* **23(4)**, pp. 82–93. doi:10.5670/oceanog.2010.07

Lai, A.W., M. Herzog, H.-F. Graf., 2015: Two key parameters for the El Nino continuum: zonal wind anomalies and Western Pacific subsurface potential temperature. *Climate Dynamics*. doi:10.1007/s00382-015-2550-0

Large, W.G., J.C. McWilliams and S.C. Doney, 1994: Oceanic vertical mixing: A review and a model with a nonlocal boundary layer parameterization. *Reviews of Geophys*ics, **32**, pp. 363–403. doi:10.1029/94RG01872

Large W. and S. Yeager, 2004: Diurnal to decadal global forcing for ocean and sea ice models: the data sets and climatologies. *Technical Report, Boulder: National Centre for Atmospheric Research*, 105 pp.

Large, W.G. and S. Yeager, 2009: The global climatology of an interannually varying air-sea flux data set. *Climate Dynamics,* **33***.* doi:10.1007/s00382-008-0441-3

Lazier, J., R. Hendry, A. Clarke, I. Yashayaev, P. Rhines, 2002: Convection and restratification in the Labrador Sea, 1990-2000. *Deep-Sea Research*, **49**, pp. 1819-1835.

Lee, H.-C., A. Rosati and M. Spelman, 2006: Barotropic tidal mixing effects in a coupled climate model: Oceanic conditions in the northern Atlantic. *Ocean Modelling,* **3–4***,* pp. 464–477.

Levitus, S., J.I.Antonov, T.P. Boyer, C. Stephens, 2000: Warming of the world ocean. Sciences, **287**, pp. 2225-2229.

Levitus, S., J.I. Antonov, and T.P. Boyer, 2005: Warming of the World Ocean, 1955-2003. *Geophysical Research Letters*, **32**, L02604. doi:10.1029/2004GL021592

Levitus, S., J.I. Antonov, T.P. Boyer, O.K. Baranova, H.E. Garcia, R.A. Locarnini, A.V. Mishonov, J.R. Reagan, D. Seidov, E.S. Yarosh, and M.M. Zweng, 2012: World ocean heat content and thermosteric sea level change (0–2000 m), 1955–2010. *Geophysical Research Letters*, **39**, L10603. doi:10.1029/2012GL051106

Marshall. J., K.C. Armour, J.R. Scott, Y. Kostov, U. Hausmann, D. Ferreira, T.G. Shepherd and C.M. Bitz, 2014: The ocean's role in polar climate change: asymmetric Arctic and Antarctic responses to greenhouse gas and ozone forcing. *Philosophical Transactions of the Royal Society A*, **372**, 20130040. doi:10.1098/rsta.2013.0040

Marsland, S.J., and J.-O. Wolff, 2001: On the sensitivity of Southern Ocean sea ice to the surface freshwater flux. J. Geophys. Res. (Oceans), **106**, pp. 2723-2741.

Meehl, G.A., J.M. Arblaster, J.T. Fasullo, A. Hu and K.E. Trenberth, 2011: Model-based evidence of deep-ocean heat uptake during surface-temperature hiatus periods. *Nature Climate Change*, **1**, pp. 360–364. doi:10.1038/nclimate1229

Meredith, M.P., A. M. Hogg, 2006: Circumpolar response of Southern Ocean eddy activity to a change in the Southern Annular Mode. *Geophysical Research Letters*, **33**, L16608. doi:10.1029/2006GL026499

Meredith, M.P., A.C.N. Garabato, A. M. Hogg and R. Farneti, 2012: Sensitivity of the Overturning Circulation in the Southern Ocean to Decadal Changes in Wind Forcing. *Journal of Climate*, **25**, pp. 99-110.

Merrifield, M.A., 2011: A Shift in Western Tropical Pacific Sea Level Trends during the 1990s. *Journal of Climate*, **24**, pp. 4126-4138. doi:10.1175/2011JCLI3932.1

Morrison, A.K., England, M.H. and Hogg, A.M., 2015: Response of Southern Ocean Convection and Abyssal Overturning to Surface Buoyancy Perturbations. *Journal of Climate*, **28**, pp. 4263-4278. doi:10.1175/JCLI-D-14-00110.1

Murray, R.J., 1996: Explicit generation of orthogonal grids for ocean models. *Journal of Computational Physics*, **126**, pp. 251–273.

Myers, P.G., D. Deacu, 2004: Labrador Sea freshwater content in a model with a partial cell topographic representation. *Ocean Modelling*, **6**, pp. 359-377.

Potter, R.A. and M.S. Lozier, 2004: On the warming and salinification of the Mediterranean outflow waters in the North Atlantic. *Geophysical Research Letters*, **31**, L01202. doi:10.1029/2003GL018161

Purkey, S.G., G.C. Johnson, 2010: Warming of Global Abyssal and Deep Southern Ocean Waters between the 1990s and 2000s: Contributions to Global Heat and Sea Level Rise Budgets. *Journal of Climate*, **23**, pp. 6336-6351.

Rayner, N. A., P. Brohan, D. E. Parker, C. K. Folland, J. J. Kennedy, M. Vanicek, T. J. Ansell, and S. F. B. Tett, 2006: Improved Analyses of Changes and Uncertainties in Sea Surface Temperature Measured In Situ since the Mid-Nineteenth Century: The HadSST2 Dataset. *Journal of Climate*, **19**, pp. 446–469. doi:10.1175/JCLI3637.1

Redi, M.H., 1982: Oceanic isopycnal mixing by coordinate rotation. *Journal of Physical Oceanography,* **12***,* pp. 1154–1158.

Rhein, M., S.R. Rintoul, S. Aoki, E. Campos, D. Chambers, R.A. Feely, S. Gulev, G.C. Johnson, S.A. Josey, A. Kostianoy, C. Mauritzen, D. Roemmich, L.D. Talley and F. Wang, 2013: Observations: Ocean. In: Climate Change 2013: The Physical Science Basis. Contribution of Working Group I to the Fifth Assessment Report of the Intergovernmental Panel on Climate Change [Stocker, T.F., D. Qin, G.-K. Plattner, M. Tignor, S.K. Allen, J. Boschung, A. Nauels, Y. Xia, V. Bex and P.M. Midgley (eds.)]. Cambridge University Press, Cambridge, United Kingdom and New York, NY, USA.

Schanze, J.J., R.W. Schmitt and L.L. Yu, 2010: The global oceanic freshwater cycle: A state-of-the-art quantification. *Journal of Marine Research*, **68**, pp.569-595.

Schmitt, R.W., 2009: Salinity and the global water cycle. *Oceanography*, **21**, pp. 12-19.

Schwarzkopf F.U. and C.W. Böning, 2011: Contribution of Pacific wind stress to multi-decadal variations in upper-ocean heat content and sea level in the tropical south Indian Ocean. *Geophysical Research Letters*, **38**, L12602. doi:10.1029/2011GL047651

Seidel, D.J., Q. Fu, W.J. Randel and T.J. Reichler, 2008: Widening of the tropical belt in a changing climate. *Nature Geoscience*, **1**, pp. 21-24. doi:10.1038/ngeo.2007.38

Simmons, H.L., S.R. Jayne, L.C.S. Laurent and A.J. Weaver, 2004: Tidally driven mixing in a numerical model of the ocean general circulation, *Ocean Modelling*, **6**, pp. 245–263.

Skliris, N., R. Marsh, S.A. Josey, S.A. Good, C. Liu, R.P. Allan, 2014: Salinity changes in the World Ocean since 1950 in relation to changing surface freshwater fluxes. *Climate Dynamics*, **43** (3-4), pp. 709-736. doi:10.1007/s00382-014-2131-7

Sloyan, B.M., I.V. Kamenkovitch, 2007: Simulation of Subantarctic Mode and Antarctic Intermediate Waters in Climate Models. Journal of Climate, **20**, pp. 5061-5080. doi:10.1175/JCLI4295.1

Smith, D.M. and J.M. Murphy, 2007: An objective ocean temperature and salinity analysis using covariances from a global climate model. *Journal of Geophysical Research*, **112**, C02022. doi:10.1029/2005JC003172

Solomon, S., D. Qin, M. Manning, M. Marquis, K. Averyt, M. M. B. Tignor, H. L. Miller Jr., and Z. Chen, Eds., 2007: Climate Change 2007: The Physical Science Basis. *Cambridge University Press*, 996 pp.

Stammer, D., 2008: Response of the global ocean to Greenland and Antarctic ice melting. *Journal of Geophysical Research*, **113**, C06022. doi:10.1029/2006JC004079

Swart, N.C., J.C. Fyfe, 2012: Observed and simulated changes in the Southern Hemisphere surface westerly wind-stress. *Geophysical Research Letters*, **39**, L16711. doi:10.1029/2012GL052810

Sweby, P., 1984: High-resolution schemes using flux limiters for hyperbolic conservation-laws. *SIAM Journal of Numerical Analysis,* **21**, pp. 995–1011.

Taylor, K.E., R.J. Stouffer and G.A. Meehl, 2012: An Overview of CMIP5 and the experiment design. *Bulletin of the American Meteorological Society*, **93**, pp. 485-498, doi:10.1175/BAMS-D-11-00094.1

Trenberth, K., L. Smith, T. Qian, A. Dai, and J. Fasullo, 2007: Estimates of the global water budget and its annual cycle using observational and model data. *Journal of Hydrometeorology*, **8**, pp. 758–769.

Uppala, S.M., P.W. Kållberg, A.J. Simmons, U. Andrae, V. Da Costa Bechtold, M. Fiorino, J.K. Gibson, J. Haseler, A. Hernandez, G.A. Kelly, X. Li, K. Onogi, S. Saarinen, N. Sokka, R.P. Allan, E. Andersson, K. Arpe, M.A. Balmaseda, A.C.M. Beljaars, L. Van De Berg, J. Bidlot, N. Bormann, S. Caires, F. Chevallier, A. Dethof, M. Dragosavac, M. Fisher, M. Fuentes, S. Hagemann, E. Hólm, B.J. Hoskins, L. Isaksen, P.A.E.M. Janssen, R. Jenne, A.P. Mcnally, J.-F. Mahfouf, J.-J. Morcrette, N.A. Rayner, R.W. Saunders, P. Simon, A. Sterl, K.E. Trenberth, A. Untch, D. Vasiljevic, P. Viterbo and J. Woollen, 2005: The ERA-40 re-analysis. *Quarterly Journal of the Royal Meteorological Society*, **131**(612), pp. 2961-3012.

Valcke, S. 2006: OASIS3 User Guide (prism 2-5). *PRISM Support Initiative*, Report No. 3, CERFACS, Toulouse, France, 68 pp.

Warren, B.A., 1983: Why is no deepwater formed in the North Pacific?. *Journal of Marine Research*, **41**(2), pp. 327-347. doi**:**10.1357/002224083788520207

Wu, R., J. L. Kinter III, and B. P. Kirtman, 2005: Discrepancy of Interdecadal Changes in the Asian Region among the NCEP–NCAR Reanalysis, Objective Analyses, and Observations. *Journal of Climate*, **18**, pp. 3048–3067. doi:10.1175/JCLI3465.1

Wu, L., W. Cai, L. Zhang, H. Nakamura, A. Timmermann, T. Joyce, M.J. McPhaden, M. Alexander, B. Qiu, M. Visbeck, P. Chang and B. Giese, 2012: Enhanced warming over the global subtropical western boundary currents. *Nature Climate Change*, **2**, pp. 161–166.

Wunsch, C., R. Ferrari, 2004: Vertical mixing, energy, and the general circulation of the oceans. *Annual Review of Fluid Mechanics*, **36**, pp. 281–314. doi:10.1146/annurev.fluid.36.050802.122121

Wunsch, C., 1998: The Work Done by the Wind on the Oceanic General Circulation. *Journal of Physical Oceanohraphy: Notes and Correspondence*, **28**, pp. 2332-2340.

Yashayaev, I., H.M. van Aken, N.P. Holliday, M. Bersch, 2007: Transformation of the Labrador Sea Water in the subpolar North Atlantic. *Geophysical Research Letters*, **34**, L22605. doi:10.1029/2007GL031812

Yin, J., R.J. Stouffer, M.J. Spelman and S.M. Griffies, 2010: Evaluating the Uncertainty Induced by the Virtual Salt Flux Assumption in Climate Simulations and Future Projections. *Journal of Climate*, **23**, pp. 80-96.

Yu, L., 2011: A global relationship between the ocean water cycle and near-surface salinity. *Journal of Geophysical Research: Oceans*, **116** (C10). doi:10.1029/2010JC006937

Zhai, 2013: On the wind mechanical forcing of the ocean general circulation. *Journal of Geophysical Research: Oceans*, **118**, pp. 1–17. doi:10.1002/2013JC009086

Zhang, X., Zwiers, F.W., Hegerl, G.C., Lambert, F.H., Gillett, N.P., Solomon, S., Stott, P.A. and Nozawa, T., 2007: Detection of human influence on twentieth-century precipitation trends. *Nature*, **448**, pp. 461-466. doi:10.1038/nature06025

Chapter 2

Simulating the role of surface forcing on observed multidecadal upper ocean salinity changes

This chapter has been removed for copyright or proprietary reasons.

It has been published as: Lago, V., Wijffels, S. E., Durack, P. J., Church, J. A., Bindoff, N. L., Marsland, S. J., 2016. Simulating the role of surface forcing on observed multidecadal upper ocean salinity changes. Journal of climate, 29(15), 5575-5588

Chapter 3

Subsurface temperature response to surface changes in a 50 year idealized ocean model simulation

Subsurface temperature response to surface changes in a 50 year idealized ocean model simulation

Véronique Lago[1], Susan E. Wijffels[1], Paul J. Durack[2,1], John A. Church[1], Simon J. Marsland[4] and Nathaniel L. Bindoff[1,3,5]

[1] CSIRO Oceans and Atmosphere, GPO Box 1538 Hobart, TAS 7001 Australia

[2]Program for Climate Model Diagnosis and Intercomparison, Lawrence Livermore National Laboratory, Mail Code L-103, 7000 East Avenue, Livermore, California 94550, U.S.A.

[3]Institute for Marine and Antarctic Studies, University of Tasmania, Private Bag 129, Hobart, TAS 7001 Australia

[4] CSIRO Oceans and Atmosphere, Private Bag 1 Aspendale, VIC 3195 Australia

[5] Antarctic Climate and Ecosystems Cooperative Research Centre, Private Bag 80, Hobart, TAS 7001 Australia

Corresponding author address: Véronique Lago, CSIRO Oceans and Atmosphere, GPO Box 1538 Hobart, TAS 7001, Australia.

E-mail: Veronique.Lago@csiro.au

Abstract

Climate change is impacting the ocean's subsurface temperature field. To understand the origin of the trend in the subsurface temperature field in relation to the surface, we decompose the surface salinity and temperature changes in a global ocean climate model. We performed experiments with changes in only the surface temperature, only the surface salinity pattern (inferred evaporation minus precipitation changes), and both of these changes together. The changes were imposed as a linear change over 50 years. These experiments are designed as idealized representations of the 50 years trend in the observed surface temperature and salinity changes. We compare the resulting evolution in the temperature field in the ocean interior with observations. This qualitative comparison of the pattern of changes shows that surface temperature increase and salinity pattern amplification are complementary in inducing the observed subsurface changes in temperature. Both of the changes in surface conditions create circulation and penetration changes that modify the subsurface temperature field and heat content. These results extend our understanding on mechanisms responsible for changes in the ocean interior water mass subsurface properties in response to climate change.

Keywords: Oceanography, temperature, ocean heat content, global change, ocean modelling, climate change

3.1 Introduction

Climate change is impacting the ocean surface temperature and salinity (Levitus *et al.*, 2005; Ishii *et al.*, 2006; Durack and Wijffels, 2010; Durack *et al.*, 2012; Rhein *et al.*, 2013). Atmospheric warming induces an increase in surface temperature and an amplification of the hydrological cycle, which affects the surface salinity (Allen and Ingram, 2002; Held and Soden, 2006; Wentz *et al.*, 2007; Durack *et al.*, 2012, Rhein *et al.*, 2013). The intensified hydrological cycle (evaporation minus precipitation) is related to an amplification of the surface salinity pattern (Schmitt, 1995; Solomon *et al.*, 2007; Helm *et al.*, 2010; Durack and Wijffels, 2010; Durack *et al.*, 2012). The changes in sea surface temperature and salinity act together in altering the temperature field within the ocean (Gregory, 2000; Banks and Gregory, 2006; Kuhlbrodt *et al.*, 2015). However, the specific role of each surface component in driving temperature change patterns is not fully understood. Ocean heat uptake impacts the rate of global warming and the steric expansion drives a large portion of sea level rise and its regional patterns (Domingues *et al.*, 2008; Vermeer and Rahmstorf, 2009; Meehl *et al.*, 2011). Therefore, the mechanisms that drive the patterns in temperature and heat content are important to understanding present and future trends in climate change.

Over the past 50 years the surface ocean has warmed, largely in the tropics and subtropics, by about 0.5°C, and the surface salinity pattern has amplified by 8%. Both effects are believed to be related to the increase in Greenhouse Gases (Rhein *et al.*, 2013). A key question is how these surface changes are related to subsurface patterns of warming and salinity change, and what processes control this.

Rates of penetration of heat into the ocean interior vary across the oceans (Huang *et al.*, 2002; Gille, 2008; Levitus *et al.*, 2009; Lyman *et al.*, 2010; Purkey and Johnson, 2010; Kouketsu *et al.*, 2011). Changes in the circulation can redistribute the heat content in the global oceans (Dickson *et al.*, 2002; Xie *et al.*, 2010; Kuhlbrodt and Gregory, 2012). Recent studies have shown that ocean surface warming is stronger in the tropics and subtropics and stronger near the surface at depth

(Cane *et al.*, 1997; Rayner *et al.*, 2006; Xie *et al.*, 2010; Levitus *et al.*, 2012). In the tropics and subtropics, the subsurface temperature increase is likely carried by flow along isopycnal surfaces from outcrops in actively subducting regions (Spall *et al.*, 2000; Levitus *et al.*, 2005; Levitus *et al.*, 2012). At the higher latitudes, the mechanisms for the observed temperature changes throughout the water column are less understood (Rhein *et al.*, 2013). To date, the independent contributions of surface temperature and salinity changes on the specific distribution of the subsurface temperature trends have not been described. Attributing temperature changes in the subsurface ocean to changing surface properties would help understand the mechanisms that drive trends in the ocean's interior temperature field.

We use a global ocean and sea ice model to isolate the role of changes in surface temperature and salinity to the observed subsurface trends in temperature and heat content patterns. Our experiments are idealized representations of the 50 years surface warming and salinity pattern amplification based on observed changes over the past few decades (Ishii *et al.*, 2005; Rayner *et al.*, 2006; Solomon *et al.*, 2007; Helm *et al.*, 2010; Durack and Wijffels, 2010).

3.2 Methods

In order to diagnose the links between the increasing surface temperature and surface salinity pattern amplification along with the subsurface changes, we use the Australian Community Climate and Earth System Simulator Ocean Model (ACCESS-OM; Bi *et al.*, 2013). ACCESS-OM is a global ocean and sea ice model that comprises the NOAA/GFDL Modular Ocean Model version 4.1 (MOM4p1; (Griffies, 2009), the Los Alamos National Laboratory Sea Ice Model version 4.1 (CICE; Hunke and Lipscomb, 2010), and the OASIS3 (Valke, 2006) coupling code. The simulations are forced with the Coordinated Ocean-ice Reference Experiments version 2 dataset (COREv2; Large and Yeager, 2004; 2009). The 500 years spin-up follows the protocols of the Normal Year Forcing CORE experiment as described by Griffies *et al.* (2009).

Three experiments were performed in addition to a control experiment. One experiment (ΔT) restores the surface temperature to the mean annual cycle but with an additional linear increase

that leads to a 0.5°C warming at 50 years. The temperature increase is uniform between 55°S and 60°N whilst the surface salinity is restored to the seasonal cycle in the last year of the spin-up (Figure 3.1a). A second experiment (ΔS) restores the surface salinity to the mean seasonal cycle but with a linear amplification of the mean salinity pattern by 8% over 50 years and with fixed seasonal cycle of surface temperature from the last year of the spin-up (Figure 3.1b). These experiments are consistent with observed changes in the surface fields over the past 50 years (Figure 3.1) (Rayner *et al.*, 2003; Ishii *et al.*, 2005; Rayner *et al.*, 2006; Durack and Wijffels, 2010; Durack *et al.*, 2012). The third experiment (ΔTΔS) increases the temperature as in ΔT and amplifies the salinity pattern as in ΔS together. The control experiment restores both the temperature and salinity to the fixed seasonal fields from the last year of the spin-up. The temperature and salinity are restored 6 hourly at the surface and all other forcings are kept constant with the normal year COREv2 forcing. These experiments are described in detail in Lago *et al.* (2016). The changes in surface temperature and salinity in the experiments, being idealized, vary regionally from the observational changes (Figure 3.1 c and d), although they have comparable changes when considered as a global average (Figure 3.1 e and f). A notable difference is stronger freshening of the subpolar and polar regions than observed (Figure 3.1 b and d).

The temperature drift in the control run is minimal compared to the changes in our experiments in the top 2000 m (Figure 3.2 a, b and c). From 2000 m to the bottom, there is a significant negative temperature trend in the control experiment of ~-0.2°C (Figure 3.2 d, e and f). This is common in global ocean model simulations under the CORE Normal Year Forcing (Griffies, 2009; Bi *et al.*, 2013). We restrict this study to the top 2000 m of the ocean where the drift is minimal and we subtract the drift from the control experiment from all the results presented in order to isolate the impact of the idealized changes at the surface.

The results of our idealized experiments are compared to the observed linear temperature changes analysed by Durack and Wijffels (2010) for the top 2000 m from observations acquired between 1950 and 2008. On zonal basin average, the amplitude and pattern of their diagnosed

trends compare well with other published temperature analyses (Figure 3.3), despite being only based on hydrographic casts and Argo profiles, where other analyses use eXpendable Bathythermograph data (which require fall rate and temperature bias corrections; Abraham *et al.*, 2013; Cheng *et al.*, 2015). Most differences are minor and are mainly found in the Southern Hemisphere, where available data are very sparse. The overall patterns of subsurface temperature changes are quite robust across studies.

This is the second paper in a series of three analysing subsurface ocean changes. For this paper, we focus on the changes in temperature in the ocean interior due to surface temperature increase and surface salinity pattern amplification. The first paper (Lago *et al.*, 2016) investigated the salinity changes in the ocean interior with increased surface temperature and amplified surface salinity pattern. The third paper will concentrate on the impact of changes in wind patterns to the temperature and salinity in the ocean interior.

3.3 Results

Many of the observed features of temperature increase in the ocean interior are reproduced with our simple idealized experiments (Figure 3.4). Some of the key observed patterns of temperature changes in each ocean (Figure 3.4 a, e and i) are present in the combined experiment, ΔTΔS (Figure 3.4 b, f and j). Notably the heating pattern found in the subtropics and tropics, where there is a build up in the ventilated subtropical gyres (marked by the isotherm bowls in each hemisphere) and penetrating into the tropics. There is also a distinct shallow warming between 100 m and 500 m around Antarctica that is also reproduced in ΔTΔS, and a warming of the subpolar gyres of both the North Atlantic and North Pacific. As found for the salinity changes in these experiments (Lago *et al.*, 2016), the pattern of trends in ΔTΔS are a combination of the results of the single forced ΔT changes in temperature (Figure 3.4 c, g and k) and ΔS (Figure 3.4 d, h and l) experiments, giving insight into the surface to interior links.

3.3.1 Changes in temperature in the ocean interior

We separate the subsurface warming into two distinct regions that highlight the different mechanisms that drive subsurface warming. We defined the ventilated gyres to be from the surface to 2000 m and between 47°S and 47°N. This region is highlighted by grey dashed lines in Figure 3.4. The ventilated gyres involve the subduction of surface changes to the ocean interior via downwelling along isopycnals (generally equatorward). The higher latitudes are defined as poleward from 47°S and 47°N and are where the deeper ocean can upwell (as in the Southern Hemisphere) or be ventilated via deep convection associated with North Atlantic Deep Water production in the far north Atlantic and Antarctic Bottom Water production around the Antarctic Continent. Thus at these higher latitudes surface anomalies can impact the deeper ocean through these subpolar regional connections. The limit defined at 47°N in the Northern Hemisphere roughly separates the subtropical gyres from the subpolar gyres and the 47°S limit in the Southern Hemisphere separates roughly the Southern Ocean from the main gyres. Here, we concentrate on the top 2000 m to allow comparison with the observed temperature changes.

3.3.1.1 VENTILATED GYRES (47°S to 47°N)

In the ventilated gyres, the temperature changes above 500 m are dominated by the subduction of the surface temperature increase in ΔT (Figure 3.4 between the grey dashed lines) producing a surface intensified warming reflecting the faster overturn in the near equatorial and shallow part of the gyre, versus the slow ventilation rates of the mode and intermediate waters found in the deeper and colder parts of the gyres. However, the ΔS experiment features a surprising and significant warming between 100 m and 2000 m which also contributes to ΔTΔS particularly below 200 m (Figure 3.4 b, d, f, h, j and l).

In order to understand the mechanisms that drives the warming in the ocean interior of the ventilated gyres in ΔS; we decomposed the components that contribute to the heat convergence. We separated the heat convergence for the vertical components into advection, diffusion and shortwave warming and horizontally into advection and diffusion. The perturbation heat budget

for the model was calculated for each component per grid cell as the sum of the directional inward and outward heat flux. The integrated heat fluxes for each time step gives the total heat content change per heating mechanism, which we convert to an equivalent temperature change. The outputs are monthly which does not allow for the budget to close, so an extra term was added as the difference between the heat content change in the grid cell and the sum of the heat convergence from all the heating components at each time step. The total temperature changes from the heat budget are the sum of all the components including the residuals. The top 250m of the oceans was omitted because the variability within the monthly output, the residual term, leads the budget.

Based on our heat budget, the warming in ΔS is due to changes in the vertical advection of heat in the Atlantic and Pacific (Figure 3.5 c and f) and a combination of vertically and horizontally advected heat in the Indian Ocean (Figure 3.5c). This is consistent with a subsurface warming due reduced upwelling in low latitudes described by Gregory (2000) and Banks and Gregory (2006) in a coupled model with an increase atmospheric CO_2. The upwelling in the low latitudes cools the ocean and by reducing this cooling effect, it creates a positive temperature change. In ΔS the upwards vertical transport under 500 m is reduced by ~1.2 Sv/50yrs in the Atlantic (Figure 3.6a), ~0.7 Sv/50yrs in the Pacific (Figure 3.6b) and ~0.4 Sv/50yrs in the Indian Ocean (Figure 3.6c). The upwelling is weakened the most in the Atlantic, which is corresponds with the stronger warming in ΔS (Figure 3.6a). Gregory (2000) described how upwelling through the thermocline is reduced in low latitudes as a consequence of reduced convection in the higher latitudes and thus a weakening of the thermohaline circulation. With the increased CO_2, their model responded with an increase in precipitation in the high latitudes, which increased near surface stratification which in turn reduces the convection. The reduced surface salinity in the high latitudes in ΔS has a similar effect. It increases the stratification which reduces the convection (Figure 3.7) and thus the upwelling in the lower latitudes (Figure 3.6).

Some zones of cooling in the Pacific and Indian Oceans between 100 m and 700 m are not reproduced with ΔTΔS. These cooling zones are likely driven by changes within the atmospheric

wind forcing (Fyfe, 2006; Schwarzkopf and Böning, 2011), as our experiments do not change the winds, these cooling regions are not simulated. Other than these cooling regions and the cooling in the North Atlantic below 1000 m, the general key features of the observed temperature changes across each ocean are reproduced simply with our combined idealized experiment, ΔTΔS.

The observations show cooling in the South Pacific and South Indian Oceans between 500 m and 2000 m (Figure 3.3 e and i). Corresponding cooling regions are found in ΔTΔS, which comes from ΔT in the Indian and a combination of ΔT and ΔS in the Pacific (Figure 3.3 f, g, h, j, k and l). These suggest changes in the interaction between the Antarctic Circumpolar Current (ACC) and the South Pacific and South Indian Oceans.

The North Atlantic cools between 1000 m to 2000 m in ΔT but warms in ΔS and ΔTΔS. These changes are linked to changes in the convection at high latitudes, so the dynamics will be discussed in the next section.

In the ventilated gyres, the mean temperature change profile with ΔTΔS in the Atlantic Ocean is comparable to the observations, although it warms less at the surface (Figure 3.7a). The warming in the top 100 m of the Atlantic in ΔTΔS is solely produced through ΔT whilst the subsurface warming in ΔS is required to keep the gradually reduced warming between 100 m and 1000 m. Deeper than 1000 m, the warming profile in ΔTΔS is almost entirely attributable to ΔS.

In the Pacific and Indian Oceans, the temperature change profile is overestimated at mid-depth by all of our experiments (Figure 3.7 b and c). The steep decline in warming between 100 m and 1000 m is mainly associated with the cancelling effect of the observed regions of cooling alongside the edge of the South Indian and South Pacific subtropical gyres. It is likely that these features are wind-driven (Alory *et al.*, 2007; Figure 3.4 e and i) and thus not reproduced in our idealized experiments. Deeper than 1000 m, ΔT produces a more accurate temperature change profile.

In the ventilated gyres, in all ocean basins, the warming is too large compared to the observations in ΔTΔS (Figure 3.7 b and c). In the Atlantic Ocean, ΔS is necessary to produce an ocean warming in ΔTΔS that is closer to the observed than in ΔT (Figure 3.7a and b), with the exception to the cooling in the North Atlantic between 1000 m and 2000 m which is linked to the dynamics at high latitudes.

3.3.1.2 HIGH LATITUDES (SOUTH OF 47°S AND NORTH OF 47°N)

There is consistent warming with ΔS in the subpolar regions between 100 m and 2000 m in each ocean, except for the North Atlantic (Figure 3.4 d, h and l). The North Atlantic has a different dynamic than the North Pacific due to the deep convection occurring at high latitudes.

Cooling in the subpolar North Atlantic in corresponds to an increase in North Atlantic Deep Water (NADW) formation (Figure 3.4a) (Dickson *et al.*, 1996; Dickson *et al.*, 2002). This cooling is not reproduced in ΔTΔS, although this cooling is visible in ΔT and cancelled out from warming in ΔS (Figure 3.4 b, c and d). The NADW cooled during the period of the observations due to increases of deep convection in the 1990s and 2000s (Dickson *et al.*, 1996; Lazier *et al.*, 2002; Dickson *et al.*, 2002; Yashayaev *et al.*, 2007). We do not warm the ocean surface at latitudes north of 60°N. Therefore, the convection in the Irminger Sea (south of Iceland) and Nordic Sea (north of Iceland, and Europe) still occur in ΔT and are enhanced. The deep convection in these sites enhances due to the increased surface temperature gradient between the subtropics and the subpolar gyre. There is evidence of a correlation between the meridional steric height gradient and the overturning circulation in the North Atlantic (Dickson *et al.*, 1996; Thorpe *et al.*, 2001; Straneo, 2006; Hurrell and Deser, 2010). Because we increase the temperature difference in ΔT, it would thus favour stronger convection. With ΔS the surface salinity decreases in the regions of deep convection (Figure 3.1b), which reduces the production of NADW due to an increase in buoyancy and stratification (Dickson *et al.*, 1996; Curry and McCartney, 2001; Häkkinen and Rhines, 2004). As deep convection decreases, the NADW becomes warmer because of isopycnal mixing with the surrounding warmer water (Lazier *et al.*, 2002; Yashayaev *et al.* 2007). In ΔTΔS the NADW warms,

which is in contradiction with the observations. We freshen the surface subpolar North Atlantic more than is observed (Figure 3.1 a and d), so the cooling with ΔT is overly compensated by ΔS.

The Southern Ocean around the Antarctic near 100-200 m warms with ΔS, which also occurs in ΔTΔS (Figure 3.4). The warming produced in ΔS is stronger than observed, but comparable in pattern. It corresponds with a reduced convection in the Weddell Sea due to the increased surface buoyancy from the fresher surface waters in ΔS (Figure 3.8 a, b and c). It is worth mentioning that although there is some depth variability in the Weddell Sea convection in the model, in the control experiment the convection varies by a maximum linear trend over 50 years of ~130 m/50yrs and minimum of ~-180 m/50yrs. In comparison, the ΔS experiment has changed by a minimum linear trend of ~-1400 m/50yrs, which is ~8 times more than the long term variability in the control experiment. Similar effects of changes in the freshwater balance at high-latitudes on oceanic convection have previously been shown by, e.g., Marsland and Wolff (2001). The convection in the Weddell Sea cools the Southern Ocean near the continent and by reducing this cooling effect in ΔS, it produces a net positive temperature trend.

The warming within the ACC, between ~50^{o}S and ~55^{o}S in ΔTΔS is produced through ΔT and most pronounced where the meridional density gradient is highest, between the Southern Ocean and the subtropical gyre (Figure 3.4). The surface temperature increase is subducted to the interior at the convergence zone. The produced warming in ΔTΔS is weaker in the Atlantic, but stronger in the Pacific and Indian. The observed data are very sparse in time and space in the Southern Ocean and the different analyses show a range of amplitude in warming (Figure 3.3). None of the observational analyses shows a warming in the ACC as strong as in ΔTΔS in the Pacific and Indian Oceans. However, Durack *et al.* (2014) suggest that observations of temperature changes in the Southern Ocean likely have a bias to smaller changes.

In ΔTΔS, there is an increased temperature in the subpolar North Pacific which is only produced in ΔS (Figure 3.4 f and h). Our perturbation heat budget shows that this is driven by increased horizontal heat advection (Figure 3.9 a and c). The advected heat originates from increase

transport between the subtropical and subpolar gyres. There is observed warming between 47°N and 60°N, although not as strong as in ΔTΔS (Figure 3.4 e and f).

The high latitudes mean temperature profile with ΔTΔS in each ocean is warmer than observed as previously mentioned (Figure 3.7 d, e, f). However, ΔTΔS accurately reproduces the observed subsurface maxima at about 300 m in each ocean. The surface warming is solely reproduced by ΔT, whilst the subsurface warming between 100 m and 500 m in the Atlantic (Figure 3.7 a, b, c and d) and between 100 m and about 1200 m in the Pacific and Indian Oceans (Figure 3.7 e, f, g, h, i, j and k) is produced through a combination of ΔT and ΔS. The deeper warming is produced solely through the changes in surface salinity in ΔS. The observations show a cooling in the deeper high latitudes North Atlantic (Figure 3.7d). This comes from cooling by increased production of the NADW as previously discussed.

3.3.2 Linearity of the temperature experiments

The temperature changes in the ocean interior from ΔT and ΔS individually sum mostly linearly to produce the changes in ΔTΔS (Figure 3.10). The difference between the sum of the effect of surface temperature and salinity and ΔTΔS in the Pacific and Indian Ocean is surprisingly negligible with root mean square of the residuals ~4% that of the sum ΔT+ΔS. The sum ΔT+ΔS has a correlation of ~ 0.997 with the ΔTΔS experiment. In the Atlantic, there are some non-linear effects on the temperature changes in the subpolar regions, however these are still small effects with root mean square of 12% compared to the total changes in the sum ΔT+ΔS or a correlation of 0.98 between ΔT+ΔS and ΔTΔS. In the subpolar regions, decreased convection in ΔS is opposed to an increase in convection in ΔT (Figure 3.8), except for the Labrador Sea (not shown). These regions of changes in convection are where these non-linear effects are strongest, but are still small compared to the total changes in temperature.

3.3.3 Regional changes in temperature

At 100 m, changes in temperature in ΔTΔS are led by ΔT through subduction of the surface warming (Figure 3.11 a, b, c and d). One exception is for the Southern Ocean south of 55^{o}S, where our ΔT experiment has no surface warming and the interior ocean warming is contributed by ΔS. Regions of cooling in the Pacific and Indian Ocean are not reproduced in ΔTΔS, these are likely wind-driven changes.

At 300 m, the warming is stronger at the edge of the ventilated gyres in ΔTΔS and ΔT, where the outcropping isopycnals penetrate to around this depth (Figure 3.11 e, f, g and h). In ΔS, there is an increased northward temperature advection in the North Pacific between the subtropical and subpolar gyres which drives the subpolar warming in ΔS as previously discussed (Figure 3.4h and Figure 3.9c). On the other hand, the North Pacific subtropical gyre is cooling in ΔS (Figure 3.11h), which is negated on the western side by the warming in ΔT (Figure 3.11g). Both this cooling and warming are induced by vertical temperature advection (Figure 3.9 b and c). The resulting pattern in ΔTΔS is consistent with the observed stronger warming on the western side of the subtropical gyre.

In the Southern Ocean at 300 m, the interior warms faster than the global mean (Figure 3.11 e, f, g and h). Just north of the ACC, the warming comes uniquely from ΔT. The surface temperature increase is subducted to depth at the convergence zone. We do not impose surface warming south of 55^{o}S with ΔT, which is approximately where the warming in depth stops with this experiment. Within the Southern Ocean, the warming in ΔTΔS is only produced in ΔS due to reduced convection (Figure 3.8 a, b and c). The warming produced is more than observed as previously discussed.

At 1000 m, the observed warming is reproduced remarkably well in ΔTΔS, through a combination of ΔS and ΔT (Figure 3.11 i, j, k and l). The observed warming in the Atlantic, Southern Ocean and North Indian are all reproduced primarily by ΔS. There is an observed zone of cooling in the North Atlantic, which originates from increased convection in ΔT north of where we imposed surface

warming as discussed earlier. The observed cooling in the South Indian and western South Pacific are reproduced with ΔT.

There is overall stronger warming at 1000 m in the Atlantic, than in the Pacific and Indian Oceans (Figure 3.11) both in the observations and ΔTΔS. The warming is stronger in the subtropical North Atlantic, where ΔS leads the temperature increase and is where the salinity is increased the most (Figure 3.11 h and l). In ΔTΔS, however, part of the stronger warming in the North Atlantic subtropical gyre with ΔS is negated by cooling in ΔT. The dynamics of this cooling was explained in the previous section.

3.3.4 Changes in heat content

The patterns of changes in heat content integrated between the surface and 2000 m with ΔTΔS are consistent with the observations (Figure 3.12 b and c), though the totals are overestimated (Figure 3.12a). There is a stronger increase in heat content in the Atlantic and Southern Ocean, than in the Pacific and Indian Ocean (Figure 3.12 b and c). There are observed reductions in ocean heat content in the Pacific and Indian Oceans that is not reproduced in ΔTΔS which is likely due to wind driven features as mentioned earlier.

Both ΔT and ΔS have total heat content change in the upper 2000 m that are individually close to the total observed of ~2.0×10^{23} J/50 years; in ΔT the total heat content increased by ~1.9×10^{23} J/50 years and in ΔS by ~2.0×10^{23} J/50 years. When combined in ΔTΔS, the total heat content change in the top 2000 m is almost double the observed with ~3.9×10^{23} J/50 years. However, Durack *et al.* (2014) suggest that the changes in ocean heat content is likely underestimated in the Southern Hemisphere where data are sparse. They evaluated that the Durack and Wijffels (2010) dataset, which we used for our comparison, is globally underestimated by around 38% for the changes in heat content in the upper 700 m. This increase applied to the upper 700 m of our observed heat content change leads to a trend of ~2.6×10^{23} J/50 years, which would suggest our ΔTΔS experiment warms the ocean 1.5 times the total observed. Furthermore, ΔT and ΔS are each respectively 74% and 76% the total observed warming. The difference between the total

heat content increase in ΔTΔS and the observed change would be at least partially countered by the cooling effect of changes in the wind pattern in the Pacific and Indian Ocean.

The asymmetry of heat content change between the Atlantic and the other oceans is accurately reproduced in ΔS. This is due to the reduced cooling effect from upwelling, which is reflected by the reduced vertical advection as previously discussed (Figure 3.6a). Even though the upwelling is reduced in the other oceans, the effect is stronger in the Atlantic.

The global zonal average of heat content change is overestimated with ΔTΔS (Figure 3.12a). The overestimated warming in our experiments might be induced by an excessive diffusivity in ACCESS-OM. Additionally, the wind-driven cooling in the Pacific and Indian Ocean at around 40^{o}N and 10^{o}S to 40^{o}S are not reproduced in these simplistic experiments which hinder the zonal average heat content change in ΔTΔS. The biggest difference with the observations is in the ACC. The regional patterns of heat content change are similar to the observations with ΔTΔS and ΔS in the ACC (Figure 3.12 b, c and d), but the increase is overestimated. Although, the observed warming in the Southern Ocean has likely a bias low, so it is hard to say whether the heat content increase in our experiment is realistic, however, it does lie within the range of estimated adjustments proposed by Durack *et al.* (2014).

3.4 Discussion

Key features of the observed changes in temperature in the ocean interior over the past 50 years are reproduced through a combination of surface temperature increase and, more surprisingly, surface salinity pattern amplification. In the ventilated gyres (47°S - 47°N), the surface temperature increase in ΔT is transferred to the interior through subduction, producing a surface intensified warming across the ventilated volume. In ΔTΔS, this adds to an increase in temperature in ΔS due to a decrease of the cooling effect of upwelling cold water from below. The warming effects in ΔT and ΔS are combined in ΔTΔS to produce a change in temperature larger to that observed below 100 m for which ΔS starts to contribute to the total temperature changes. The excess heat is likely due to excessive heat diffusivity in ACCESS-OM which enhances

the warming effect from both ΔT and ΔS and the absence of the cooling effect from changes in the wind patterns in these experiments.

In the Southern Ocean, the warming in ΔTΔS is mainly produced through ΔS and has a pattern that is consistent with the observations, but with larger amplitude. It is also possible that due to the lack of observations, the warming in the Southern Hemisphere might be underestimated. Durack *et al.* (2014) estimated that warming of the Southern Hemisphere is underestimated by 89% in the Durack and Wijffels (2010) temperature observational data we use for comparison. This adjustment makes the comparison of the warming in ΔTΔS closer to the observations, but still overestimated. The Southern Ocean warms in ΔS due to a reduction of the cooling effect from weaker deep convection. The decreased surface salinity increases the stratification and hinders the convection (c.f. Marsland and Wolff, 2001).

There is also significant warming induced in the subpolar North Pacific with ΔS. In ΔS, there is more heat advected between the subtropical and subpolar gyres. The Kuroshio Current is too strong in ACCESS-OM (Bi *et al.*, 2013). The amplification of the surface salinity pattern is likely amplifying this bias. The warming in ΔS is added to warming in ΔT in the combined ΔTΔS experiment, which produces an increased temperature that exceeds the observed warming.

The changes in temperature in the ocean interior with ΔT and ΔS sum mainly linearly to produce the result of the full dual forced experiment ΔTΔS. Non-linear effects are mostly found in the subpolar regions of the Atlantic, but remain small with differences of about 12% the amplitude of the total temperature changes. The effect of temperature and salinity on the penetration of heat through changes in convection, diffusion, mixing and advection are complex and sensitive to small differences, but still act linearly upon the pattern of temperature change in these experiments.

The total change in heat content in the ocean is nearly double the observations in the ΔTΔS experiment. The changes in surface temperature and salinity pattern taken individually induce a total change in heat content that is 96% and 99% that of the observed total respectively.

However, Durack *et al.* (2014) suggests that the Durack and Wijffels (2010) observed heat content increase is globally 38% underestimated in the top 700 m. With this adjustment, the total heat content change in ΔTΔS is 1.5 times the total observed warming, ΔT and ΔS individually are 74% and 76% the total observed warming respectively. The overestimated change in heat content is at least partially due to the absence of the wind-driven cooling in the Pacific and Indian Ocean in our experiments and the excessive heat diffusivity in our model. However, even if the total warming is overestimated, our experiments suggest that the dynamical changes induced by the amplification of the surface salinity pattern have an impact on the heat content in the ocean that is comparable in amplitude to that induced by surface warming.

The interior warming in the ventilated gyres induced by the amplified surface salinity pattern added to the warming due to the subducted surface warming together reproduce the observed subsurface temperature increase maxima. Additionally, the warming at high latitudes is reproduced through a combination of ΔT and ΔS in the Northern Hemisphere and solely through ΔS in the Southern Ocean. However, our experimental design does not impose any surface warming south of 55^{o}S, which explains the absence of temperature changes induced with ΔT in the Southern Ocean. The observed temperature changes suggest that there is little overall warming at the surface in the Southern Ocean. However, the available data are sparse and thus biased which hinders the interpretation of the results with ΔT in the Southern Ocean. In our experiments, the changes in temperature in the ocean interior are a combination of the effect of the amplification of the surface salinity pattern and the increased surface temperature. This point to the important role surface salinity changes has on the temperature changes in the ocean interior. Both the surface warming and the surface salinity pattern amplification are acting linearly together to induce temperature changes of similar amplitude.

Acknowledgments

The work of V.L., S.E.W., J.A.C. and S.J.M. is supported by the Australian Government Department of Environment, the Bureau of Meteorology and CSIRO through the Australian Climate Change Science Program. This research was undertaken with the assistance of resources provided at the NCI National Facility systems at the Australian National University through the National Computational Merit Allocation Scheme supported by the Australian Government. The work of P.J.D. from Lawrence Livermore National Laboratory is a contribution to the U.S. Department of Energy, Office of Science, Climate and Environmental Sciences Division, Regional and Global Climate Modelling Program under contract DE-AC52-07NA27344. The work of V.L. and N.L.B. from the Institute of Marine and Antarctic Studies is supported by the University of Tasmania and the Centre of Excellence for Climate System Science.

References

Allen, M.R. and W.J. Ingram, 2002: Constraints on future changes in climate and the hydrologic cycle. *Nature*, **419**, pp. 224-232. doi:10.1038/nature01092

Alory, G., S. Wijffels, M. Meyers, 2007: Observed temperature trends in the Indian Ocean over 1960-1999 and associated mechanisms. *Geophysical Research Letters*, **34** (2): Art. No. L02606 JAN 20 2007

Banks, H.T., J.M. Gregory, 2006: Mechanisms of ocean heat uptake in a coupled climate model and the implications for tracer based predictions of ocean heat uptake. *Geophysical Research Letters*, **33**, L07608. doi:10.1029/2005GL025352

Bi, D., S.J. Marsland, P. Uotila, S. O'Farrell, R. Fiedler, A. Sullivan, S.M. Griffies, X. Zhou, and A.C. Hirst, 2013: ACCESS-OM: the Ocean and Sea ice Core of the ACCESS Coupled Model. *Australian Meteorology and Oceanography Journal*, **63**(1), pp. 213-232.

Cane, M.A., A.C. Clement, A. Kaplan, Y. Kushnir, D. Pozdnyakov, R. Seager, S.E. Zebiak, R. Murtugudde, 1997: Twentieth-Century Sea Surface Temperature Trends. *Science*, **257**, pp. 957-960. doi:10.1126/science.275.5302.957

Curry, R.G. and M. S. McCartney, 2001: Ocean Gyre Circulation Changes Associated with the North Atlantic Oscillation. *Journal of Physical Oceanography*, **31**, pp. 3374–3400. doi:10.1175/1520-0485(2001)031<3374:OGCCAW>2.0.CO;2

Dickson, R., J. Lazier, J. Meincke, P. Rhines, and J. Swift, 1996: Long-term coordinated changes in the convective activity of the North Atlantic. *Progress in Oceanogr*aphy, **38**, pp. 241-295.

Dickson, B., I. Yashayaev, J. Meincke, B. Turrell, S. Dye and J. Holfort, 2002: Rapid freshening of the deep North Atlantic Ocean over the past four decades. *Nature*, **416**, pp. 832-837. doi:10.1038/416832a

Domingues, C.M., J.A. Church, N.J. White, P.J. Gleckler, S.E. Wijffels, P.M. Barker and J.R. Dunn, 2008: Improved estimates of upper-ocean warming and multi-decadal sea-level rise. *Nature*, **453**, pp. 1090-1093. doi:10.1038/nature07080

Durack, P.J. and S.E. Wijffels, 2010: Fifty-Year Trends in Global Ocean Salinities and Their Relationship to Broadscale Warming. *Journal of Climate*, **23**, pp. 4342-4362. doi:10.1175/2010JCLI3377.1

Durack, P.J., S.E. Wijffels and R.J. Matear, 2012: Ocean Salinities Reveal Strong Global Water Cycle Intensification During 1950 to 2000. *Science*, **336**, pp. 455-458. doi:10.1126/science.1212222

Durack, P.J., J. P. Gleckler, F.W. Landerer and K. E. Taylor, 2014: Quantifying underestimates of long-term upper-ocean warming. *Nature Climate Change*, **4**, pp. 999-1005. doi:10.1038/NCLIMATE2389

Fyfe, J.C., 2006: Southern Ocean warming due to human influence. *Geophysical Research Letters*, **33**, L19701. doi:10.1029/2006GL027247

Gille, S.T., 2008: Decadal-Scale Temperature trends in the Southern Hemisphere Ocean. *Journal of Climate*, **21**, pp. 4749-476. doi:10.1175/2008JCLI2131.1

Good, S.A., M.J. Martin and N.A. Rayner, 2013: EN4: Quality controlled ocean temperature and salinity profiles and monthly objective analyses with uncertainty estimates. *Journal of Geophysical Research: Oceans*, **118**, pp. 6704-6716. doi:10.1002/2013JC009067

Gregory, J.M., 2000: Vertical heat transports in the ocean and their effect on time-dependant climate change. *Climate Dynamics*, **16**, pp. 501-515.

Griffies, S.M., 2009: Elements of MOM4p1: GFDL Ocean Group Tech. Rep. 6. NOAA/Geophysical Fluid Dynamics Laboratory, 444 pp.

Häkkinen, S. and P.B. Rhines, 2004: Decline of Subpolar North Atlantic Circulation During the 1990s. *Science*, **304**, pp. 555-559. doi:10.1126/science.1094917

Held, I.M. and B.J. Soden, 2006: Robust Responses of the Hydrological Cycle to Global Warming. *Journal of Climate*, **19**, pp. 5686-5699. doi:10.1175/JCLI3990.1

Helm, K.P., N.L. Bindoff and J.A. Church, 2010: Changes in the global hydrological-cycle inferred from ocean salinity. *Geophysical Research Letters*, **37**, L18701. doi:10.1029/2010GL044222

Huang, B., P.H. Stone, A.P. Sokolov and I.V. Kamenkovich, 2002: The Deep-Ocean Heat Uptake in Transient Climate Change. *Journal of Climate*, **16**, pp. 1352-1363.

Hunke, E.C. and Lipscomb, W.H., 2010: CICE: the Los Alamos Sea ice Model Documentation and Software 504 User's Manual. LA-CC-06-012 Tech. Rep., 1–76.

Hurrell J.W. and C. Deser, 2010: North Atlantic climate variability: The role of the North Atlantic Oscillation. *Journal of Marine Systems*, **79**, pp. 231-244.

Ishii, M., A. Shouji, S. Sugimoto, and T. Matsumoto, 2005: Objective analyses of sea-surface temperature and marine meteorological variables for the 20th century using icoads and the Kobe collection. *International Journal of Climatology*, **25**, pp. 865–879.

Ishii, M., M. Kimoto, K. Sakamoto and S. Iwasaki, 2006: Steric sea level changes estimated from historical ocean subsurface temperature and salinity analyses. *Journal of Oceanography*, **62**, Issue 2, pp. 155-170.

Ishii, M. and M. Kimoto, 2009: Reevaluation of historical ocean heat content variations with time-varying XBT and MBT depth bias corrections. *Journal of Oceanography*, **65**, pp. 287-299.

Kouketsu, S., T. Doi, T. Kawano, S. Masuda, N. Sugiura, Y. Sasaki, T. Toyoda, H. Igarashi, Y. Kawai, K. Katsumata, H. Uchida, M. Fukasawa, and T. Awaji, 2011: Deep ocean heat content changes estimated from observation and reanalysis product and their influence on sea level change. *Journal of Geophysical Research*, **116**, C03012. doi:10.1029/2010JC006464

Kuhlbrodt, T. and J.M. Gregory, 2012: Ocean heat uptake and its consequences for the magnitude of sea level rise and climate change. *Geophysical Research Letters*, **39**, L18608. doi:10.1029/2012GL052952

Kuhlbrodt, T., J.M. Gregory and L.C. Shaffrey, 2015: A process based analysis of ocean heat uptake in an AOGCM with an eddy- permitting ocean component. *Climate Dynamics*. doi:10.1007/s00382-015-2534-0

Lago, V., S.E. Wijffels, P.J. Durack, J.A. Church, N.L. Bindoff and S.J. Marsland, in revision: Simulating the role of surface forcing on observed multidecadal upper ocean salinity changes. *Journal of Climate*. doi:10.1175/JCLI-D-15-0519.1

Large, W. and Yeager, S., 2004: Diurnal to decadal global forcing for ocean and sea ice models: the data sets and flux climatologies. CGD Division of the National Center for Atmospheric Research, NCAR Technical Note: NCAR/TN-460+STR

Large, W.G. and S. Yeager, 2009: The global climatology of an interannually varying air-sea flux data set. *Climate Dynamics, **33.*** doi:10.1007/s00382-008-0441-3

Lazier, J., R. Hendry, A. Clarke, I. Yashayaev, P. Rhines, 2002: Convection and restratification in the Labrador Sea, 1990-2000. *Deep-Sea Research*, **49**, pp. 1819-1835.

Levitus, S., J. Antonov and T. Boyer, 2005: Warming of the world ocean, 1995-2003. *Geophysical Research Letters*, **32**. doi:10.1029/2004GL021592

Levitus, S., J. Antonov, T. Boyer, R.A. Locarnini and H.E. Garcia, 2009: Global ocean heat content 1955-2008 in light of recently revealed instrumentation problems. *Geophysical Research Letters*, **36**. doi:10.1029/2008GL037155

Levitus, S., J.I. Antonov, T.P. Boyer, O.K. Baranova, H.E. Garcia, R.A. Locarnini, A.V. Mishonov, J.R. Reagan, D. Seidov, E.S. Yarosh, and M.M. Zweng, 2012: World ocean heat content and

thermosteric sea level change (0–2000 m), 1955–2010. *Geophysical Research Letters*, **39**, L10603. doi:10.1029/2012GL051106

Lyman, J.M., S.A. Good, V.V. Gouretski, M. Ishii, G.C. Johnson, M.D. Palmer, D.M. Smith and J.K. Willis, 2010: Robust warming of the global upper ocean. *Nature*, **465**, pp. 334–337. doi:10.1038/nature09043

Marsland, S.J., and J.-O. Wolff, 2001: On the sensitivity of Southern Ocean sea ice to the surface freshwater flux. J. Geophys. Res. (Oceans), 106, pp. 2723-2741.

Meehl, G.A., J.M. Arblaster, J.T. Fasullo, A. Hu and K.E. Trenberth, 2011: Model-based evidence of deep-ocean heat uptake during surface-temperature hiatus periods. *Nature Climate Change*, **1**, pp. 360–364. doi:10.1038/nclimate1229

Purkey, S.G., G.C. Johnson, 2010: Warming of Global Abyssal and Deep Southern Ocean Waters between the 1990s and 2000s: Contributions to Global Heat and Sea Level Rise Budgets. *Journal of Climate*, **23**, pp. 6336-6351.

Rayner, N. A., *et al.*, 2003: Global analyses of sea surface temperature, sea ice, and night marine air temperature since the late nineteenth century. *Journal of Geophysical Research: Atmospheres*, **108**. doi:10.1029/2002JD002670

Rayner, N. A., P. Brohan, D. E. Parker, C. K. Folland, J. J. Kennedy, M. Vanicek, T. J. Ansell, and S. F. B. Tett, 2006: Improved Analyses of Changes and Uncertainties in Sea Surface Temperature Measured In Situ since the Mid-Nineteenth Century: The HadSST2 Dataset. *Journal of Climate*, **19**, pp. 446–469. doi:10.1175/JCLI3637.1

Rhein, M., S.R. Rintoul, S. Aoki, E. Campos, D. Chambers, R.A. Feely, S. Gulev, G.C. Johnson, S.A. Josey, A. Kostianoy, C. Mauritzen, D. Roemmich, L.D. Talley and F. Wang, 2013: Observations: Ocean. In: Climate Change 2013: The Physical Science Basis. Contribution of Working Group I to the Fifth Assessment Report of the Intergovernmental Panel on Climate Change [Stocker, T.F., D.

Qin, G.-K. Plattner, M. Tignor, S.K. Allen, J. Boschung, A. Nauels, Y. Xia, V. Bex and P.M. Midgley (eds.)]. Cambridge University Press, Cambridge, United Kingdom and New York, NY, USA.

Schmitt, R.W., 1995: The ocean component of the global water cycle. *Reviews of Geophysics*, **33** (S2), pp. 1395-1409.

Schwarzkopf, F.U., C.W. Böning, 2011: Contribution of Pacific wind stress to multi-decadal variations in upper-ocean heat content and sea level in the tropical south Indian Ocean. *Geophysical Research Letters*, **38**, L12602. doi:10.1029/2011GL047651

Smith, D.M. and J.M. Murphy, 2007: An objective ocean temperature and salinity analysis using covariances from a global climate model. *Journal of Geophysical Research*, **112**, C02022. doi:10.1029/2005JC003172

Solomon, S., D. Qin, M. Manning, M. Marquis, K. Averyt, M. M. B. Tignor, H. L. Miller Jr., and Z. Chen, Eds., 2007: Climate Change 2007: The Physical Science Basis. Cambridge University Press, 996 pp.

Spall, M.A., R.A. Weller and P.W. Furey, 2000: Modelling the three-dimensional upper ocean heat budget and subduction rate during the Subduction Experiment. *Journal of Geophysical Research*, **105** (C11), pp. 26,151-26,166.

Straneo, F., 2006: On the Connection between Dense Water Formation, Overturning, and Poleward Heat Transport in a Convective Basin. *Journal of Physical Oceanography*, **36**, pp. 1822-1840.

Thorpe, R.B., J. M. Gregory, T. C. Johns, R. A. Wood, and J. F. B. Mitchell, 2001: Mechanisms Determining the Atlantic Thermohaline Circulation Response to Greenhouse Gas Forcing in a Non-Flux-Adjusted Coupled Climate Model. *Journal of Climate*, **14**, pp. 3102-3116.

Valcke, S., 2006: OASIS3 User Guide (prism 2-5). *PRISM Support Initiative*, Report No. 3, CERFACS, Toulouse, France, 68 pp.

Vermeer, M. and S. Rahmstorf, 2009: Global sea level linked to global temperature, *Proceedings of the National Academy of Sciences*, **106** (51), pp. 21,527-21,532. doi:10.1073/pnas.0907765106

Wentz, F.J., L. Ricciardulli, K. Hillburn and C. Mears, 2007: How Much More Rain Will Global Warming Bring? *Science*, **317**, pp. 233-235. doi:10.1126/science.1140746

Xie, S., C. Deser, G.A. Vecchi, J. Ma, H. Teng, and A.T. Wittenberg, 2010: Global Warming Pattern Formation: Sea Surface Temperature and Rainfall. *Journal of Climate*, **23**, pp. 966–986. doi:10.1175/2009JCLI3329.1

Yashayaev, I., H.M. van Aken, N.P. Holliday, M. Bersch, 2007: Transformation of the Labrador Sea Water in the subpolar North Atlantic. *Geophysical Research Letters*, **34**, L22605. doi:10.1029/2007GL031812

Figures

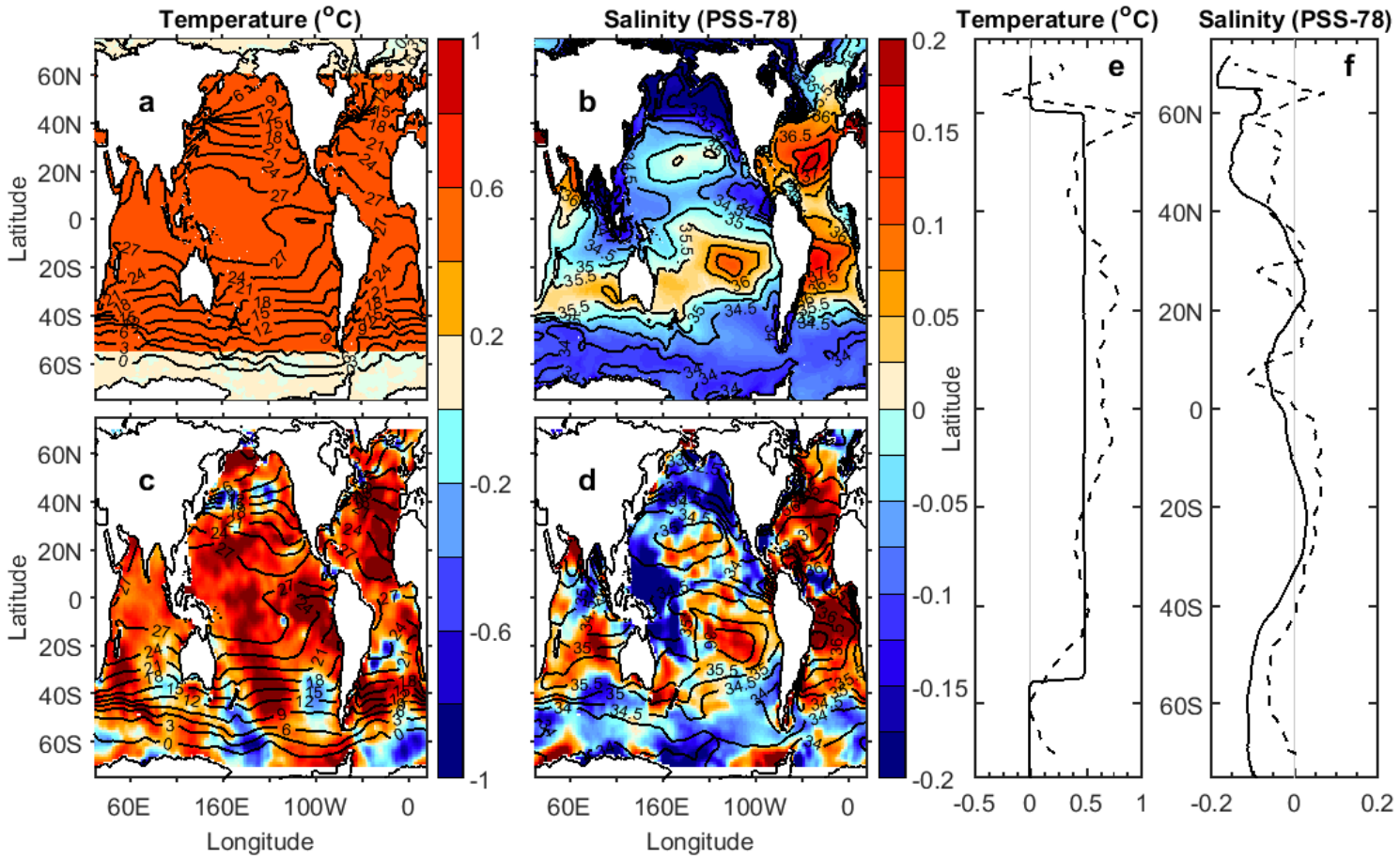

Figure 3.1. Temperature (°C; a, c) and salinity (PSS-78; b, d) changes for a 50 years period. The top row (a, b) has the changes imposed in the model and the bottom row (c, d); the observed changes for the period 1950-2000. The black contours are the mean field every 3°C and every 0.5 PSS-78 for the temperature and salinity respectively. The plots on the right show the global zonally averaged temperature (e) and salinity (f) changes from the experiments (solid line) and observations (dashed line).

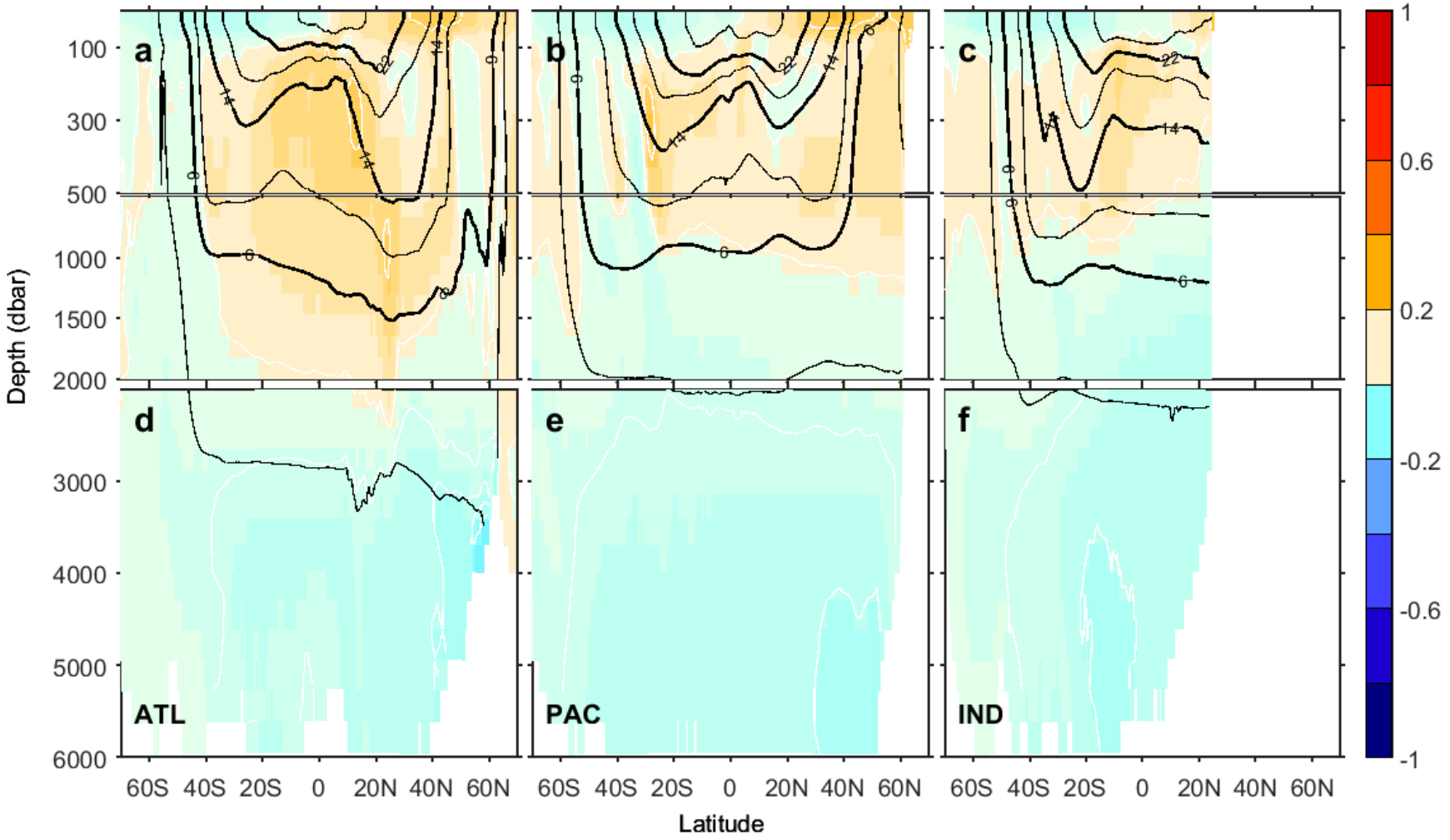

Figure 3.2. Zonally averaged potential temperature changes (°C per 50 years) in the control experiment for the Atlantic (a, d) Pacific (b, e) and Indian (c, f) Oceans. The scale matches the scale use for the results. The black contours are the mean temperature every 4°C and the white contours are the changes every 0.1°C.

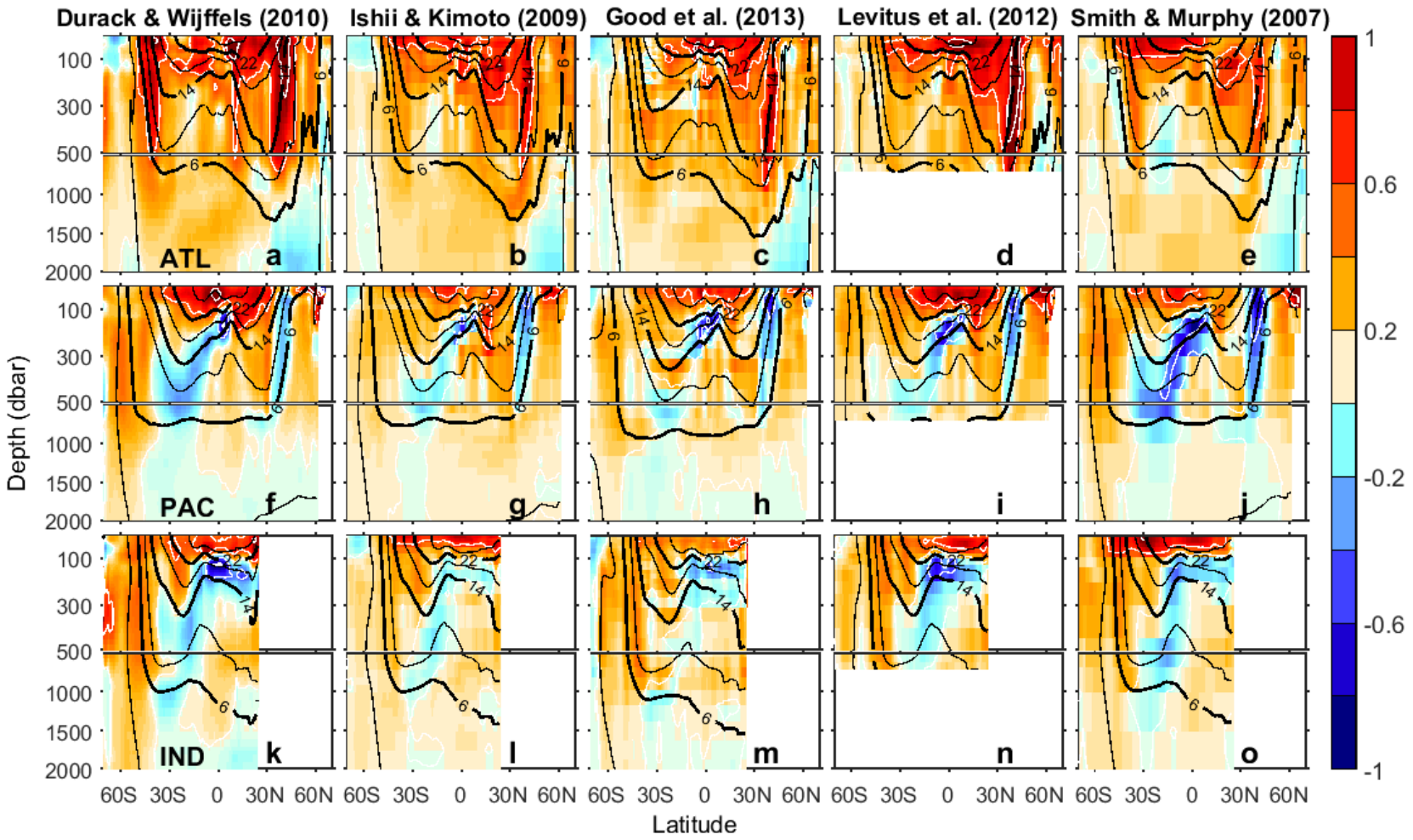

Figure 3.3. Comparison of the zonally averaged potential temperature changes (°C per 50 years) in the Atlantic (a,b,c,d) Pacific (e,f,g,h) and Indian (i,j,k,l) Oceans for the top 2000m for different observational datasets. The columns correspond from left to right to the datasets of Durack and Wijffels (2010), Ishii and Kimoto (2009), Good et al. (2013), Levitus et al. (2012) and Smith and Murphy (2007). The white contours are the temperature trend every 0.5°C. The black contours are the mean temperature every 8°C (thick lines) and 4°C (thin lines).

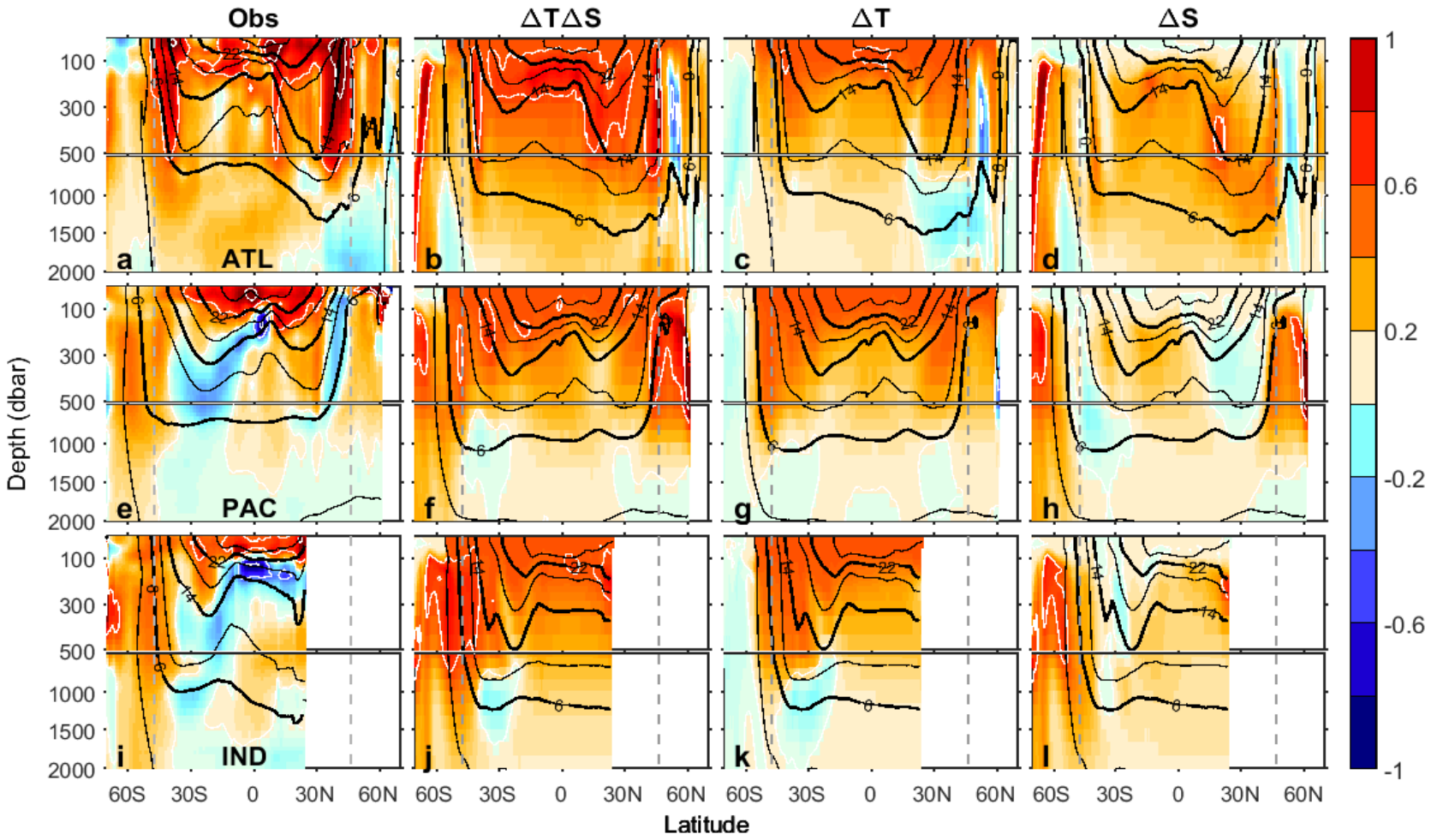

Figure 3.4. Zonally averaged potential temperature changes (°C per 50 years) in the Atlantic (a,b,c,d) Pacific (e,f,g,h) and Indian (i,j,k,l) Oceans for the top 2000m of the ocean. The columns correspond from left to right to the observations, ΔTΔS, ΔT and ΔS. The white contours are the temperature trend every 0.5°C. The black contours are the mean temperature every 8°C (thick lines) and 4°C (thin lines). The dashed grey lines are the latitudes selected as the limit for the ventilated gyres and the high latitudes as described in the results.

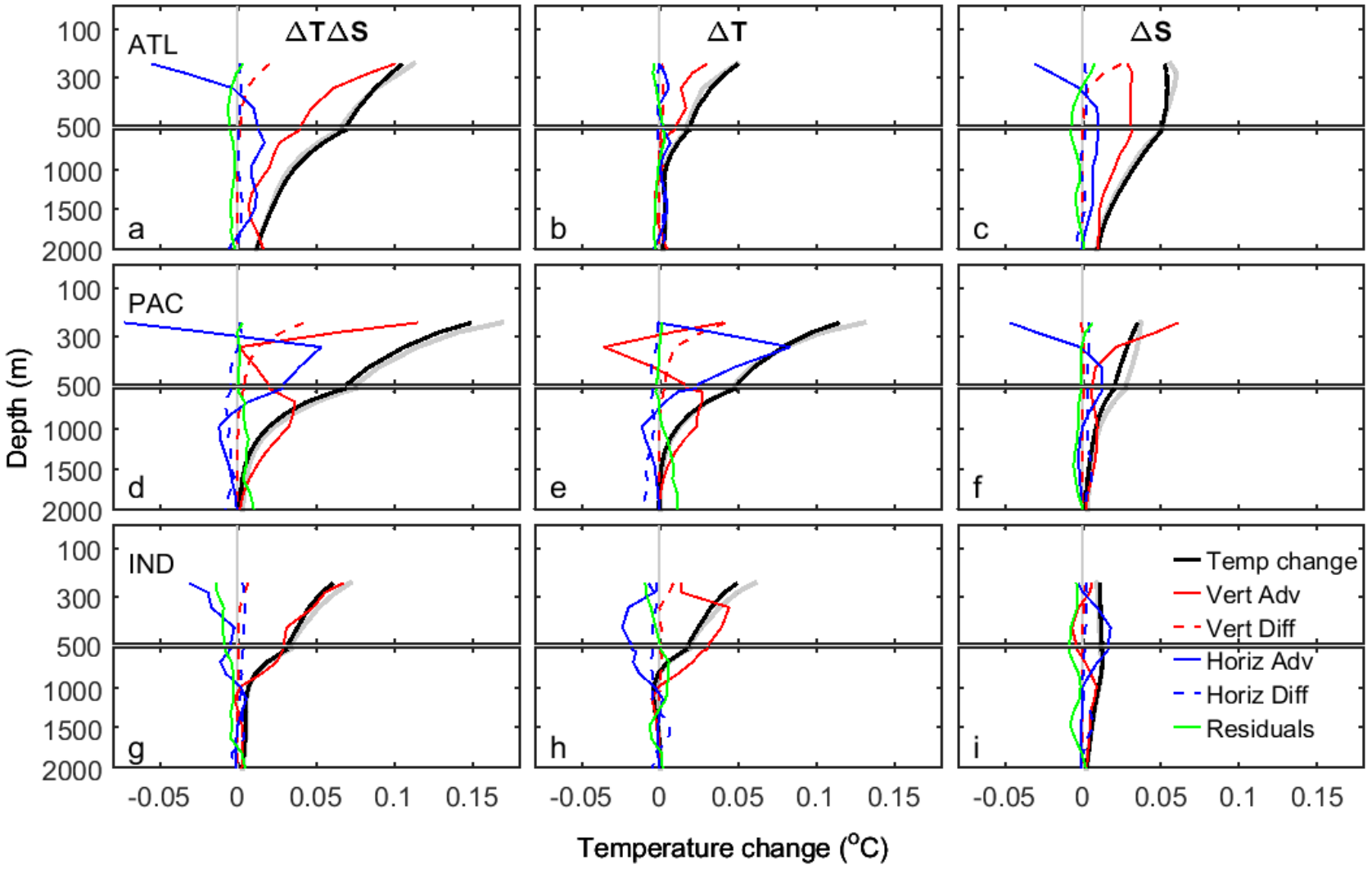

Figure 3.5. Mean temperature change due to each component of the heat budget for each ocean basin between 30°S and 30°N. The paler solid line is the total temperature change from all of the components and the darker solid line is the temperature change directly from the model's temperature outputs.

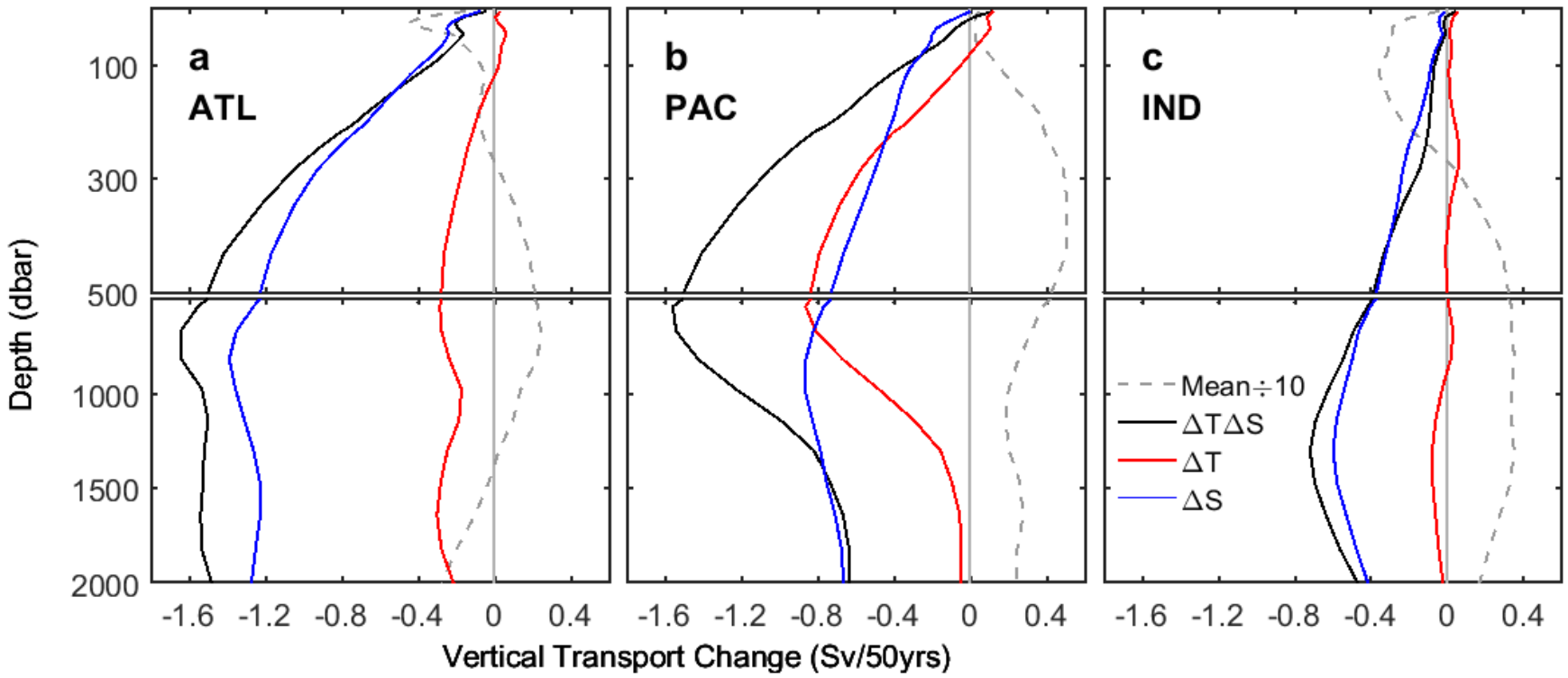

Figure 3.6. Total vertical transport change integrated between 30°S and 30°N in the Atlantic (a), Pacific (b) and Indian (c) Oceans for each experiment. Positive is defined as upwards and the change is defined as the differences between the experiment and the control 50 years trend. The dashed grey line is the mean vertical transport in the control experiment divided by 10 to give an indication of the mean transport's direction.

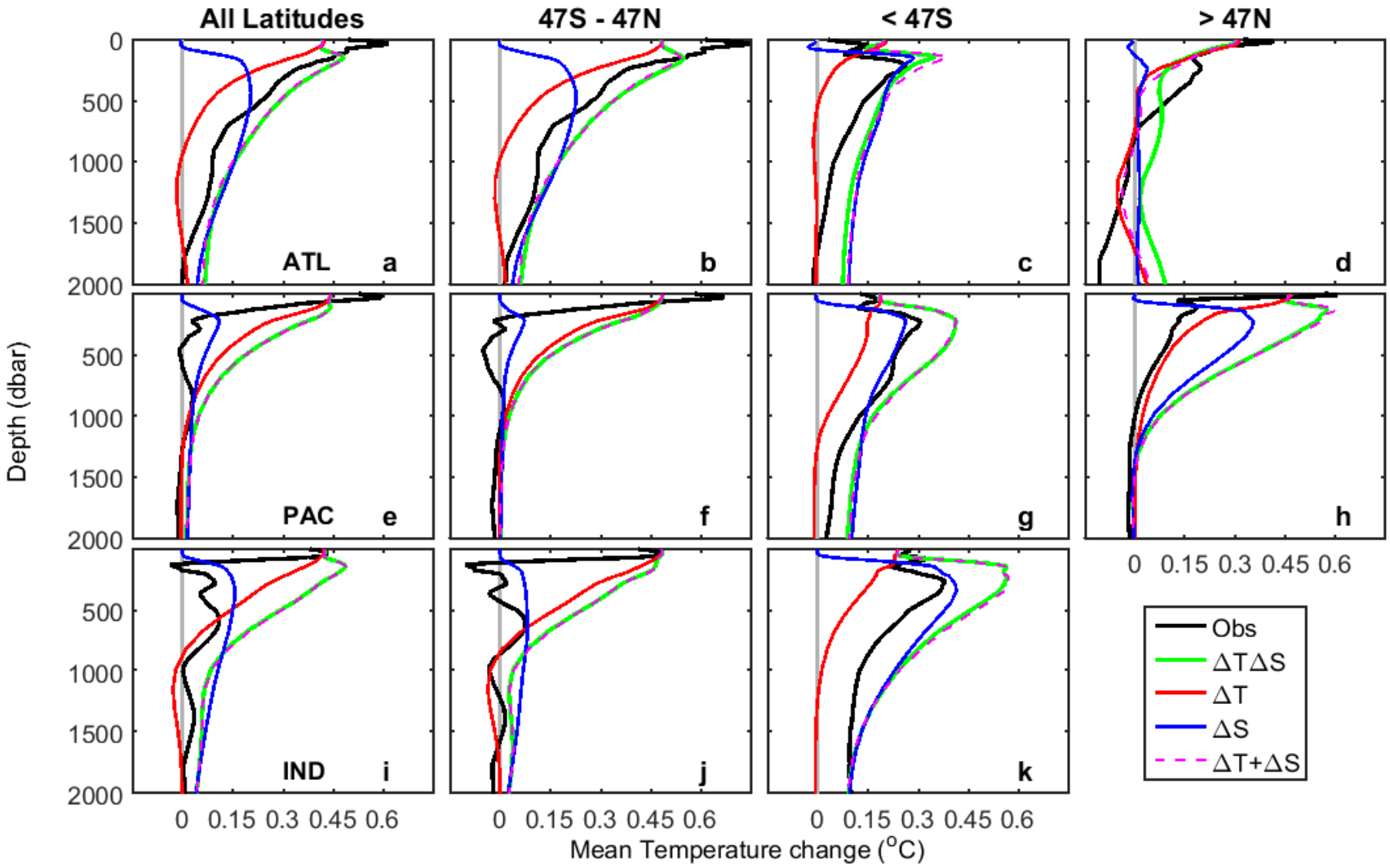

Figure 3.7. Total average temperature change for the Atlantic (a,b,c,d), the Pacific (e,f,g,h) and the Indian Ocean (I,j,k). The first column has the average temperature change for all latitudes (a,e,i), the second column the latitudes between 47°S and 47°N (b,f,j), the third column for latitudes lower than 47°S (c,g,k) and the last column for latitudes higher than 47°N (d,h).

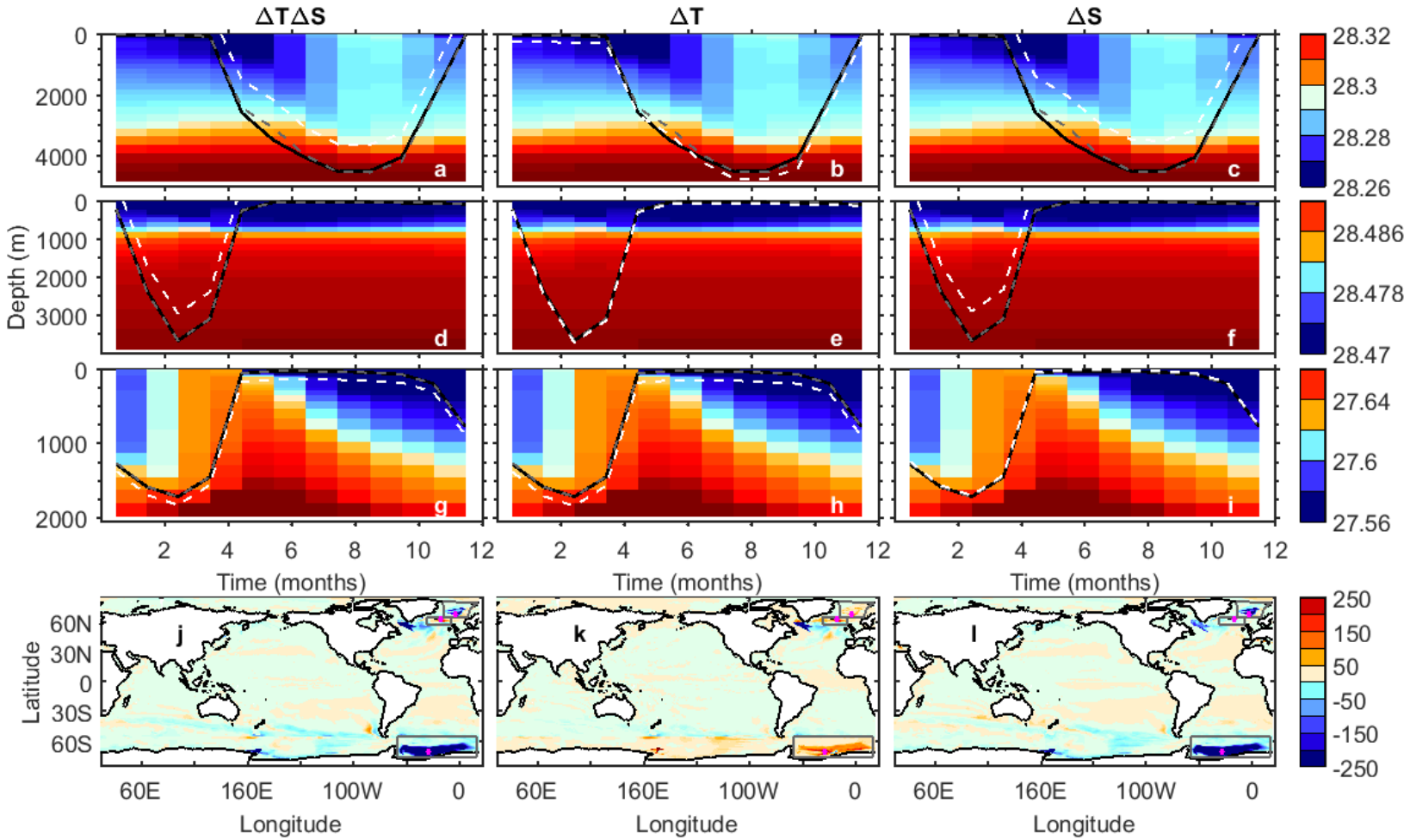

Figure 3.8. Mixed layer depth in the Weddell Sea (panels a,b,c), Nordic Seas (panels d,e,f) and Irminger Sea (panels g,h,i). For each experiment, the grey dashed line is the MLD at year 1, the white dashed line is the 50 years MLD trend added to the year 1 yearly cycle and the solid black line is the mean annual cycle. The colours in panels a to i are the mean density at this location in kg/m^3. The location is chosen where the deepest MLD occurs within the grey box in panels j, k and l, as indicated by the magenta dot. The colours in j, k and l are the MLD changed (in meters per 50 years).

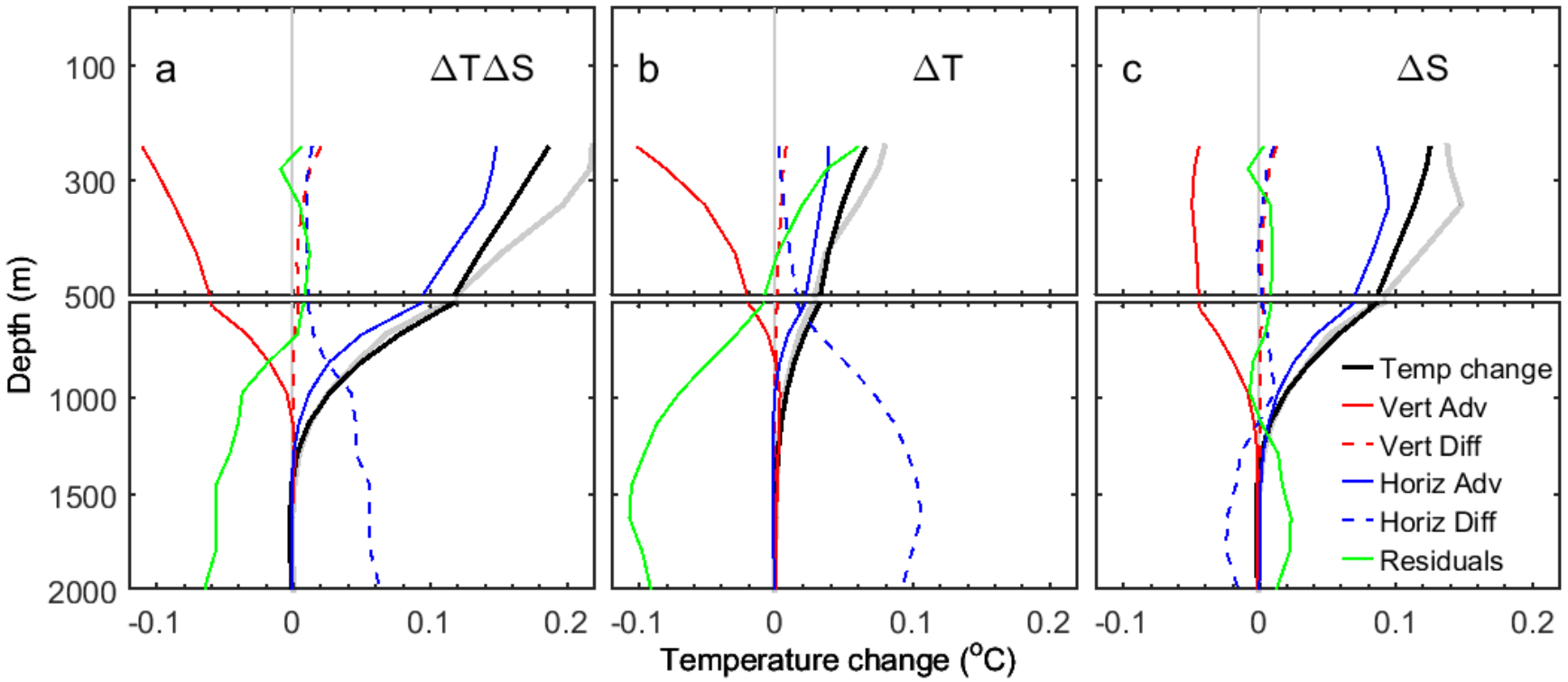

Figure 3.9. Mean temperature change due to each component of the heat budget in the North Pacific Ocean between 30°N and 65°N. The paler solid line is the total temperature change from all of the components and the darker solid line is the temperature change directly from the model's temperature outputs.

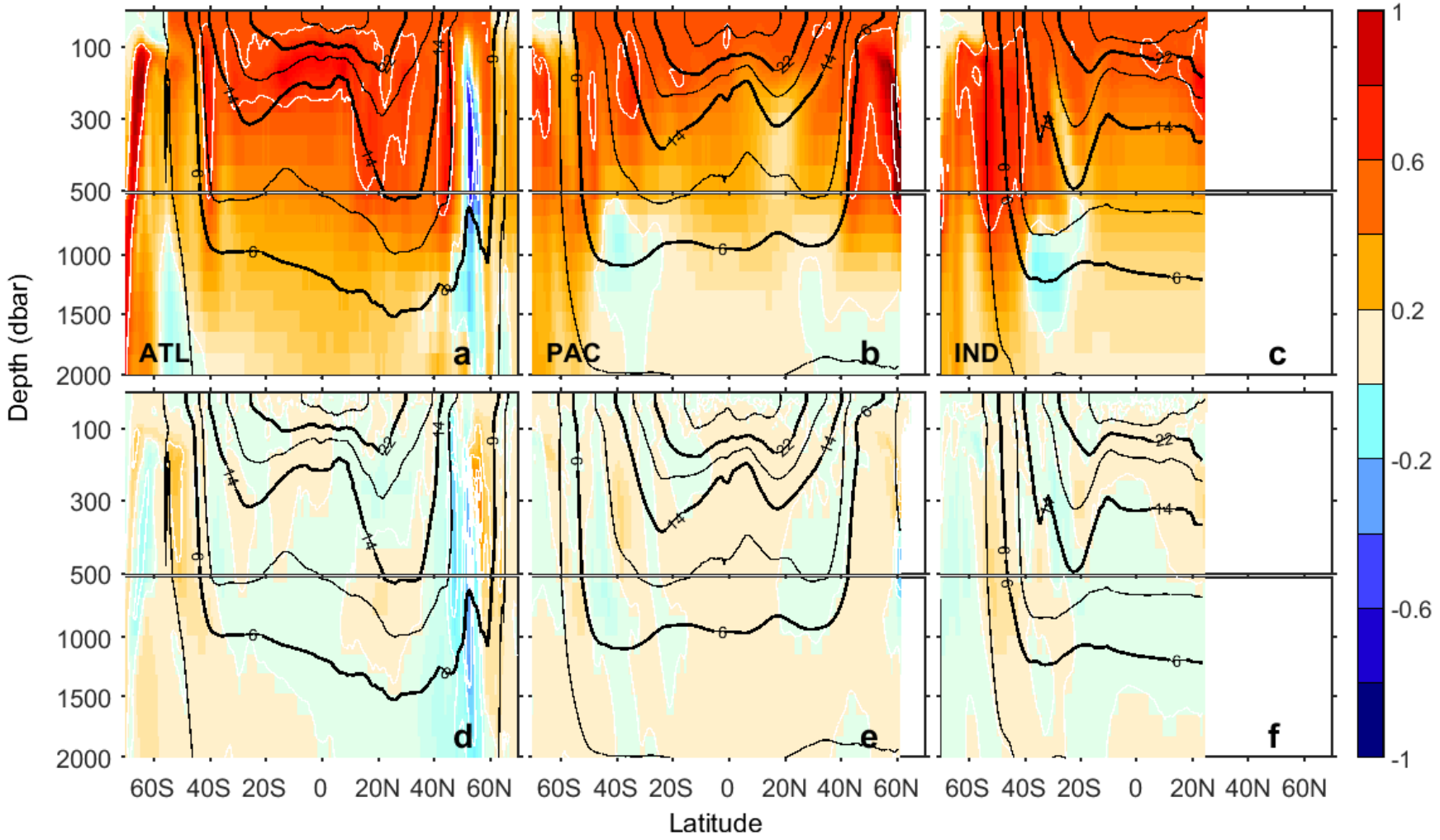

Figure 3.10. Zonally averaged temperature changes (°C per 50 years). The top row (a, b, c) is for the sum of ΔT and ΔS and the bottom row (d, e, f) for the sum of ΔT and ΔS minus ΔTΔS the scale matches the corresponding scale in Figure 4. The white contours are the temperature trend every 0.5°C (a,b,c) and every 0.1°C (d,e,f). The black contours are the mean temperature every 8°C (thick lines) and 4°C (thin lines).

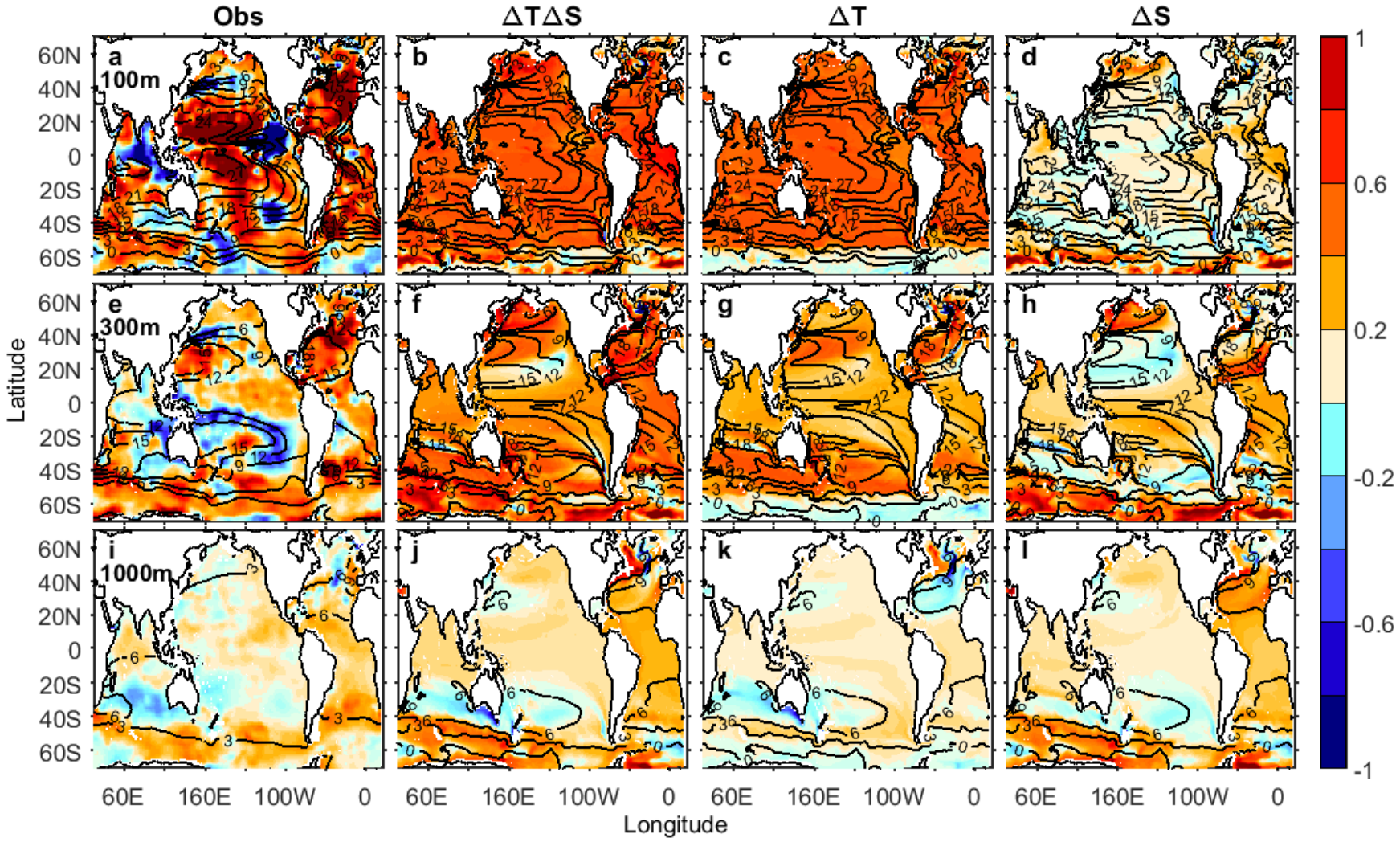

Figure 3.11. Temperature changes (°C per 50 years) at 100 m (a,b,c,d), 300 m (e,f,g,h) and 500 m (i,j,k,l). The columns correspond from left to right to the observations, ΔTΔS, ΔT and ΔS. The black contours are the mean temperature every 8°C (thick lines) and 4°C (thin lines).

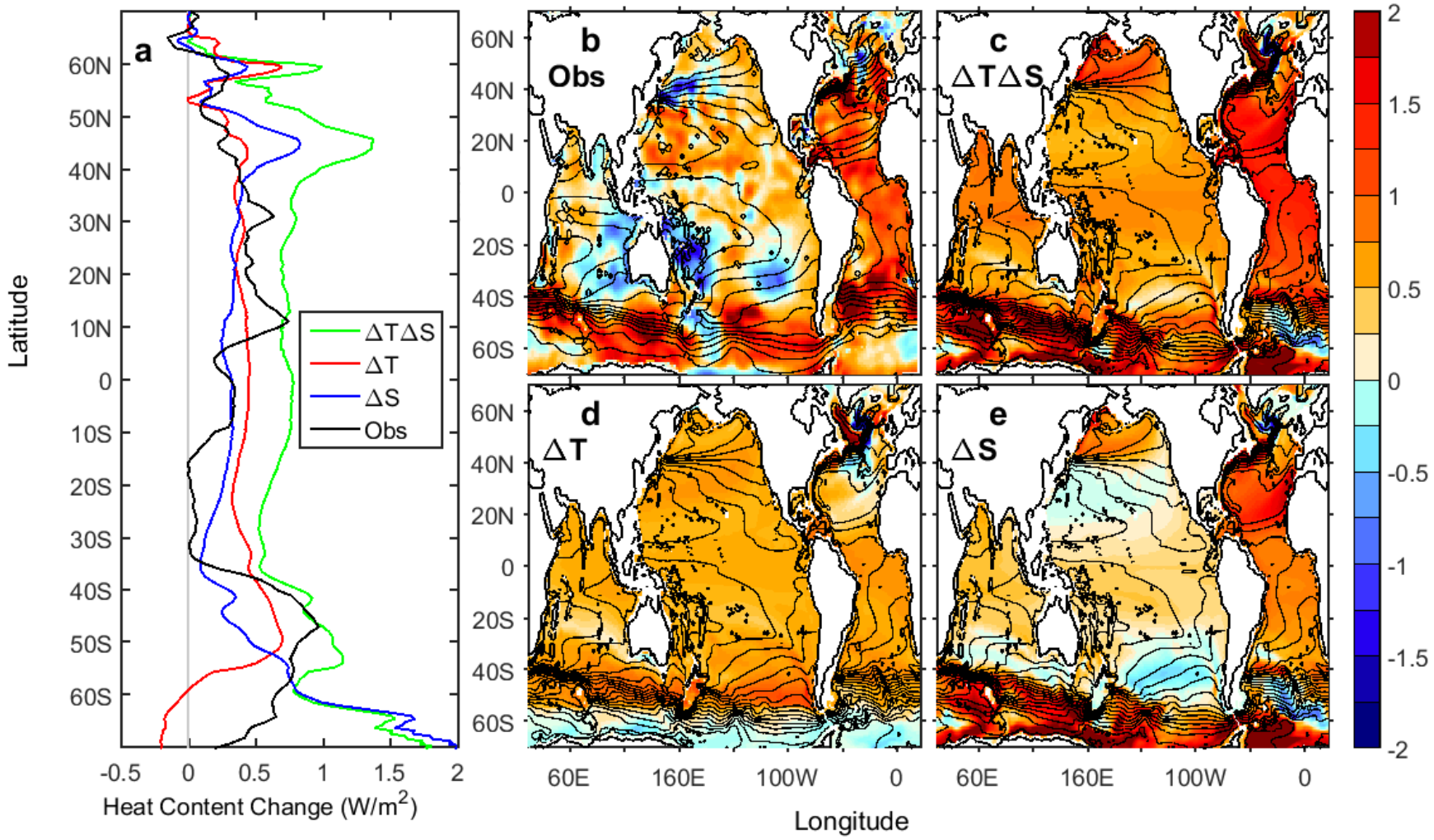

Figure 3.12. Depth integrated heat content (W/m^2) for each experiment and observations integrated from 0 m to 2000 m zonally averaged (a) and mapped (b,c,d,e). The black contours are the mean heat content every 0.5x10^{10} W/m^2.

Chapter 4

Oceans temperature and salinity response to 50 years changes in wind pattern

Abstract

Climate change has impacted the atmospheric and oceanic properties over the last decades. An increased air temperature and amplified hydrological cycle were coincident to changes in the atmospheric circulation. These changes drove trends in the ocean's surface temperature, salinity and momentum which impacts the penetration changes in the properties at the surface. A series of idealized experiments in a global ocean model are set to test the changes in the ocean interior induced from changes in the surface conditions. An idealized representation of the observed trends at sea surface temperature and salinity are implemented at the surface of the ocean with fixed and changing winds. The 50 years wind changes are taken as linear trends from three wind reanalyses datasets (ERA-40, JRA-55 and NOAA-20CR) and the mean of all three of these datasets. Additionally, a 50 years wind trend from the CMIP5 multi-model ensemble is tested. The long-term wind trends from the wind reanalyses datasets recreate the observed equatorial cooling and warming trends in the ocean interior. However, in the mid-latitudes strong changes in temperature and salinity are induced through the effect of changes in the wind stress curl which are unrealistic. With the CMIP5 multi-model ensemble, the temperature and salinity changes are more realistic in the tropical and subtropical regions than when using the wind data reanalyses. The results suggest that the temperature trends in the equatorial region are driven by the strengthening of the trade winds shown in the wind data reanalysis. Outside of the equatorial regions, the wind stress curl from these reanalyses induces inaccurate patterns of temperature and salinity changes whilst the wind changes in CMIP5 render more realistic patterns. Finally, the Southern Ocean warms with a strengthening of the westerlies in the wind data reanalyses, but does not warm with the strengthened westerlies in CMIP5 which is not sufficient to increase the eddy diffusion that leads to warming of the Southern Ocean.

Keywords: Wind stress, ocean modelling, temperature, salinity, CMIP5, wind reanalysis

4.1 Introduction

Changes in the momentum flux (wind stress), temperature and salinity at the ocean surface control changes in physical properties in the ocean interior. In the previous chapters the role of surface temperature and salinity in reproducing the observed changes in subsurface salinity and temperature were investigated. In this chapter the effect of changes in wind speed and pattern on the variability in the ocean interior are examined. Winds have been changing in the last decades and these changes reflect on the patterns of changes in ocean temperature and salinity (Xue *et al.*, 2010; Hakkinen *et al.*, 2011; Merrifield, 2011; Swart and Fyfe, 2012, Wu *et al.*, 2012, Balmaseda *et al.*, 2013; England *et al.*, 2014; Lai *et al.*, 2015). There are uncertainties as to the exact nature of the changes in the wind field (Vecchi *et al.*, 2006; Gravensen *et al.*, 2007). However, there is evidence that the westerly wind has strengthened over the Southern Ocean (Xue *et al.*, 2010; Swart and Fyfe, 2012) and the trade winds over the Tropical Pacific have also likely increased (Merrifield, 2011). Additionally, Wu *et al.* (2012) find a possible poleward expansion of the Hadley circulation. The changes in the wind pattern are described in further details in section 1.3 of Chapter 1. To investigate the contribution of the wind change to the multidecadal variability in the ocean interior, we use the 50 years wind speed trends from a variety of reanalysis products, and assess their accuracy through the changes they induce in the ocean interior.

4.2 Methods

The experiments use the Australian Community Climate and Earth System Simulator Ocean Model (ACCESS-OM; Bi *et al.*, 2013). The wind is imposed in ACCESS-OM through the CORE forcings version 2 (COREv2; Large and Yeager, 2004; 2009). The wind stress on the ocean surface is calculated from the wind speed through the OASIS3 coupler (Valcke, 2006). The model used was previously described in further details in sections 1.4 of Chapter 1 and 2.1 of Chapter 2.

Three wind reanalyses datasets were chosen to produce 50 years wind speed changes: ERA-40 (Uppala *et al.*, 2005), JRA-55 (Japanese 55-year Reanalysis; Kobayashi *et al.*, 2015) and NOAA-20CR (National Oceanic and Atmospheric Administration 20th Century Reanalysis; Compo *et al.*, 2011) (Figure 4.1 panels a to h). We selected these three datasets to span a wide range of possible wind changes because of the inconsistencies between the available data reanalyses. The 50 years change was calculated per surface grid cell between 1958 and 2003 for ERA-40, between 1958 and 2014 for JRA-55 and between 1950 and 2008 for NOAA-20CR. The time span was chosen to match as closely as possible to the time span and years of the observations from Durack and Wijffels (2010) with which we compare our ocean results. We create an additional dataset with the mean trend of ERA-40, JRA-55 and NOAA-20CR which we will refer to as Mean Trend. The 50 years trend of each dataset and the mean trend of the three datasets are used as idealized linear changes of the wind pattern in the experiments. Finally, another 50 years wind trend pattern was produced from the CMIP5 multi-model ensemble with the wind data from 1950 to 2008 (Table 4.1). The pattern of 50 years linear trend produced from the CMIP5 multi-model ensemble is applied in an independent experiment. The difference in the time span of these experiments can induce differences in the long-term trends. It is noteworthy that the time span used to produce the 50 years wind changes from the NOAA-20CR reanalysis and CMIP5 multi-model ensemble have are identical and match the time span used to produce the Durack and Wijffels (2010) temperature and salinity 50 years trend with which we compare the results. The time span used to produce the trends with the ERA-40 and JRA-55 reanalyses differs from those, however, their patterns of wind changes are qualitatively very similar to that of NOAA-20CR and differ mainly quantitatively (Figure 4.1).

Wind change trends from reanalysis products are based on atmospheric observations and numerical model analyses and the CMIP5 wind change trends are derived solely from model simulations. However, in contrast to the surface temperature and salinity changes used in this and the two earlier chapters, the wind field changes have yet to be more completely attributed to human influences from rising greenhouse gases (Bindoff *et al.*, 2013). So in this chapter, the level of confidence in the wind field trends as representing a change caused by humans is much

lower and reflects a greater uncertainty in the scientific understanding of the causes in the trends in the winds.

In these wind change experiments, we apply the 50 years trend in wind speeds from the datasets through a linear change to the COREv2 forcing in ACCESS-OM (Figure 4.1 k and l). The wind forcing on the 50 years period is thus composed of the natural variations of wind represented by COREv2 and the slow 50 year trend of the observed changes. At each timestep, we add the time dependent proportion of the total 50 years trend to the COREv2 normal year forcing. ACCESS-OM uses the wind velocity as a model input and calculates the wind stress.

For the wind changes experiments (Table 4.2; ΔERA-40, ΔJRA-55, ΔNOAA-20CR, ΔMeanTrend and ΔCMIP5), the 50 year trends are applied in the model whilst restoring the surface temperature and salinity 6 hourly to a fixed field with an annual seasonal cycle. The experiment ΔMeanTrend was run with the mean of the 50 year trends from ERA-40, JRA-55 and NOAA-20CR and fixed surface salinity and temperature (Table 4.2). The mean wind trend is also applied together with a surface temperature increase of 0.5^{o}C between 55^{o}S and 60^{o}N and a surface salinity pattern amplification of 8%to compare the combined effect of changes in all three surface forcings with the observations. The surface temperature increase and salinity pattern amplification are described in further details in Chapter 2. The surface temperature increase and salinity pattern amplification are also applied with a fixed wind field (CORE normal year) to compare with the effect of changes in surface temperature and salinity without wind changes. Finally, a control experiment was run in which the surface temperature, surface salinity and wind are all fixed to subtract the residual drift from the experiments for all results presented. The fixed surface temperature and salinity fields used are the surface field in the last year of the spin-up. The normal year of COREv2 is used for the fixed wind field.

The wind datasets used for the experiments contain some differences in the location and amplitudes of wind changes. The strongest wind change is in the amplification of the westerly winds over the Southern Ocean (Figure 4.1 a, c, e, g, i and m). The main difference in the southern hemisphere westerly wind amplification is its latitudinal location. The maximum increase in

westerly winds is at 62°S with ERA-40 (Figure 4.1 a and m), around 56°S with JRA-55 (Figure 4.1 c and m), 52°S with NOAA-20CR (Figure 4.1 e and m), 56°S with the mean trend (Figure 4.1 g and m) and 58°S with CMIP5 (Figure 4.1 i and m). The CORE mean pattern has a zonal average maximum strength at 52°S, which mean that the only wind trend pattern that does not have a southward migration of the location of the westerly wind is NOAA-20CR. The wind pattern trend with ERA-40 have the stronger southward shift of the westerly wind. Some observations suggest that the westerlies over the Southern Ocean might have shifted poleward (Fyfe *et al.*, 1999; Kushner *et al.*, 2001; Cai *et al.*, 2003; Oke and England, 2004; Fyfe *et al.*, 2007). As a result of the difference in location between the datasets, the resulting mean trend dataset has weaker wind amplification than all three reanalyses over the Southern Ocean (Figure 4.1 g and m). In the northern hemisphere, the westerly winds amplify similarly in all datasets (Figure 4.1 a, c, e, g and i). Of the three reanalyses, the zonal average in JRA-55 shows less westerly amplification between 40°N and 60°N, because of negative trends over the Asian and North American land masses. Over the oceans, the wind speed increases similarly across the reanalyses, but significantly less with the CMIP5 multi-model ensemble.

All datasets but CMIP5 have increased trade winds over the Atlantic and South Indian Ocean (Figure 4.1 a, c, e and g between 40°S and 40°N). The increased trade winds over the Atlantic are stronger in ERA-40 and weaker in NOAA-20CR. Over the South Indian Ocean, the increase is stronger in JRA-55 and weaker in ERA-40. Over the North Indian Ocean, the mean winds are eastwards and are amplified in all datasets. Over the low latitudes Pacific, the wind changes are not consistent in the different datasets, except CMIP5. In ERA-40, the trade winds over the Pacific are overall weakened, except in the low latitudes on the western side of the Pacific. In JRA-55 the trade winds are overall increased over the Pacific, except over the equatorial eastern Pacific where they weaken. In NOAA-20CR, over the Pacific, the trade winds are overall weakened, except over the equatorial western Pacific and the South Pacific around 25°S on the western and eastern sides where the trade wind amplifies. The mean trend dataset has the trade winds amplified over the western side of the Pacific and weakened over the eastern side of the Pacific with the exception of near zero changes over the eastern Pacific around 25°S. In CMIP5, all the

trade winds are slightly weakened, by less than 0.2 m/s. The eastward wind over the North Indian is also weakened in CMIP5.

The meridional wind trends of the ERA-40 dataset have the overall strongest changes (Figure 4.1b). Over the Southern Ocean, only NOAA-20CR has increased northward wind south of 60^{o}S (Figure 4.1f). Over the Antarctic Circumpolar Current (ACC), the mean meridional wind is southward and under 2 m/s (Figure 4.1l). There are regional differences in the reanalysis datasets wind trends with both weakening and strengthening of the southward winds (Figure 4.1 b, d, f and h). However, with CMIP5 the southward winds are mainly strengthened (Figure 4.1 j). ERA-40 and JRA-55 show weakened southward wind in the Southern Ocean over the Pacific and Indian sectors. Only NOAA-20CR almost exclusively intensifies the southward wind. The mean trend mainly strengthens the southward wind over the Southern Ocean, except for a weakening over the south Indian Ocean.

Over the Atlantic, Pacific and Indian Oceans, the northward winds in the southern hemispheres and subpolar northern hemisphere are amplified in all datasets, except for the eastern South Pacific and equatorial Pacific with ERA-40 and equatorial eastern Pacific in Mean Trend (Figure 4.1 b, d, f, h, j and l). The southward winds over the eastern North Pacific and North Atlantic are slightly strengthened in all datasets as well, except in NOAA-20CR where the eastern North Pacific southward winds are weaker and in CMIP5 where there is no clear long term change (Figure 4.1 b, d, f, h, j and l).

In general, in the datasets, the winds are strengthened except for the trade winds over the Pacific. The wind trends in CMIP5 are generally much weaker than in the data reanalyses. The trends in trade winds speed over the Pacific are not consistent in the datasets with some geographically different strengthening and weakening. The only consistent differences over the low-latitudes Pacific are the amplified western equatorial and South Pacific trade winds and weakened eastern equatorial Pacific trade winds. In the Southern Ocean, the latitude of the mean westerly wind amplification varies between 50^{o}S and over 60^{o}S. In summary, there are qualitative similarities between the long-term wind changes in the three wind reanalyses, but there are quantitative

differences, even with the difference in time span used to create the 50 years trends, and the wind changes in CMIP5 are smaller in amplitude and qualitatively different than in the reanalyses.

4.3 Results

Changes in the model input of atmospheric wind speed are transmitted to the ocean through wind stress, which impacts on the penetration of temperature and salinity in the ocean interior and on the ocean circulation. Just like the wind speed, the wind stress is overall intensified in all datasets (Figure 4.2). Most differences between the datasets are in the zonal wind stress of the low latitudes Pacific and in the location of the changes in the zonal wind stress in the Southern Ocean (Figure 4.2 a, c, e, g, i and m). However, the wind stress changes pattern in CMIP5 is different than in the reanalyses and the intensity of the trends are much smaller. The wind stress in the Southern Ocean is also strengthened by an average of about 0.007 N/m^2 more in ΔNOAA-20CR than in ΔERA-40 and ΔJRA-55 (Figure 4.2m). The experiment with Mean Trend has an average of 0.004 N/m^2 less than in ΔERA-40 and ΔJRA-55 because of the differences in the meridional location of the main strengthening (Figure 4.2m). In CMIP5, the wind stress over the Southern Ocean is increased on average by 0.01 N/m^2 less than the reanalysis Mean Trend. The differences in wind stress between the experiments reflect their differences in wind speed previously discussed.

Outside of the Southern Ocean and equatorial oceans, the changes in the wind stress curl has a bigger influence on the oceans dynamics and drives Ekman pumping. The wind stress curl over the ocean has mainly increased in the Southern Hemisphere and subpolar North Hemisphere of the wind reanalyses and mainly decreased in the North Indian and the subtropical North Pacific (Figure 4.3 a, b, c, d and f). However, ΔERA-40 has decreased wind stress curl in the South Pacific at mid-latitudes (Figure 4.3a). As for the wind speed and wind stress, the pattern of changes in ΔCMIP5 is distinctly different than in the reanalyses (Figure 4.3e). The ΔCMIP5 wind stress curl has not significantly changed in the low and mid-latitudes, but decreased off the east coast of Russia in the North Pacific and increased at the northern end of the ACC in the Southern

Hemisphere (Figure 4.3e). The strongest changes in the wind stress curl are in the Southern Hemisphere mid and high latitudes, where there is strong Ekman pumping at the junction of the ACC and the Southern Hemisphere gyres (Figure 4.3g).

4.3.1 Changes in temperature in the ocean interior

There are significant differences in the patterns of temperature changes between each experiment (Figure 4.4 and Figure 4.5). In particular, ΔCMIP5 has a pattern of temperature change that differs from the temperature trend induced by the wind reanalyses dataset experiments. The oceans are cooled under the ventilated gyres in ΔCMIP5 whilst the other experiments induce a combination of warming and cooling areas in the low latitudes (Figure 4.4). Subsurface cooling regions in the equatorial Pacific and Indian Ocean are consistent in the wind reanalyses changes experiments, and is consistent with the observations (Figure 4.4 f, g, h, i, k, l, m, n and Figure 4.5 h and l). However, in ΔNOAA-20CR the subsurface cooling in the Indian Ocean is virtually non-existent. All wind reanalyses experiments create warming below 1000 m in each ocean basin (Figure 4.5 and Figure 4.5 d, i and n). This deeper warming combined with the warming in the ΔTΔS experiment overestimates the observed warming at these depths (Figure 4.5 a, b, f, g, k and l). When the warming induced by the ΔTΔS experiment is added to the ΔCMIP5 temperature change, the warming is still overestimated, but it is closer to the observed field.

4.3.1.1 ZONAL TEMPERATURE CHANGES

In the Atlantic Ocean, consistent features in the different reanalyses wind experiments include warming in the subtropical North Atlantic and around 45^{o}N (Figure 4.4 a, b, c and d and Figure 4.5d). The warming around 45^{o}N produced in ΔTΔSΔMean is improving the comparison with the pattern in the observations compared with ΔTΔS (Figure 4.5 a, b and e). This suggests that the increased wind in the subpolar North Atlantic is at least qualitatively realistic. However, the warming in the subtropical North Atlantic is not consistent with the observations (Figure 4.4 a, b, c and d). The observed temperature trend is close to 1^{o}C change in the top 100 m and less than 0.5^{o}C warming under 200 m (Figure 4.4a). The wind reanalyses have warming reaching above

0.5°C around 300 m, it is particularly pronounced in ΔNOAA-20CR (Figure 4.4 b, c, d and Figure 4.5d). The ΔCMIP5 experiment induces 0.2°C warming at around 200 m and cooling elsewhere, which when combined with ΔTΔS still overestimates the warming with ~0.5°C, but is more realistic than the >1°C warming induced in ΔTΔSΔMean (Figure 4.4d and Figure 4.5 b, c).

In the equatorial Atlantic, there is warming in the western Atlantic and cooling in the eastern Atlantic in all wind change experiments except ΔNOAA-20CR and ΔCMIP5 (Figure 4.6). This is consistent with increased trade winds in ΔERA-40, ΔJRA-55 and ΔMeanTrend and minimal wind changes in ΔNOAA-20CR and ΔCMIP5 (Figure 4.6 f, h, j, l and n). The increased trade winds lead to increased accumulation of the surface heat on the western side and upwelling on the eastern side of the Atlantic. When the surface warming and salinity pattern amplification are included, in ΔTΔSΔMean, a generalized subsurface warming reduces significantly the zonal difference induced in ΔMeanTrend (Figure 4.6c). Similarly, in the observations there is a pattern of western warming and eastern cooling, although significantly reduced compared to the wind stress experiment alone (Figure 4.6a). Our experiment ΔTΔSΔMean has too much warming and so it is difficult to say if the ΔMeanTrend trade winds increase is realistic. However, from the zonal pattern in the observations, it is likely that the trade winds over the Atlantic did increase to a certain degree.

In the subpolar South Pacific Ocean, there is an observed cooling to the north of the ACC, between ~45°S and ~15°S that is consistent across the wind experiments, but extending at lesser depths and restricted to higher latitudes (Figure 4.3 e, f, g h and Figure 4.4 e, f, g). That cooling is consistent with the increased Ekman pumping due to the strengthened westerlies over the Southern Ocean in all wind datasets. The increased exchange between the Southern Ocean and the south of the other oceans means an increase in cold water carried northward and warm water southward (Oke and England, 2004; Meredith and Hogg, 2006; Alory *et al.*, 2007; Hogg *et al.*, 2007; Abernathey *et al.*, 2011). When the increased westerlies are added to surface changes in temperature and salinity, this cooling feature is reduced by the warming induced by the other forcings (Figure 4.5 g, h and j). The observations have a cooling pattern of similar amplitude than

in ΔTΔSΔMean, although it extends further north (Figure 4.5e). This cooling north of the ACC is also observed in the Indian Ocean and is reproduced to a lesser extent in all the experiments but ΔERA-40 (Figure 4.4 k, l, m, n, o and Figure 4.5n). In ΔTΔSΔMean this cooling is countered by the warming induced in ΔTΔS. In the sum ΔTΔS+ΔCMIP5, only the deeper end of the cooling is still present. These cooling patterns are further explored in the regional pattern subsection 4.2.1.2.

In the equatorial Pacific Ocean, the observed cooling reproduced in the wind data reanalyses experiments is consistent with increased upwelling on the eastern side and downwelling on the western side due to increased trade winds on the western side (Figure 4.6 a, g, i, k and m). With ΔCMIP5, there is mainly cooling induced with no zonal dichotomy, which is consistent with the quasi-absence of trend in the trade winds over the Pacific (Figure 4.6 n and o). In the wind reanalysis experiments, the increased trade winds over the western Pacific lead to increased subduction of heat in the subtropical regions (Figure 4.4 g, h and i and Figure 4.5i). It also leads to increased upwelling towards the eastern Pacific (Figure 4.6 g, l, k and m). The effect of increased trade winds on the ocean dynamics in the equatorial region has been described by England *et al.* (2014) for changes in the wind field over the Pacific in the past two decades. This effect is consistent with the observed equatorial cooling (Figure 4.4f and Figure 4.6a). Although in the subtropical Pacific, the heat subducted in the wind experiment is much greater than observed, especially in ΔERA-40 and ΔJRA-55 (Figure 4.4 g and h), suggesting that the lesser strengthening of the equatorial wind over the Pacific in ΔNOAA-20CR might be more realistic (Figure 4.1e).

The subsurface cooling in the Pacific is transferred to the Indian Ocean through the Indonesian Throughflow (ITF) (Figure 4.6). In ΔNOAA-20CR and ΔCMIP5, the Indian Ocean does not cool to the same extent as in the other wind reanalyses experiments as they do not show this cooling through the ITF (Figure 4.6 m and o). Additionally, ΔNOAA-20CR has the strongest warming throughout the water column east of the ITF, which transfer to the Indian Ocean (Figure 4.6m). The combined experiment ΔTΔSΔMean also warms throughout the water column near the ITF due to the combined effect of the surface warming and salinity pattern amplification (Figure

4.6c). In the observations, the western Pacific cools through to the ITF and transmits the cooling to the Indian Ocean (Figure 4.6a) similarly to the connection induced in ΔERA-40, ΔJRA-55 and ΔMeanTrend. This cooling in the Indian Ocean from the ITF is visible in the zonal temperature average of the Indian Ocean (Figure 4.4 k, l, m and Figure 4.5 k, l and n). In ΔTΔSΔMean, as previously mentioned, the warming induced by ΔTΔS almost fully counters the cooling from ΔMeanTrend (Figure 4.5 k, l, n and o). This suggests that either the warming in ΔTΔS is overestimated or that the cooling in ΔMeanTrend is underestimated.

Schwarzkopf and Böning (2011) pointed out that the equatorial subsurface cooling in the Indian Ocean is attributed to a combination of the effect of wind changes over both the Pacific Ocean and Indian Ocean. They noted that the western side of the Indian Ocean is more influenced by the changes in the wind field over the Indian Ocean. Between 5^{o}S and 5^{o}N, the mean wind is positive, so a positive trend in Figure 4.6 means a wind strengthening. The two experiments with the stronger wind increase over the Indian Ocean, ΔERA-40 and ΔJRA-55, also have the strongest cooling throughout the water column (Figure 4.6 h, i, j and k). Likewise, ΔNOAA-20CR, which has the smallest wind increase, has the least cooling (Figure 4.6 l and m). The only experiment with a small weakening of the wind over the equatorial Indian Ocean is ΔCMIP5, which induces warming of the western equatorial Indian Ocean (Figure 4.6 n and o). In ΔTΔSΔMean, the cooling in the equatorial Indian Ocean from the ΔMeanTrend wind change is countered by warming from the surface warming and salinity pattern amplification and reduces the extent of the cooling.

4.3.1.2 REGIONAL TEMPERATURE CHANGES

The temperature changes at 100 m in the wind experiments are most pronounced in the equatorial oceans (Figure 4.7 b, c, d, e and Figure 4.8d). The equatorial Atlantic Ocean has cooled on the eastern side and warmed on the western side in all wind experiments except ΔCMIP5 (Figure 4.7 b, c, d, e and Figure 4.8d). In ΔNOAA-20CR this change pattern is less prominent and is also the wind reanalyses experiment with the smallest increase in the trade winds over the equatorial Atlantic (Figure 4.1 e, i and Figure 4.2 e, i). This warming (cooling) pattern is driven by the strengthened trade winds which enhance the western downwelling (eastern upwelling).

There is a similar cooling effect of the enhanced upwelling in the eastern Pacific consistent between the wind experiments, even slightly visible in ΔCMIP5 (Figure 4.7 b, c, d, e and Figure 4.8d). This effect in the Pacific and Atlantic Oceans was described previously (Figure 4.6). In ΔCMIP5, the Trade winds are weakened over the equatorial Pacific which reduces the eastern upwelling from the equatorial overturning. The observed temperature changes at 100 m have equatorial western warming and eastern cooling in the Atlantic and Pacific Ocean that is similar to that induced in the wind reanalyses experiments. This result gives confidence that the wind reanalyses dataset used have realistic increases in the trade winds over the Pacific and Atlantic Oceans, particularly in ERA-40 and JRA-55, and that the equatorial wind changes in CMIP5 are unrealistic.

In the North Indian Ocean, there is cooling on the western side and warming on the eastern side in the wind reanalyses experiments which is inconsistent with the observed temperature changes (Figure 4.7 a, b, c, d and Figure 4.8 d). The strengthened eastward wind in these experiments induce this zonal gradient (Figure 4.1 a, c, e, g and Figure 4.2 a, c, e, g). However, the temperature change in the North Indian Ocean is of opposite signs with ΔCMIP5, which does correspond to the observed trends (Figure 4.7 a and e). Each wind reanalyses, no matter the time range used to produce the wind trend, have a strengthening of the eastward wind over the North Indian Ocean. This shows that the differences between the time range used to produce the wind change pattern is not the cause of this inaccuracy. Also, the year range used with NOAA-20CR is an exact match to the range used to produce the observations and it also induce an unrealistic pattern. This suggests that the multidecadal eastward wind stress trend over the equatorial Indian Ocean might have decreased rather than increased as it is in the ΔCMIP5 experiment (Figure 4.1i and Figure 4.2i).

Outside of the equatorial oceans, the temperature changes are not consistent between the wind experiments at 100 m. The equatorial temperature changes significantly improve the regional pattern in ΔTΔSΔMean from ΔTΔS (Figure 4.8 b and e) in the Pacific and Atlantic Oceans. In the Indian Ocean, the temperature changes in ΔTΔSΔMean are comparable to the observations in

amplitude, but are the opposite signs on each side of the Indian Ocean. Although ΔCMIP5 does have the right signs of temperature change in the Indian Ocean, the amplitude is not sufficient to reproduce the observed pattern when added to ΔTΔS (Figure 4.8 a, c and e). This suggest the weakening of the eastward wind over the equatorial Indian Ocean in ΔCMIP5 is likely underestimated (Figure 4.1i and Figure 4.2i).

At 300 m, the wind reanalyses experiments produce significant temperature changes at all latitudes and smaller changes in ΔCMIP5 (Figure 4.7 g, h, i, j and Figure 4.8i). However, there are few coherent patterns repeated in all the wind change experiments. Changes in temperature vary significantly in sign, amplitude and extent across the wind experiments, notably in the North Pacific and Atlantic Oceans. These are signs of the changes in wind stress curl in the wind data reanalyses experiments which drives the Sverdrup transport and thus increases Ekman pumping (Figure 4.3 a, b, c and d). In ΔCMIP5, the wind stress curl in the tropics does not change by more than $\pm 0.1 \times 10^{7}$ N/m^2, which results in little changes in temperature under the subtropical gyres (Figure 4.3e). These smaller changes in wind stress curl are reflected in the little changes in temperature at 300 m under the subtropical gyres (Figure 4.7j).

Consistent temperature changes between the wind reanalyses experiments at 300 m include warming of the Southern Ocean of smaller amplitude and extent than observed (Figure 4.7 f, g, h, i and Figure 4.8i). The wind change in ΔERA-40 is the only dataset that has a southward shift of the westerlies over the Southern Ocean (Figure 4.1 a, m and Figure 4.2 a, m). The temperature changes produced in the Southern Ocean with ΔERA-40 is also the smallest of the wind reanalyses experiments (Figure 4.7g). The strongest westerlies strengthening without shift is in ΔNOAA-20CR (Figure 4.1 e, m and Figure 4.2 a, m) which also has the strongest Southern Ocean warming, especially in the Southern Indian Ocean (Figure 4.7i). The stronger warming in ΔNOAA-20CR is closer to the observed warming. However, ΔTΔS also significantly warm the Southern Ocean and contribute to produce a total temperature change that is significantly more than observed (Figure 4.8 g and j). The ΔCMIP5 experiment induces a small cooling that approaches zero in the Southern Ocean (Figure 4.7j). The westerlies were also strengthened over the Southern Ocean in ΔCMIP5,

but by nearly half the amplitude than in the wind reanalyses experiments (Figure 4.1m and Figure 4.2m). This suggest that a linear strengthening of the westerlies over the Southern Ocean by a zonal average of ~0.7 m/s over a period of 50 years does not induce the increase in eddy transport that result in a noticeable warming in the Southern Ocean interior. Because the total warming with ΔTΔSΔMean is overestimated, it is hard to reach any conclusion as to which wind change is more realistic over the Southern Ocean, especially that the warming induced in ΔTΔS alone is already overestimated.

The Southern Pacific significantly cools around 45^{o}S in all wind change experiments (Figure 4.7 g, h, i, j and Figure 4.8i). In ΔTΔSΔMean, this cooling pattern compares with the observations, although it is further south than observed (Figure 4.8 f and g). At the location of the observed cooling, all of the experiments induce a warming, which adds to the ΔTΔS warming to produce unrealistic changes in temperature that reaches higher than 1^{o}C. The cooling in ΔCMIP5 is lesser than in the other experiments and when added to ΔTΔS almost fully disappear and does not compare with the observations (Figure 4.7i and Figure 4.8h). However, ΔCMIP5 has lesser warming north of the mid-latitudes cooling, which is more realistic.

The western equatorial Pacific cools at 300 m in the wind change experiments, except for ΔCMIP5, which is consistent with the increased circulation driven by the strengthened trade winds as previously mentioned (Figure 4.7 g, h, i, j and Figure 4.8i). The observations show mostly increased temperature in the western equatorial Pacific with cooling on the western coastlines and around 10^{o}S (Figure 4.7f). This asymmetry around the equator is also seen in the wind reanalyses experiments, which have less cooling north of the equator and is more realistic in ΔMeanTrend (Figure 4.7i). In ΔTΔSΔMean, the warming from ΔTΔS combined with the asymmetrical cooling of ΔMeanTrend produces a pattern that is more realistic than in ΔTΔS or ΔMeanTrend alone, except for the western cooling along the coastlines (Figure 4.8 f, g, i and j).

At 300 m depth the Indian Ocean cools with ΔERA-40 and ΔJRA-55, warms with ΔNOAA-20CR and shows little change in ΔCMIP5 (Figure 4.7 g, h, i and j). The cooling in ΔERA-40 and ΔJRA-55 was described earlier as due to differences of the western Pacific temperature changes being

transferred through the ITF. The ITF is cooler in ΔERA-40 and ΔJRA-55 whilst warmer in ΔNOAA-20CR and near constant in ΔCMIP5. The cooling in the western equatorial Pacific is further south in ΔNOAA-20CR than the Pacific opening on the ITF, which explains this difference (Figure 4.7i). In ΔMeanTrend, the Indian Ocean cools, although not enough to compensate for the ΔTΔS warming in ΔTΔSΔMean and neither is the small cooling induced in ΔCMIP5 when added to ΔTΔS (Figure 4.8 g, h, i and j). The observations show near zero change in temperature in the Indian Ocean (Figure 4.8f). This could possibly be produced with a wind experiment that cools the Indian Ocean more than ΔMeanTrend such as ΔERA-40 or ΔJRA-55.

There are changes in temperature at 500 m of amplitude greater than observed in the wind reanalyses experiment and smaller amplitude in ΔCMIP5. The temperature change at 500 m varies greatly among the wind experiments, especially in the Northern Hemisphere (Figure 4.7 k, l, m, o and Figure 4.8n). The Atlantic mainly cools in ΔERA-40 and ΔCMIP5 whilst it warms in ΔJRA-55 and ΔNOAA-20CR. The North Pacific cools in ΔNOAA-20CR and ΔCMIP5 whilst it warms in ΔERA-40 and ΔJRA-55. The equatorial eastern Pacific warms in ΔNOAA-20CR and ΔERA-40 and does not significantly change in ΔJRA-55 and ΔCMIP5. Also, the temperature trend is of different sign in the Indian Ocean in ΔNOAA-20CR than in ΔERA-40. ΔJRA-55 and ΔCMIP5 like at the shallower depths. In the mid-latitude South Indian Ocean, ΔERA-40 warms while ΔJRA-55, ΔNOAA-20CR and ΔCMIP5 cools. The wind experiments create temperature change at 500 m that are not consistent in most of the oceans and there are not two experiments that agree on the overall pattern of change. With the mean wind trend, in ΔMeanTrend, the temperature trends are more constant regionally, at smaller amplitude and more realistic (Figure 4.8n).

However, there are some agreements between the experiments in the Southern Ocean and mid-latitudes South Pacific. The observed Southern Ocean at this depth mostly warms, except for slight cooling south of Africa and New Zealand (Figure 4.7k). The temperature change pattern at 500 m in ΔTΔS is comparable to the observed pattern but with stronger warming (Figure 4.8o). In ΔMeanTrend, the temperature is mainly warming, and when added in ΔTΔSΔMean, the Southern Ocean at 500 m warms more than observed (Figure 4.8 k, l and o). In ΔCMIP5, the

Southern Ocean slightly cools at 500 m, however, it still produces overestimated temperature change when added to ΔTΔS (Figure 4.7o and Figure 4.8 k, m). Durack *et al.* (2014) show that there is a likely bias low in the observed temperature change in the Southern Ocean. It is thus hard to determine if the amplitude of temperature change in the Southern Ocean is realistic, but the pattern of change is consistent with the observations (Figure 4.8 k, l and m).

In the mid-latitude South Pacific at 500 m, there is strong cooling in all the wind experiments around 30^{o}S, which is consistent in amplitude with the observations (Figure 4.7 k, l, m, n and o). Although, this cooling is much more restrained to lower latitudes in the experiments. This is the deeper end of the cooling previously discussed at 300 m and in the zonal integration (Figure 4.4 f, g, h, i, j and Figure 4.5 f, g, h, i, j). These cooling patterns are consistent in their regional location and vertical extent with an increase in Ekman transport from the Southern Ocean due to the strengthened westerly wind (Oke and England, 2004; Hogg *et al.*, 2007; Abernathey *et al.*, 2011).

At 500 m, the sum of ΔCMIP5 with ΔTΔS is closer to the observed pattern of temperature change than with ΔTΔSΔMean. This is mainly due to the overestimation of the warming at this depth in the combination of ΔMeanTrend and ΔTΔS whilst ΔCMIP5 counters part of the warming induced in ΔTΔS.

The wind reanalyses experiments produce strong regional temperature change throughout the water column which varies greatly between each experiment. It shows how sensitive the temperature field in the ocean interior is to the differences across the wind data reanalyses. The wind reanalyses experiments have similar temperature changes in the shallower equatorial Pacific, shallower equatorial Indian Ocean, mid-latitudes South Pacific and in the Southern Ocean. With the CMIP5 multi-model ensemble wind change the temperature change in the ocean interior are significantly smaller and mainly negative. In the ΔCMIP5 experiment, the observed temperature changes in the equatorial oceans are not reproduced. In the mid-latitudes ΔCMIP5 induce more realistic changes in temperature whilst at low latitudes the wind reanalyses induce more realistic temperature changes. In the Southern Ocean, when the temperature change is

combined to the warming induced in ΔTΔS, the warming is overestimated with all wind experiments, but have similar pattern than in the observations.

4.3.2 Changes in salinity in the ocean interior

The changes in the surface winds induce subsurface salinity trends that generally do not compare with those observed (Figure 4.9 and Figure 4.10). The salinity changes induced by the wind trend are particular strong under the subtropical gyres in the Atlantic and Pacific Oceans with the wind reanalyses experiments where the salinity increases and freshens by ~0.05 to 0.15 PSS-78 (Figure 4.9 b, c, d, g, h, i and Figure 4.10 d and i). In the subtropical gyres, the circulation is driven by the wind stress curl (Figure 4.3), so these regions are particularly sensitive to small differences in the wind field. The pattern of salinity changes in ΔTΔSΔMean is less realistic than in ΔTΔS (Figure 4.10). This suggests that multidecadal trends in the wind data reanalyses are not fully accurate in the subtropical regions as they produce changes in the water masses that do not correspond with the observed changes for the same time span. With ΔCMIP5, the salinity changes are smaller, in the range ~0.05 PSS-78 (Figure 4.9 e, j and o). The wind changes with CMIP5 induces freshening under the ventilated gyres and increased salinity in the upper 200 m and high latitudes. The smaller amplitude of changes is consistent with the very small changes in the wind stress curl in ΔCMIP5 (Figure 4.3e). When these are added to the salinity changes induces by ΔTΔS, the pattern of salinity trends looks closer to the observations (Figure 4.10 c, h and m).

It is possible that the simplicity of our linearly changed wind experiments induce the unrealistic changes in the ocean salinity field. The omission of the higher frequency interannual variability in the wind field might induce the strong unrealistic changes in the physical properties of the ocean interior. Zhai (2013) points to the important role the wind fluctuations at small timescale in the long term change of energy input to the ocean. The changes in salinity induced by our idealized experiments suggest that at least the multidecadal trends in the wind field from the data reanalyses alone are unrealistic in the salinity changes they induce.

4.3.3 Correlations

Correlation coefficients between the changes in the ocean interior for the top 2000 m induced in the model and the observations gives an idea of the accuracy of the results and relative contribution to the total pattern of change for each experiment (Table 4.2 and Table 4.3). However, the location of the water masses and water mass changes are not necessarily identical between the model and reality which restricts the interpretation of these correlation coefficients.

The correlations between the temperature changes in the wind experiments and the observations are very weak in the Atlantic Ocean (Table 4.3). The trends induced by the wind change in ΔTΔSΔMean reduce the correlation with the observed temperature trend in the Atlantic compared with the same experiment with fixed winds, ΔTΔS. The pattern correlation between the sum of ΔCMIP5+ΔTΔS and the observations is improved in the Pacific and Global Oceans compared to ΔTΔS alone and is slightly reduced in the Atlantic and Indian Ocean. In the Pacific, ΔERA-40, ΔJRA-55, ΔMeanTrend and ΔCMIP5 correlate better with the observed temperature trends then ΔNOAA-20CR, however ΔCMIP5 have near a 0 correlation coefficient in the Indian Ocean. ΔERA-40 and ΔJRA-55 have correlations of 0.23 and 0.32 respectively in the Pacific Ocean and 0.42 and 0.59 respectively in the Indian Ocean due mainly to the reproduced equatorial cooling. In NOAA-20CR, there is very little cooling in the Indian Ocean and too much warming due to the warmer ITF, unlike the observed temperature trend. This leads to the negative correlation between ΔNOAA-20CR and the observations in the Indian Ocean. With ΔCMIP5, the correlation coefficients are close to zero and negative in the Atlantic and Indian Ocean, but 0.38 in the Pacific Ocean which is reflected on the correlation coefficient for the Global Ocean with 0.35. These correlations are mainly due to the accurately reproduced increased Ekman pumping driven cooling in the South Pacific as previously discussed and the smaller temperature changes under 500 m as compared with the other wind experiments (Figure 4.4j).

In contrast to the correlations for the Atlantic, in the Pacific, Indian and Global Oceans, the wind changes added to the surface temperature and salinity changes in ΔTΔSΔMean improves the

correlation with the observed temperature pattern compared to ΔTΔS alone. The comparison is mostly improved in the Indian Ocean, where the observed cooling regions are partly reproduced in the zonal averages when the wind change ΔMean is added to the ΔTΔS forcings in ΔTΔSΔMean. All of the wind reanalyses experiments correlate in each ocean with ΔTΔSΔMean, except for the Indian Ocean with ΔNOAA-20CR. This correlation indicate the relative contribution of the temperature changes induced by each wind reanalysis forcing to the total pattern of change in the model with all forcings together. Their strong correlation is indicative of the strong temperature changes induced by the wind stress trends in these experiments compared to the changes induced by the surface salinity and temperature changes. This correlation shows that the amplitude of the temperature changes induced by the wind stress alone is significant in the total pattern of changes induced by changes in all three surface conditions.

The salinity changes from the wind experiments show little correlation to the observed trends (Table 4.4). The wind experiments anti-correlate or is near zero almost everywhere. One exception is the salinity changes induced by ΔCMIP5 in the Indian Ocean that has a correlation coefficient of 0.44 with the observations. It is the only wind experiment that reproduces the observed increased salinity in the North Indian upper 500 m, increased salinity in the upper 300 m around 30^{o}S along with cooling across most of the Indian Ocean under 500 m (Figure 4.9o). However, the pattern is roughly similar to the observed, the amplitude of changes and variations of amplitude is very small.

The wind change experiments do correlate with the experiment that combines all surface forcings, ΔTΔSΔMean. This is an indication that the amplitude of salinity changes produced in the wind reanalyses experiments compares with the total salinity changes induced by the changes in the surface temperature and salinity fields. However, even though the salinity changes induced in the ΔMeanTrend compares in amplitude to those produced in ΔTΔS alone, they differ from the observations. In each ocean, the ΔTΔSΔMean experiment reduces the correlation to the observations compared to the same experiment with fixed winds, ΔTΔS. It is indicative of the

inaccuracy of these wind reanalyses in the subtropics and/or a too sensitive reaction of the model to these wind changes in the subtropics.

By opposition, the salinity changes induced by ΔCMIP5 improves the total pattern of salinity change from ΔTΔS in the Atlantic and Indian Oceans as shown by the correlation coefficients between the sum ΔTΔS+ΔCMIP5. The salinity changes induced by ΔCMIP5 are overall less than 0.05 in amplitude in each ocean, but have a realistic pattern in the Indian Ocean which complements the salinity pattern induced by ΔTΔS. In the Atlantic Ocean, the pattern of salinity changes in itself does not correlate with the observations with a correlation coefficient of 0.02. However, it complements partly to the pattern induced in ΔTΔS by reducing the increased salinity under 300 m in the low latitudes and reduce the reduced salinity in the subpolar North Atlantic and improving the correlation by a small margin (Figure 4.9e and Figure 4.10 c and e).

The inaccurate salinity changes in the wind reanalyses experiments mostly occur due to the wind stress curl changes in the subtropics and ΔCMIP5 has significantly smaller wind stress curl changes in these latitudes (Figure 4.3). Because ΔCMIP5 has more realistic pattern of salinity changes, it does indicate that the changes in the wind stress curl in these wind reanalyses are over estimated.

4.3.4 Linearity

The wind changes imposed in the model act linearly with the increased surface temperature and salinity pattern amplification in their induced changes in temperature and salinity within the scale of our experiments (Figure 4.11). The main small differences between the changes in the temperature and salinity in ΔTΔSΔMean, and the sum of the changes in ΔTΔS and ΔMeanTrend are in the high latitude Atlantic (Figure 4.11 b and d). These regions have strong variability and are highly non-linear, yet only small differences are seen in the 50 years trends. Even though the changes in the wind pattern produced strong temperature and salinity trends in the ocean interior, which are highly sensitive to small variations in the wind pattern imposed, these are still

very linear in response to the changes induced by our idealized variations in the surface properties.

4.4 Discussion

The 50 years trend of three different wind data reanalyses applied individually in idealized experiments produce pronounced and highly variable temperature and salinity changes. The patterns of change in the wind data reanalyses are overall similar, although they differ regionally in the strength of the trends. These differences are enough to induce trends in temperature and salinity of opposite signs with strong regional differences that are unrealistic outside of the equatorial region. The 50 years linear wind trend from the CMIP5 multi-model ensemble is of an order of magnitude weaker than the wind data reanalyses, except for the westerlies over the Southern Ocean that is about half the strengthening seen in the reanalyses. These weaker wind change induce change in salinity and temperature that are more realistic in the tropics and subtropics, but less realistic in the equatorial area.

The wind reanalysis experiments are in agreement for some temperature changes in the equatorial oceans shallower than 300 m, the mid-latitudes South Pacific and in the Southern Ocean. In the equatorial Pacific and Atlantic, the strengthened trade winds increase the downwelling on the western side of the ocean and upwelling on the eastern side. The changes in temperature due to this effect compares well with the observed changes. In the equatorial Indian Ocean, there is a combination of effects from the changes in wind over the Pacific connecting through the ITF and the local change in winds, as previously suggested by Schwarzkopf and Böning (2011). The changed wind over the Pacific induces a subsurface cooling through the ITF which propagates into the Indian Ocean. However, the wind trend from the NOAA-20CR data reanalysis does induce a warming of the ITF and thus a warming Indian Ocean, which is opposite to the observed temperature trends.

In the North Indian Ocean, the wind experiments produce a western cooling and eastern warming, which is opposite to that observed. In CMIP5, the eastward wind has weakened, which

induces a more realistic western warming and eastern cooling, although at significantly smaller amplitude than observed. This suggests that the weakened eastward wind over the North Indian Ocean in CMIP5 might be more accurate, although the trend might be too small to reproduce the full cooling pattern observed.

In the Southern Ocean, the changes in temperature due to the strengthened westerlies are mainly deeper than 100 m. The largest warming is produced with the NOAA-20CR data trend. It is also the only data that does not have a southward shift of the westerlies. The pattern of temperature change in the Southern Ocean does compare well with the observed temperature changes. The Southern Ocean warming and cooling in the southern Pacific and Indian Oceans is consistent with increase Ekman transport due to the strengthened westerlies (Oke and England, 2004; Meredith and Hogg, 2006; Hogg *et al.*, 2007). However, when added to the surface temperature increase and surface salinity pattern amplification, the warming exceeds that observed. The westerlies over the Southern Ocean in CMIP5 has increased by at ~0.25 m/s less than the trend produced as the mean of all three reanalyses, which has the lesser strengthening of the westerlies within the wind reanalyses experiments. With this wind change, the Southern Ocean has not warmed. This suggests that wind driven warming in the Southern Ocean requires a minimum wind speed increase of the westerlies that is at least greater than 0.7 m/s at its zonal average maximum before eddy diffusion warms the Southern Ocean over this period of 50 years. However, the warming induced solely by surface warming and salinity pattern amplification is greater than in the observations, so even when the temperature change induced by the CMIP5 wind trend is added, the total warming is overestimated. It is hard to say which of the temperature change in the Southern Ocean is more realistic within our experiments since it has been shown that the observed temperature changes are likely underestimated (Durack *et al.*, 2014).

These wind data reanalysis experiments also induce salinity changes in the ocean interior that reach values greater than 0.2 PSS-78 on global zonal average. These changes on the pattern of salinity are not in agreement between the experiments. Furthermore, the changes in salinity they

produce do not compare with the observations. However, the wind change in CMIP5 induces trends in salinity that are no greater than 0.02 PSS-78 on global zonal average, the pattern produced in the Atlantic and Indian Ocean are complementary to the subsurface salinity changes due to changes in the surface temperature and salinity fields. When added together, the salinity pattern induced by the CMIP5 wind trend slightly improves the comparison with the observed subsurface salinity trends. However, when the surface wind data reanalyses trends are added to the surface temperature increase and salinity pattern amplification, the pattern of salinity changes compares less well with the observations than with fixed winds.

In the model, the changes in the surface wind pattern act linearly with changes in the temperature and salinity of the ocean interior with the effect of surface temperature and salinity changes. There are small non-linear interactions, mainly in the higher latitudes of the Atlantic Ocean. Since the temperature and salinity changes induced by the changes in wind pattern are inaccurate, it might be different with a better representation of the wind trends. However, it is still noteworthy to mention that in the complex interaction between the changes in momentum induced by the wind changes and the change in the density structure induced by variations in the surface temperature and salinity, the model renders patterns that are linearly additive in their combined effect.

Changes in salinity and temperature in the ocean interior are very sensitive to the imposed changes in the wind pattern in the tropical gyres. The ocean circulation in the tropics is driven by the wind stress curl and is thus more sensitive to small variations in the wind field. Small variations between the wind reanalyses produce strong differences in the pattern of temperature and salinity changes in the ocean interior. The changing wind pattern has a stronger effect on the subsurface temperature field than it has on the salinity field. However, the subsurface changes in temperature and salinity in the tropics and subtropics compare poorly with the observed changes. This suggests that either the wind data reanalyses or the model's response to them is inaccurate. The changes in wind stress curl in CMIP5 are of much smaller amplitude within the tropics and subtropics, which renders more accurate temperature and salinity changes in the

ocean interior in these regions. Although, these changes are possibly too small to provide an accurate simulation of the temperature and salinity trends in the interior when added to the changes induced by variations in the surface temperature and salinity.

The unrealistic changes in the temperature and salinity fields outside of the equatorial oceans and Southern Ocean with the wind data reanalyses might be due to the idealized nature of our experiments. The linearly imposed multidecadal wind trends, without the higher frequency changes, might impact on the results in the regions more sensitive to small differences in the wind stress curl. Changes in the intra-annual structure of the wind pattern or decadal variability might be of importance in setting the wind-driven changes in temperature and salinity outside of the equator and Southern Ocean as suggested by Zhai (2013). However, our results also suggest that the equatorial changes in temperature and possibly the wind-induced warming of the Southern Ocean are driven by the multi-decadal changes in the wind field as they are in the three wind data reanalyses.

Acknowledgments

The data used from the CMIP5 multi-model ensemble comes from the World Climate Research Programme's Working Groups on Coupled Modelling. We thank the climate modelling groups listed in Table 4.1 for producing and making available their model outputs. The work of V.L., S.E.W., J.A.C. and S.J.M. is supported by the Australian Government Department of Environment, the Bureau of Meteorology and CSIRO through the Australian Climate Change Science Program. This research was undertaken with the assistance of resources provided at the NCI National Facility systems at the Australian National University through the National Computational Merit Allocation Scheme supported by the Australian Government. The work of P.J.D. from Lawrence Livermore National Laboratory is a contribution to the U.S. Department of Energy, Office of Science, Climate and Environmental Sciences Division, Regional and Global Climate Modelling Program under contract DE-AC52-07NA27344. The work of V.L. and N.L.B. from the Institute of Marine and Antarctic Studies is supported by the University of Tasmania and the Centre of Excellence for Climate System Science.

References

Abernathey R., J. Marshall and D. Ferreira, 2011: The Dependence of Southern Ocean meridional overturning on wind stress. *Journal of Physical Oceanography*, **41**, pp.2261-2278. doi:10.1175/JPO-D-11-0.23.1

Alory, G., S. Wijffels, M. Meyers, 2007: Observed temperature trends in the Indian Ocean over 1960-1999 and associated mechanisms. Geophys. Res. Lett., 34 (2): Art. No. L02606 JAN 20 2007

Balmaseda, M.A., K.E. Trenberth and E. Kallen, 2013: Distinctive climate signals in reanalysis of global ocean heat content. *Geophysical Research Letters*, **40**, pp.1754-1759. doi:10.1002/grl.50382

Bi, D., S.J. Marsland, P. Uotila, S. O'Farrell, R. Fiedler, A. Sullivan, S.M. Griffies, X. Zhou, and A.C. Hirst, 2013: ACCESS-OM: the Ocean and Sea ice Core of the ACCESS Coupled Model. *Australian Meteorological and Oceanographic Journal*, **63(1)**, pp. 213-232.

Bindoff, N.L. and P.A. Stott, M. AchutaRao, M.R. Allen, N. Gillett, D. Gutzler, K. Hansingo, G. Hegerl, Y. Hu, S. Jain, I.I. Mokhov, J. Overland, J. Perlwitz, R. Sebbari and X. Zhang, Detection and attribution of climate change: from global to regional, Climate Change 2013 The Physical Science Basis: Working Group I Contribution to the Fifth Assessment Report of the Intergovernmental Panel on Climate Change, Cambridge University Press, TF Stocker, D Qin, G-K Plattner, MMB Tignor, SK Allen, J Boschung, A Nauels, Y Xia, V Bex, PM Midgle (ed), Cambridge, UK, pp. 867-952. ISBN 978-1-107-66182-0 (2013)

Cai, W., P. H. Whetton, and D.J. Karoly, 2003: The Response of the Antarctic Oscillation to Increasing and Stabilized Atmospheric CO2. *Journal of. Climate*, **16**, pp. 1525–1538. doi:10.1175/1520-0442-16.10.1525

Compo, G. P., Whitaker, J. S., Sardeshmukh, P. D., Matsui, N., Allan, R. J., Yin, X., Gleason, B. E., Vose, R. S., Rutledge, G., Bessemoulin, P., Brönnimann, S., Brunet, M., Crouthamel, R. I., Grant,

A. N., Groisman, P. Y., Jones, P. D., Kruk, M. C., Kruger, A. C., Marshall, G. J., Maugeri, M., Mok, H. Y., Nordli, Ø., Ross, T. F., Trigo, R. M., Wang, X. L., Woodruff, S. D. and Worley, S. J., 2011: The Twentieth Century Reanalysis Project. *Quaterly Journal of the Royal Meteorological Society*, **137**, pp. 1–28. doi:10.1002/qj.776

Durack, P.J. and S.E. Wijffels, 2010: Fifty-year trends in global ocean salinities and their relationship to broadscale warming. *Journal of Climate*, **23**, pp. 4342-4362. doi:10.1175/2010JCLI3377.1

Durack, P.J., P.J. Gleckler, F.W. Landerer and K.E. Taylor, 2014: Quantifying underestimates of long-term upper-ocean warming. *Nature Climate Change*, **4**, pp. 999-1005. doi:10.1038/nclimate2389

England M.H., S. McGregor, P. Spence, G.A. Meehl, A. Timmermann, W. Cai, A.S. Gupta, M.J. McPhaden, A. Purich and A. Santoso, 2014: Recent intensification of wind-driven circulation in the Pacific and the ingoing warming hiatus. *Nature Climate Change*, **4**, pp. 222-227. doi:10.1038/NClimate2106

Fyfe, J., G. Boer, and G. Flato, 1999: The Arctic and Antarctic Oscillations and their projected changes under global warming. *Geophysical Research Letter*, **26**, pp. 1601–1604.

Fyfe, J.C., O.A. Saenko, K. Zickfeld, M. Eby, and A.J. Weaver, 2007: The Role of Poleward-Intensifying Winds on Southern Ocean Warming.*Journal of Climate*, **20**, pp. 5391–5400. doi:10.1175/2007JCLI1764.1

Gravensen, R.G., E. Källén, M. Tjernström and H. Körnich, 2007: Atmospheric mass-transport inconsistencies in the ERA-40 reanalysis. *Quaterly Journal of the Royal Meteorological Society*, **133**, pp. 673-680. doi:10.1002/qj.35

Hakkinen, S., P.B. Rhines and D.L. Worthen, 2011: Warm and saline events embedded in the meridional circulation of the northern North Atlantic. *Journal of Geophysical Research*, **116**, C03006. doi:10.1029/2010JC006275

Hogg, A.M., M.P. Meredith, J.R. Blundell and C. Wilson, 2007: Eddy Heat Flux in the Southern Ocean: Response to Variable Wind Forcing. *Journal of Climate*, **21**, pp. 608-620.

Kobayashi, S., Y. Ota, Y. Harada, A. Ebita, M. Moriya, H. Onoda, K. Onogi, H. Kamahori, C. Kobayashi, H. Endo, K. Miyaoka and K. Takahashi, 2015: The JRA-55 Reanalysis: General Specifications and Basic Characteristics. *Journal of the Meteorological Society of Japan*, **93**, No. 1, pp. 5−48. doi:10.2151/jmsj.2015-001

Kushner, P. J., I. M. Held, and T. L. Delworth, 2001: Southern Hemisphere atmospheric circulation response to global warming. *Journal of Climate*, **14**, pp. 2238–2249.

Lai, A.W., M. Herzog, H.-F. Graf., 2015: Two key parameters for the El Nino continuum: zonal wind anomalies and Western Pacific subsurface potential temperature. *Climate Dynamics*. doi:10.1007/s00382-015-2550-0

Large, W. and Yeager, S., 2004: Diurnal to decadal global forcing for ocean and sea ice models: the data sets and flux climatologies. CGD Division of the National Center for Atmospheric Research, NCAR Technical Note: NCAR/TN-460+STR.

Large, W.G. and S. Yeager, 2009: The global climatology of an interannually varying air-sea flux data set. *Climate Dynamics,* **33.** doi:10.1007/s00382-008-0441-3

Meredith, M.P., A. M. Hogg, 2006: Circumpolar response of Southern Ocean eddy activity to a change in the Southern Annular Mode. *Geophysical Research Letters*, **33**, L16608. doi:10.1029/2006GL026499

Merrifield, M.A., 2011: A Shift in Western Tropical Pacific Sea Level Trends during the 1990s. *Journal of Climate*, **24**, pp. 4126-4138. doi:10.1175/2011JCLI3932.1

Oke, P.R., M.H. England, 2004: Oceanic Response to Changes in the Latitude of the Southern Hemisphere Subpolar Westerly Winds. *Journal of Climate*, **17**, pp. 1040-1054.

Swart N.C. and J.C. Fyfe, 2012: Observed and simulated changes in the Southern Hemisphere surface westerly wind-stress. *Geophysical Research Letters*, **39**, L16711. doi:10.1029/2012GL052810

Schwarzkopf F.U. and C.W. Böning, 2011: Contribution of Pacific wind stress to multi-decadal variations in upper-ocean heat content and sea level in the tropical south Indian Ocean. *Geophysical Research Letters*, **38**, L12602. doi:10.1029/2011GL047651

Uppala, S.M., P.W. Kållberg, A.J. Simmons, U. Andrae, V. Da Costa Bechtold, M. Fiorino, J.K. Gibson, J. Haseler, A. Hernandez, G.A. Kelly, X. Li, K. Onogi, S. Saarinen, N. Sokka, R.P. Allan, E. Andersson, K. Arpe, M.A. Balmaseda, A.C.M. Beljaars, L. Van De Berg, J. Bidlot, N. Bormann, S. Caires, F. Chevallier, A. Dethof, M. Dragosavac, M. Fisher, M. Fuentes, S. Hagemann, E. Hólm, B.J. Hoskins, L. Isaksen, P.A.E.M. Janssen, R. Jenne, A.P. Mcnally, J.-F. Mahfouf, J.-J. Morcrette, N.A. Rayner, R.W. Saunders, P. Simon, A. Sterl, K.E. Trenberth, A. Untch, D. Vasiljevic, P. Viterbo and J. Woollen, 2005: The ERA-40 re-analysis. *Quarterly Journal of the Royal Meteorological Society*, 131(612), pp.2961-3012.

Valcke, S., 2006: OASIS3 User Guide (prism 2-5). *PRISM Support Initiative*, Report No. 3, CERFACS, Toulouse, France, 68 pp.

Vecchi, G. A., B. J. Soden, A. T. Wittenberg, I. M. Held, A. Leetmaa, and M. J. Harrison, 2006: Weakening of tropical Pacific atmospheric circulation due to anthropogenic forcing. *Nature*, **441**, pp. 73–76.

Wu, L., W. Cai, L. Zhang, H. Nakamura, A. Timmermann, T. Joyce, M.J. McPhaden, M. Alexander, B. Qiu, M. Visbeck, P. Chang and B. Giese, 2012: Enhanced warming over the global subtropical western boundary currents. *Nature Climate Change*, **2**, pp. 161–166.

Xue, Y., B. Huang, Z.-Z. Hu, A. Kumar, C. Wen, D. Behringer, and S. Nadiga, 2010: An assessment of oceanic variability in the NCEP climate forecast system reanalysis. Clim. Dyn., **37**, pp. 2541–2550.

Zhai, 2013: On the wind mechanical forcing of the ocean general circulation. *Journal of Geophysical Research: Oceans*, **118**, pp. 1–17. doi:10.1002/2013JC009086

Tables

Table 4.1. List of models used for the CMIP5 multi-model ensembles wind pattern experiment.

Modelling Centre (or Group)	Institute ID	Model Name
Commonwealth Scientific and Industrial Research Organization (CSIRO) and Bureau of Meteorology (BOM), Australia	CSIRO-BOM	ACCESS1.0 ACCESS1.3
College of Global Change and Earth System Science, Beijing Normal University	GCESS	BNU-ESM
Canadian Centre for Climate Modelling and Analysis	CCCMA	CanESM2
Centre National de Recherches Météorologiques / Centre Européen de Recherche et Formation Avancée en Calcul Scientifique	CNRM-CERFACS	CNRM-CM5
Commonwealth Scientific and Industrial Research Organization in collaboration with Queensland Climate Change Centre of Excellence	CSIRO-QCCCE	CSIRO-Mk3.6.0
NOAA Geophysical Fluid Dynamics Laboratory	NOAA GFDL	GFDL-CM3 GFDL-ESM2G GFDL-ESM2M
NASA Goddard Institute for Space Studies	NASA GISS	GISS-E2-H GISS-E2-R
Met Office Hadley Centre (additional HadGEM2-ES realizations contributed by Instituto Nacional de Pesquisas Espaciais)	MOHC (additional realizations by INPE)	HadGEM2-CC HadGEM2-ES
Institut Pierre-Simon Laplace	IPSL	IPSL-CM5A-LR IPSL-CM5A-MR IPSL-CM5B-LR
Japan Agency for Marine-Earth Science and Technology, Atmosphere and Ocean Research Institute (The University of Tokyo), and National Institute for Environmental Studies	MIROC	MIROC-ESM MIROC-ESM-CHEM
Atmosphere and Ocean Research Institute (The University of Tokyo), National Institute for Environmental Studies, and Japan Agency for Marine-Earth Science and Technology	MIROC	MIROC5
Meteorological Research Institute	MRI	MRI-CGCM3
Norwegian Climate Centre	NCC	NorESM1-M

Table 4.2. List of experiment nomenclature and corresponding imposed ocean surface conditions.

Experiment	Wind trend dataset	Temperature change (°C)	Salinity Pattern amplification (%)
ΔERA-40	ERA-40	0	0
ΔJRA-55	JRA-55	0	0
ΔNOAA-20CR	NOAA-20CR	0	0
ΔMeanTrend	(ERA-40+JRA-55+NOAA-20CR)/3	0	0
ΔTΔSΔMean	(ERA-40+JRA-55+NOAA-20CR)/3	0.5	8
ΔTΔS	None	0.5	8
Control	None	0	0

Table 4.3. Correlation coefficients for the zonal temperature changes per ocean basin.

Experiment	Ocean basin	Observations	ΔTΔSΔMean
ΔERA-40	Atlantic	0.003	0.54
	Pacific	0.23	0.68
	Indian	0.42	0.63
	Global	0.24	0.54
ΔJRA-55	Atlantic	0.03	0.62
	Pacific	0.32	0.72
	Indian	0.59	0.64
	Global	0.32	0.52
ΔNOAA-20CR	Atlantic	0.06	0.54
	Pacific	0.14	0.45
	Indian	-0.34	-0.03
	Global	0.002	0.40
ΔMeanTrend	Atlantic	0.03	0.67
	Pacific	0.30	0.77
	Indian	0.48	0.67
	Global	0.28	0.59
ΔCMIP5	Atlantic	-0.14	-
	Pacific	0.38	-
	Indian	-0.007	-
	Global	0.35	-
ΔTΔSΔMean	Atlantic	0.44	-
	Pacific	0.47	-
	Indian	0.58	-
	Global	0.65	-
ΔTΔS+ΔCMIP5	Atlantic	0.60	-
	Pacific	0.42	-
	Indian	0.14	-
	Global	0.62	-
ΔTΔS	Atlantic	0.59	0.86
	Pacific	0.32	0.50
	Indian	0.15	0.43
	Global	0.51	0.61

Table 4.4. Correlation coefficients for the zonal salinity changes per ocean basin.

Experiment	Ocean basin	Observations	ΔTΔSΔMean
ΔERA-40	Atlantic	-0.14	0.33
	Pacific	0.03	0.53
	Indian	-0.18	0.11
	Global	-0.03	0.40
ΔJRA-55	Atlantic	-0.15	0.39
	Pacific	-0.02	0.44
	Indian	-0.22	0.12
	Global	0.01	0.28
ΔNOAA-20CR	Atlantic	-0.04	0.59
	Pacific	-0.11	0.22
	Indian	-0.08	0.52
	Global	-0.07	0.28
ΔMeanTrend	Atlantic	-0.13	0.51
	Pacific	0.001	0.53
	Indian	-0.25	0.39
	Global	0.007	0.42
ΔCMIP5	Atlantic	0.02	-
	Pacific	-0.14	-
	Indian	0.44	-
	Global	-0.01	-
ΔTΔSΔMean	Atlantic	0.51	-
	Pacific	0.43	-
	Indian	0.23	-
	Global	0.60	-
ΔTΔS+ΔCMIP5	Atlantic	0.68	-
	Pacific	0.50	-
	Indian	0.48	-
	Global	0.70	-
ΔTΔS	Atlantic	0.64	0.95
	Pacific	0.50	0.89
	Indian	0.39	0.86
	Global	0.67	0.93

Figures

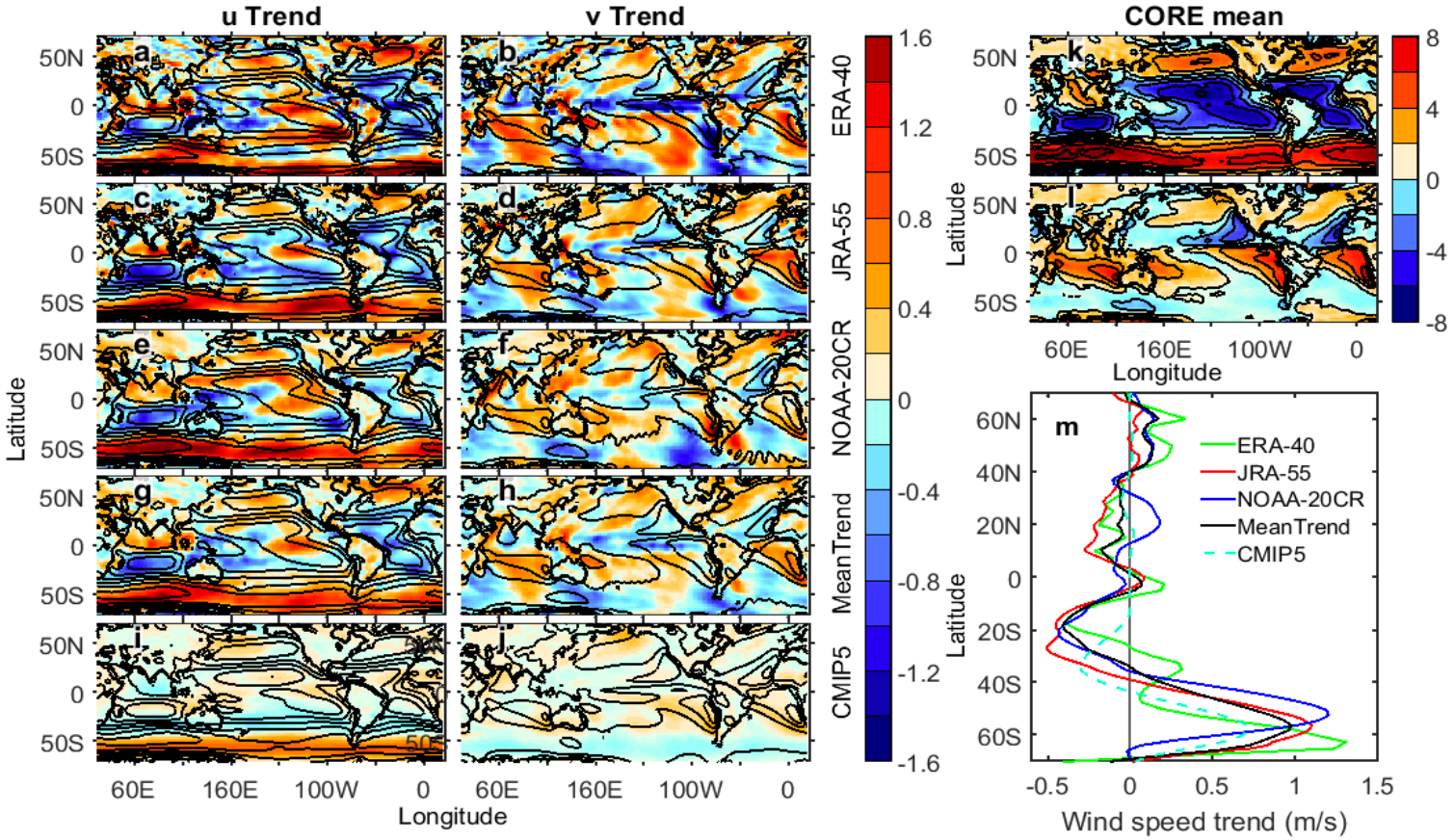

Figure 4.1. Zonal wind change (a,c,e,g,i) and meridional wind change at 10 m (b,d,f,h,j) imposed at the surface (m/s per 50 years) for each dataset used in the experiments. Panels k and l shows the mean COREv2 wind (zonal velocity: panel k and meridional velocity: panel l). The year range used to produce the 50 years linear trends are ERA-40: 1958-2003; JRA-55: 1958-2014; NOAA-20CR: 1950-2008 and CMIP5: 1950-2008. The black contours are the mean field every 2 m/s. Panel m shows the zonally averaged wind speed change (m/s per 50 years) for each dataset used in the experiments.

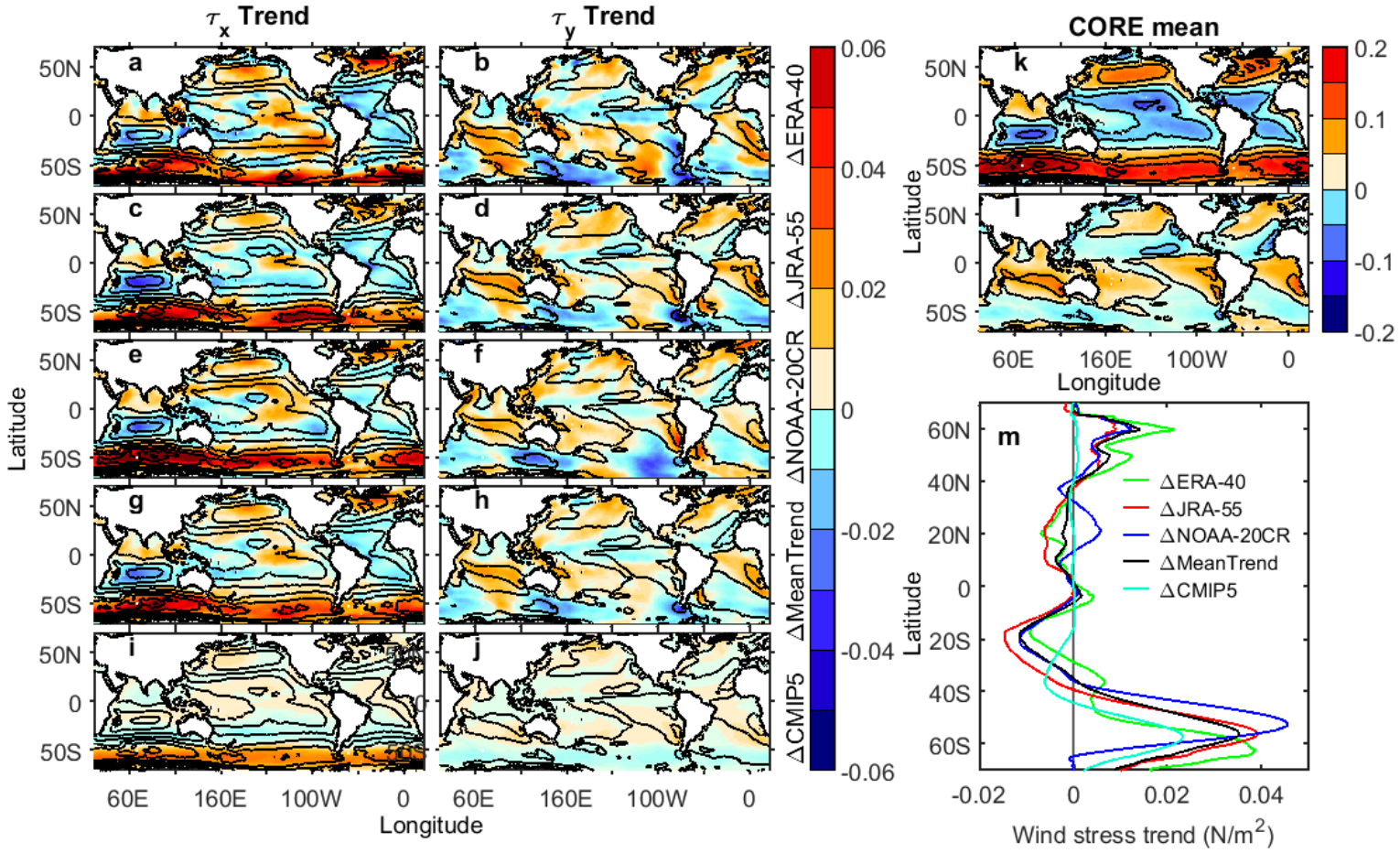

Figure 4.2. Zonal wind stress change (a,c,e,g,i) and meridional wind stress change (b,d,f,h,j) at the surface (N/m^2 per 50 years) for each wind experiment. Panels k and l shows the annual mean COREv2 wind stress (zonal wind stress: panel k and meridional wind stress: panel l). The black contours are the mean field every 0.05 N/m^2. Panel m shows the zonally averaged wind stress change (N/m^2 per 50 years) for each wind experiment.

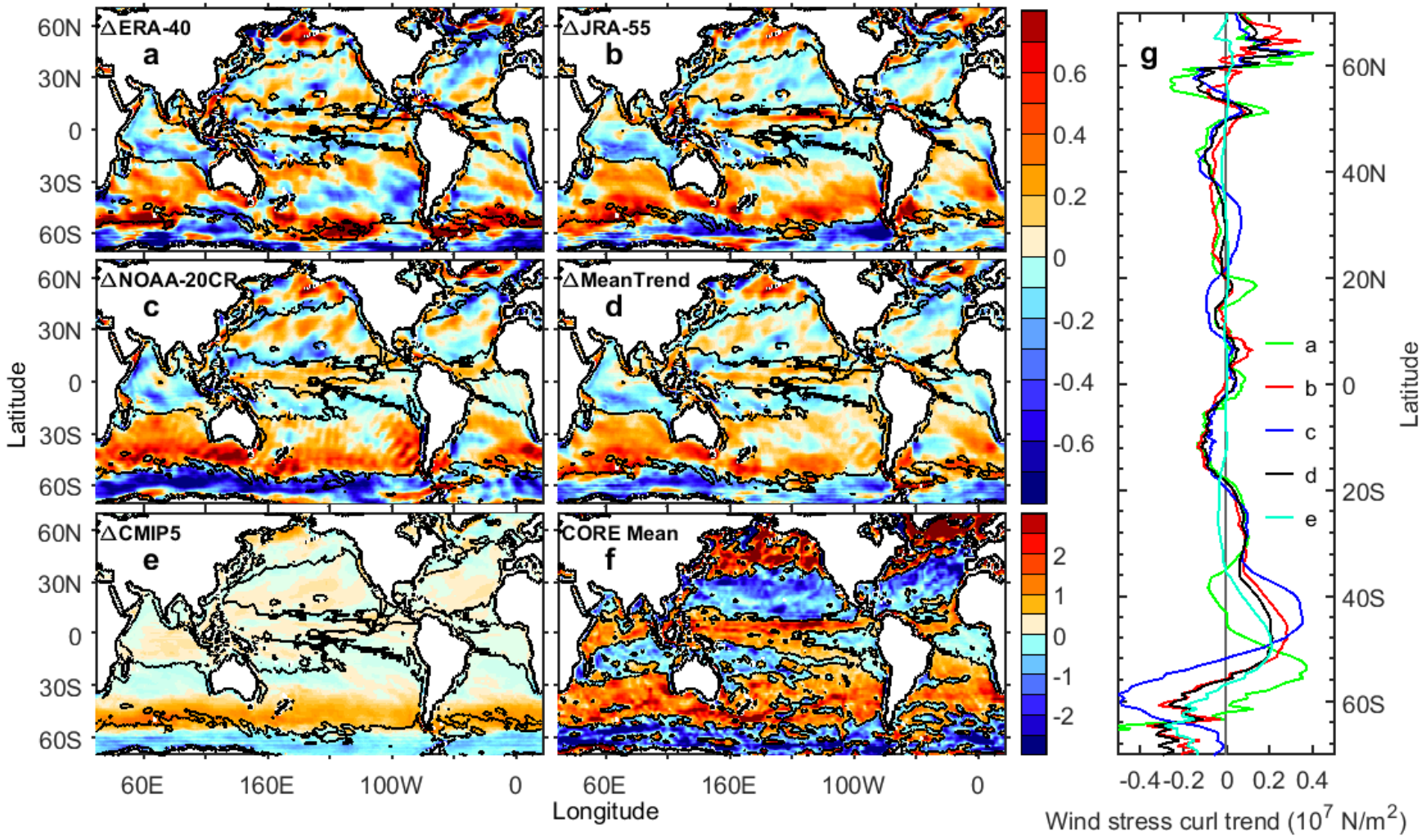

Figure 4.3. Wind stress curl change (a,b,c,d,e) at the surface (10^7 N/m^2 per 50 years) for each wind experiment (upper colourbar). Panel f shows the annual mean COREv2 wind stress curl (lower colourbar). The black contours are the mean field at 0 N/m^2. Panel g shows the zonally averaged wind stress curl change (10^7 N/m^2 per 50 years) for each wind experiment.

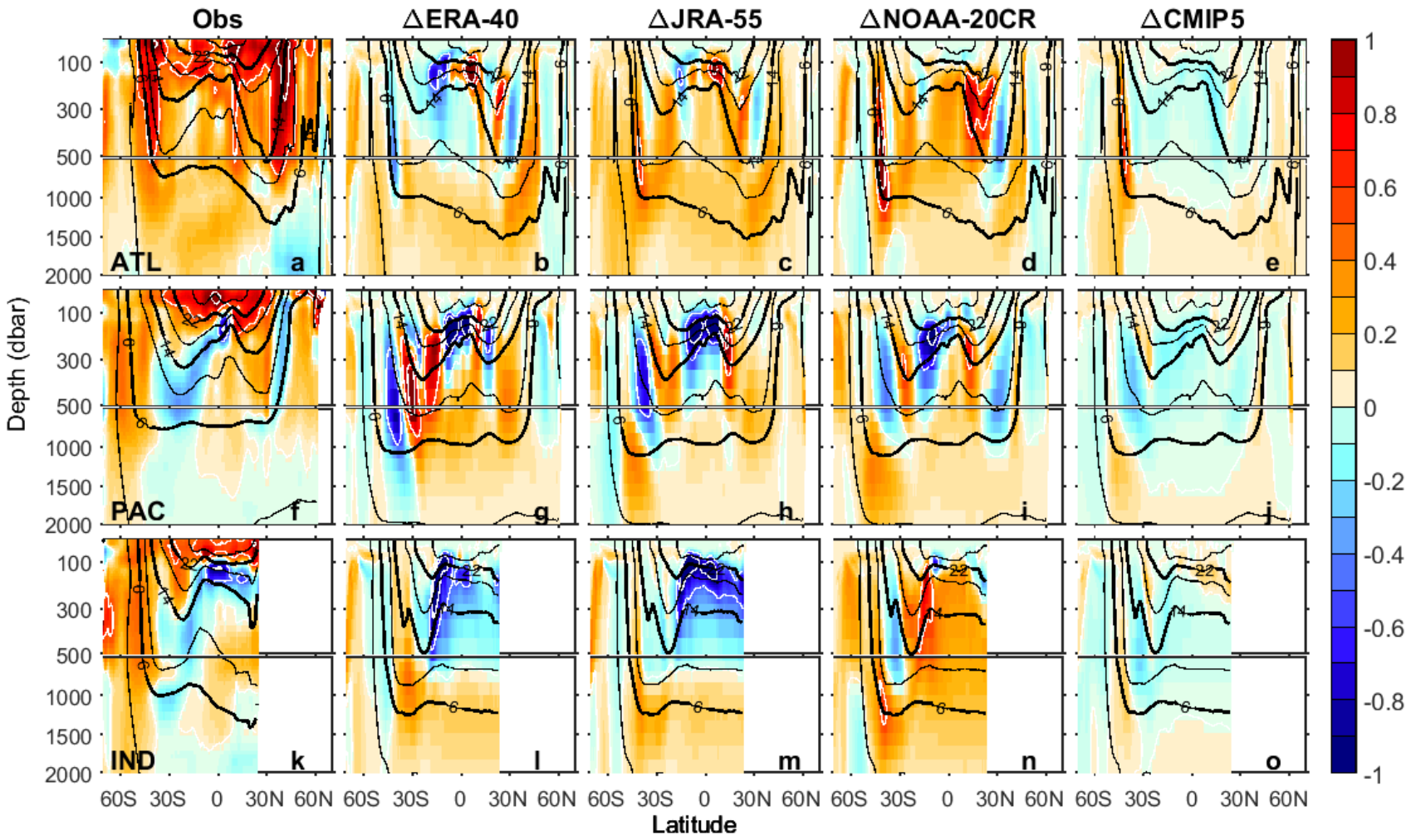

Figure 4.4. Comparison of the zonally averaged potential temperature changes (°C per 50 years) in the Atlantic (a,b,c,d,e) Pacific (f,g,h,i,j) and Indian (k,l,m,n,o) Oceans for each wind dataset experiment. The columns correspond from left to right to the observations, ΔERA-40, ΔJRA-55, ΔNOAA-20CR and ΔCMIP5. The white contours are the temperature trend every 0.5°C. The black contours are the mean temperature every 8°C (thick lines) and 4°C (thin lines).

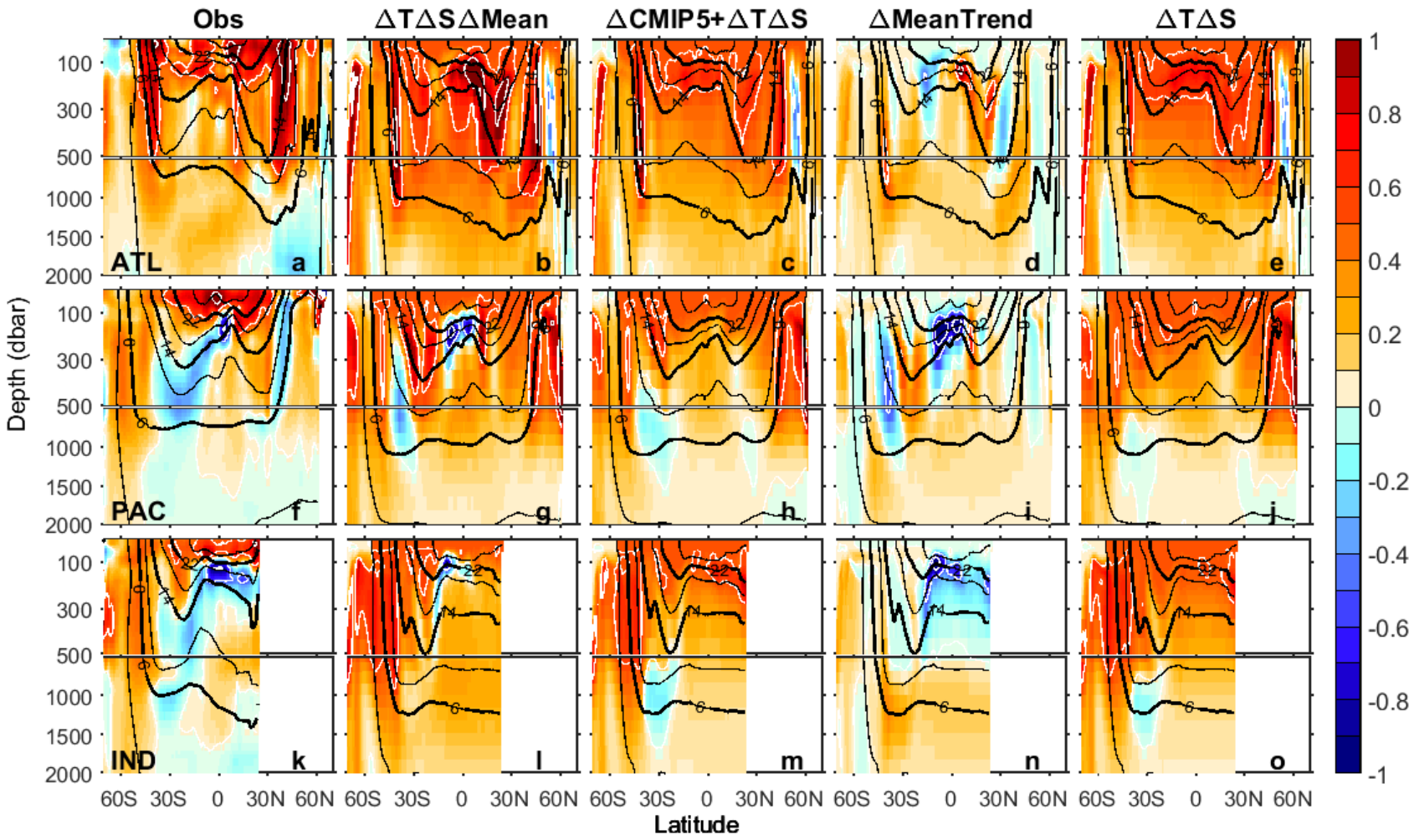

Figure 4.5. Comparison of the zonally averaged potential temperature changes (°C per 50 years) in the Atlantic (a,b,c,d,e) Pacific (f,g,h,I,j) and Indian (k,l,m,n,o) Oceans. The columns correspond from left to right to the observation, the ΔTΔSΔMean experiment, the sum of ΔCMIP5 and ΔTΔS, the ΔMeanTrend experiment and the ΔTΔS experiment. The white contours are the temperature trend every 0.5°C. The black contours are the mean temperature every 8°C (thick lines) and 4°C (thin lines).

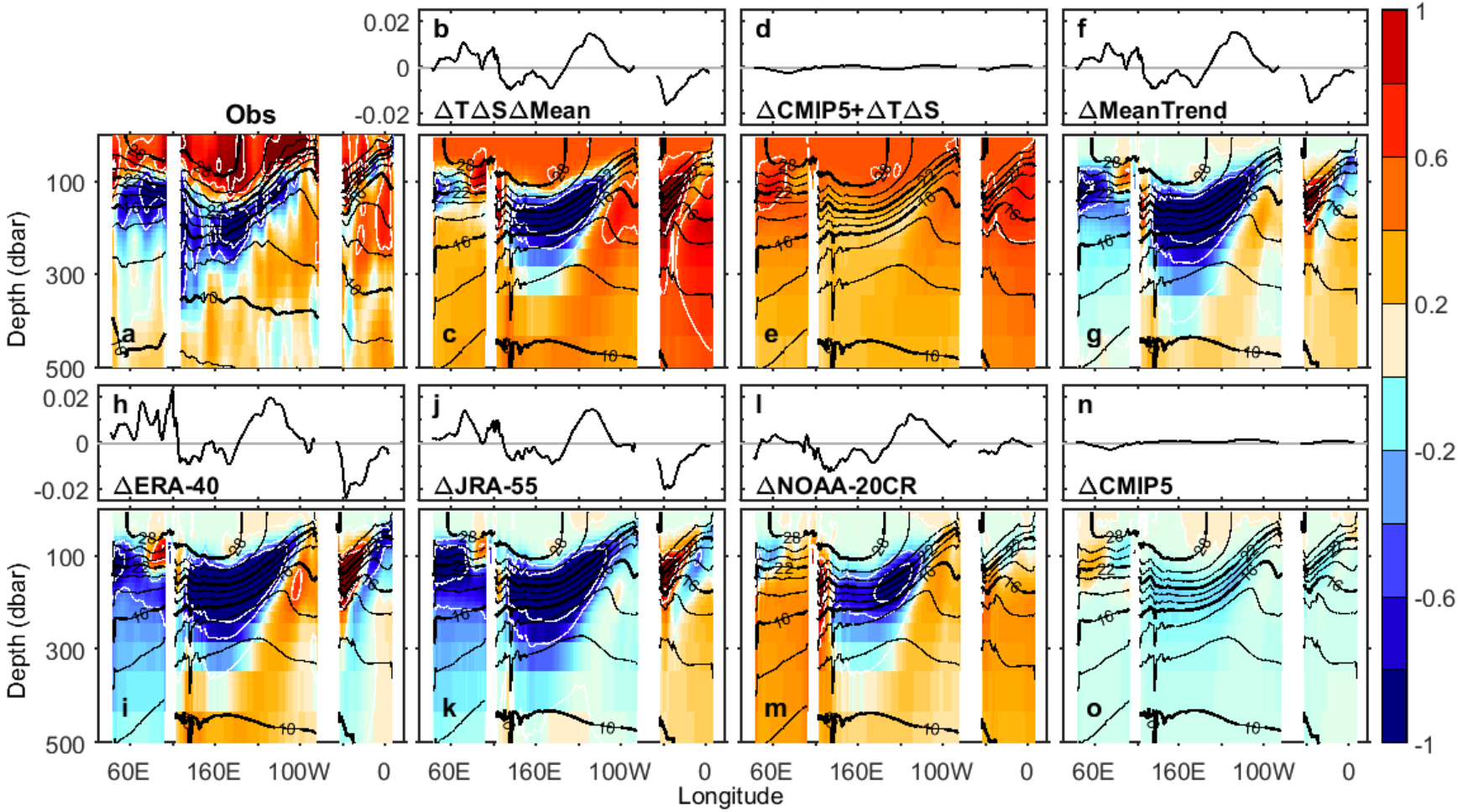

Figure 4.6. Comparison of the meridionally averaged potential temperature changes (°C per 50 years) between 5°S and 5°N along longitude for the observations (a) and the wind experiments (c, e, g, I, k, m and o) The white contours are the temperature trend every 0.5°C. The black contours are the mean temperature every 6°C (thick lines) and 2°C (thin lines). Above the temperature change of each experiment are the corresponding mean zonal wind stress changes (N/m^2 per 50 years) (b, d, f, h, j, l and n).

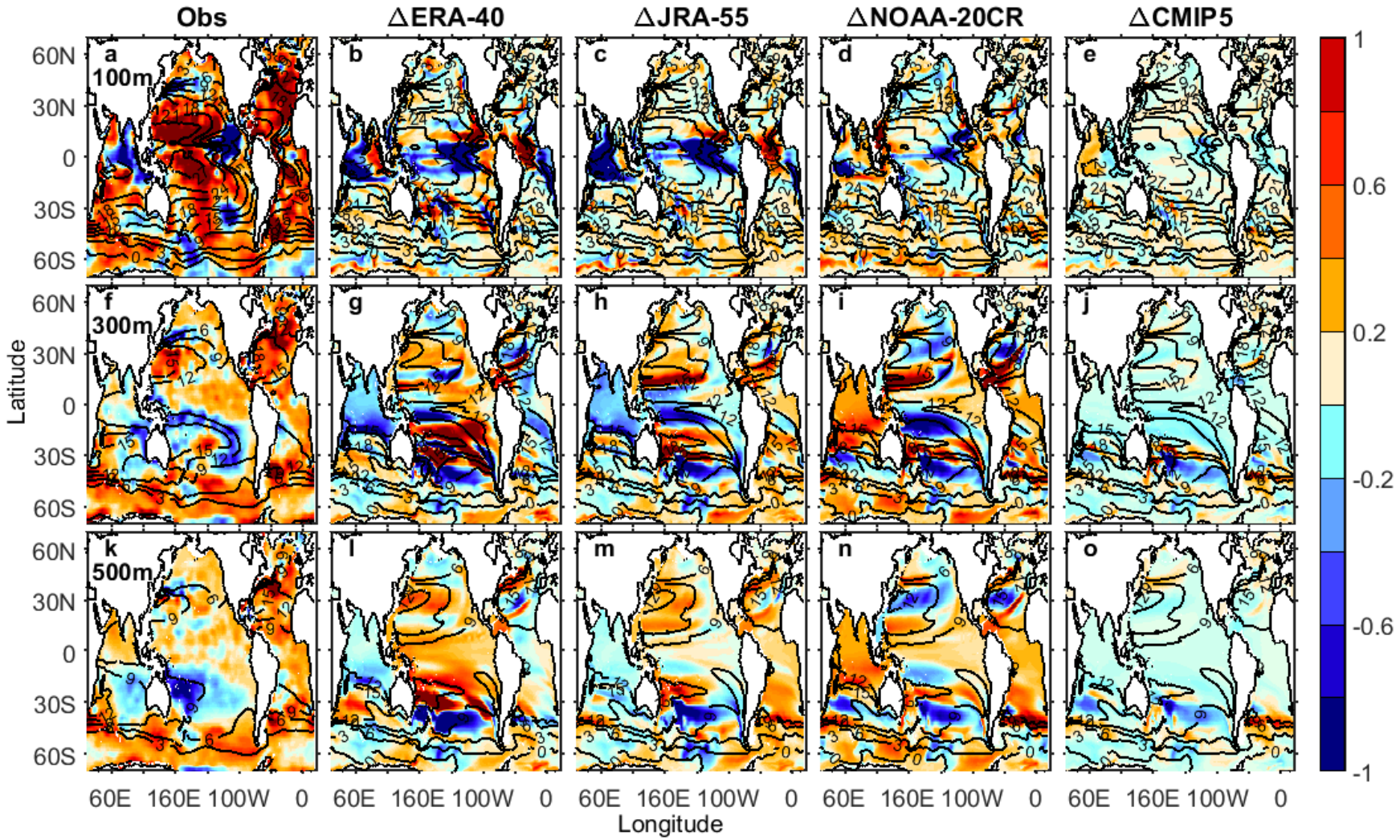

Figure 4.7. Temperature changes (°C per 50 years) at 100m (a,b,c,d,e), 300 m (f,g,h,i,j) and 500 m (k,l,m,n,o). The columns correspond from left to right to the observations, ΔERA-40, ΔJRA-55, ΔNOAA-20CR and ΔCMIP5. The black contours are the mean temperature every 8°C (thick lines) and 4°C (thin lines).

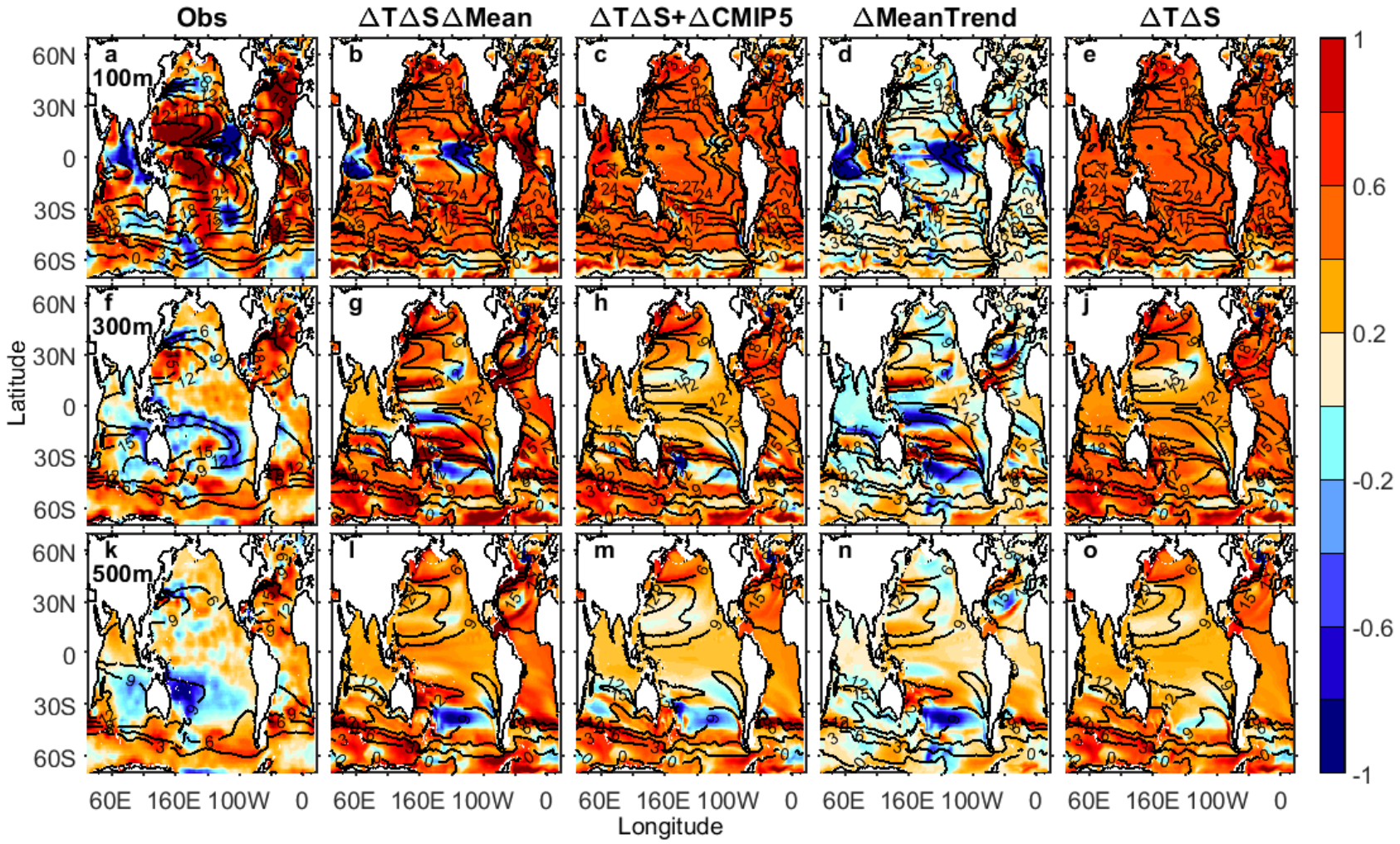

Figure 4.8. Temperature changes (°C per 50 years) at 100m (a,b,c,d,e), 300 m (f,g,h,i,j) and 500 m (k,l,m,n,o). The columns correspond from left to right to the observations, ΔTΔSΔMean, the sum of ΔTΔS and ΔCMIP5, ΔMeanTrend and ΔTΔS. The black contours are the mean temperature every 8°C (thick lines) and 4°C (thin lines).

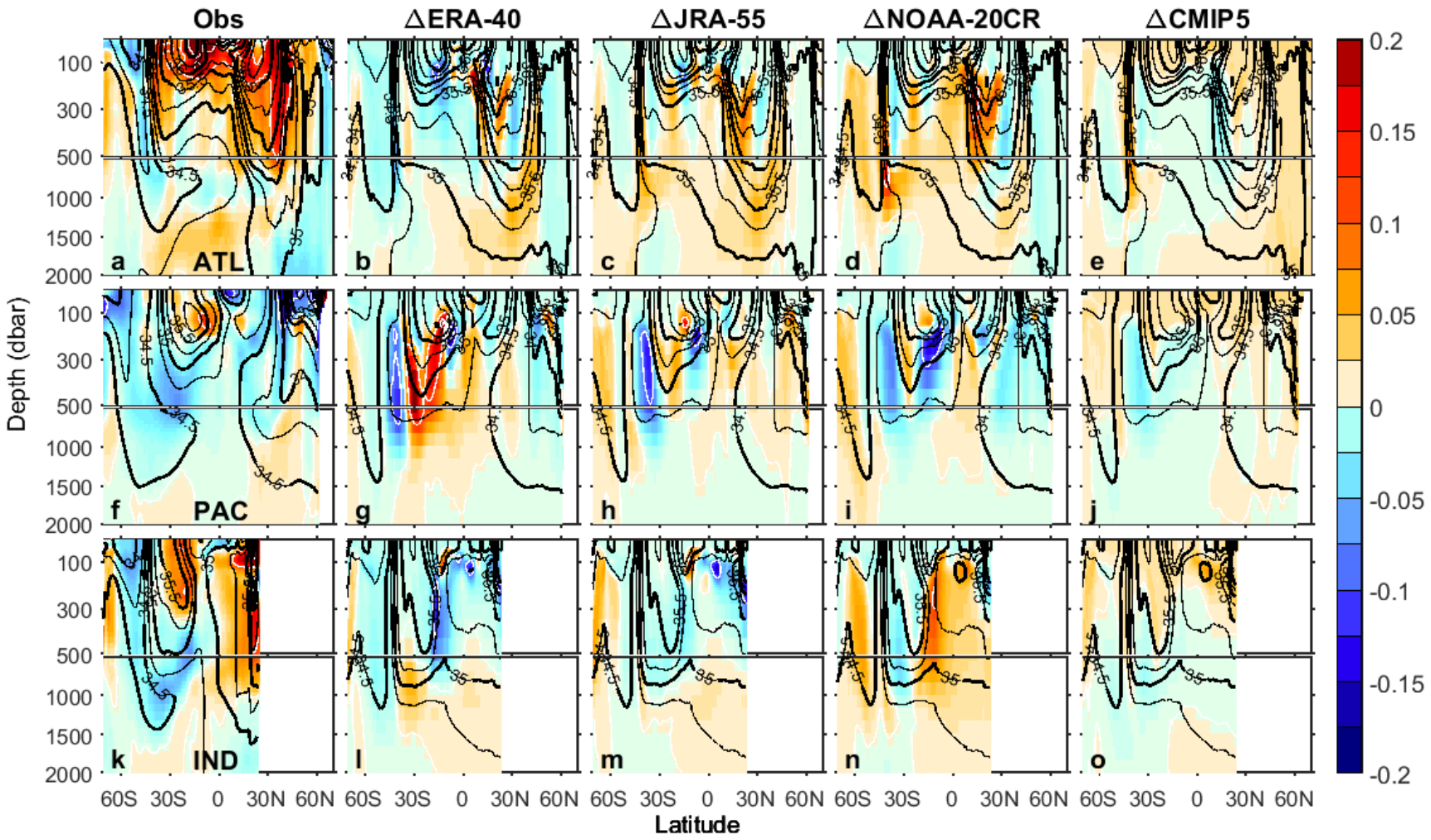

Figure 4.9. Comparison of the zonally averaged salinity changes (PSS-78 per 50 years) in the Atlantic (a,b,c,d,e) Pacific (f,g,h,i,j) and Indian (k,l,m,n,o) Oceans. The columns correspond from left to right to the observations, ΔERA-40, ΔJRA-55, ΔNOAA-20CR and ΔCMIP5. The white contours are the salinity trend every 0.1 PSS-78. The black contours are the mean salinity every 0.5 PSS-78 (thick lines) and 0.25 PSS-78 (thin lines).

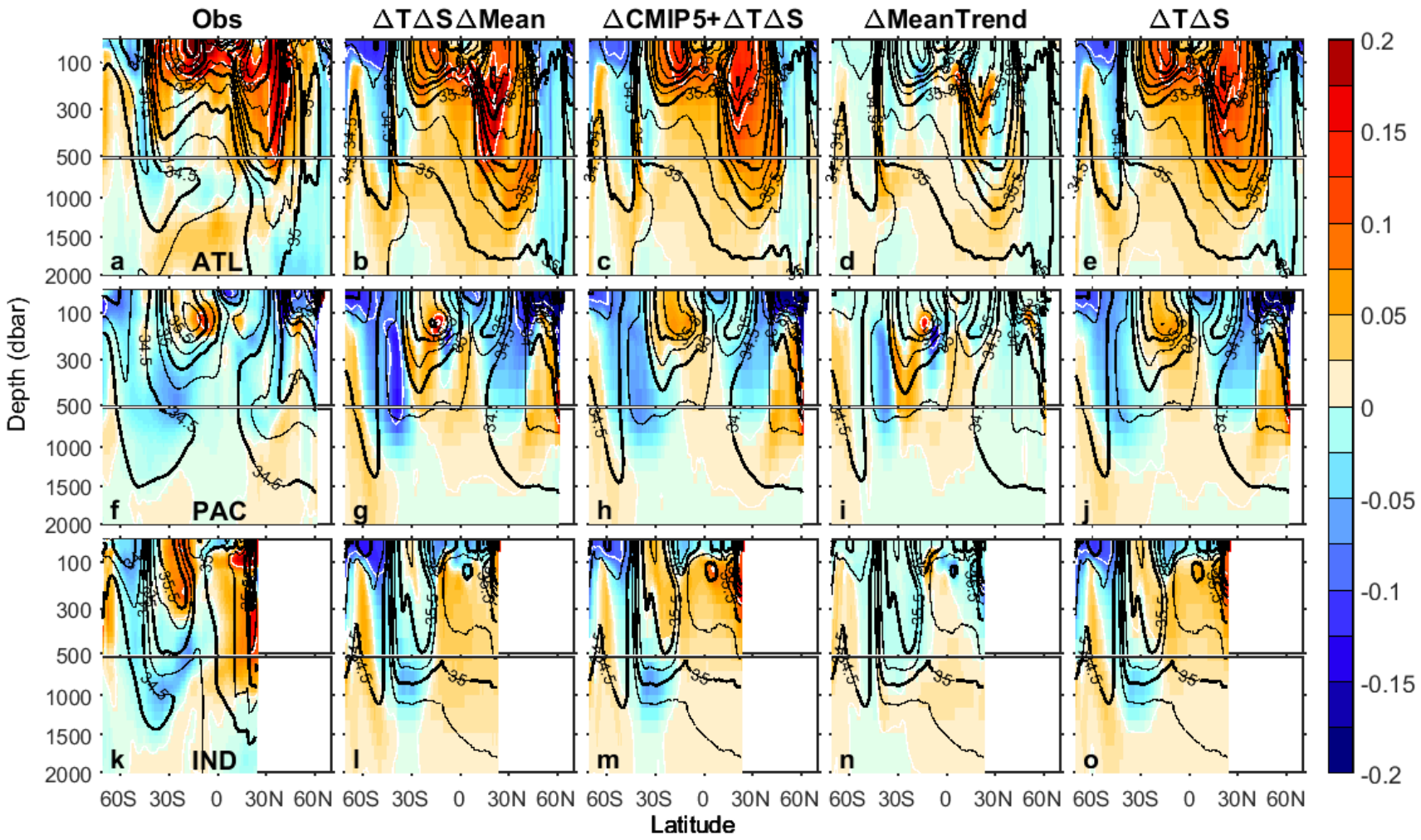

Figure 4.10. Comparison of the zonally averaged salinity changes (PSS-78 per 50 years) in the Atlantic (a,b,c,d,e) Pacific (f,g,h,i,j) and Indian (k,l,m,n,o) Oceans. The columns correspond from left to right to the observations, the ΔTΔSΔMean experiment, the sum of ΔTΔS and ΔCMIP5, the ΔMeanTrend experiment and the ΔTΔS experiment. The white contours are the salinity trend every 0.1 PSS-78. The black contours are the mean salinity every 0.5 PSS-78 (thick lines) and 0.25 PSS-78 (thin lines).

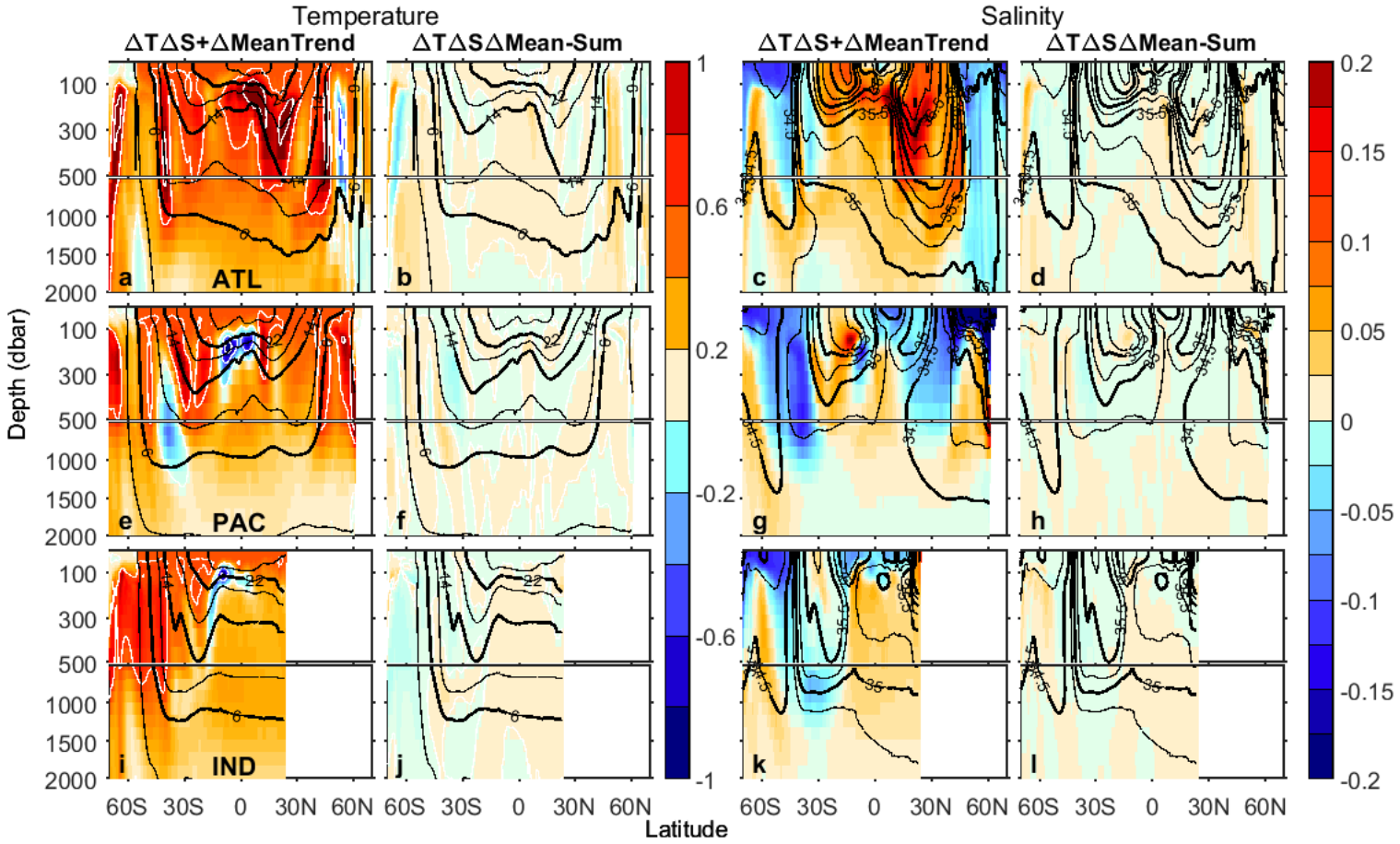

Figure 4.11. Zonally averaged temperature and salinity changes (°C and PSS-78 per 50 years) in the Atlantic (a,b,c,d) Pacific (e,f,g,h) and Indian (i,j,k,l) Oceans. The first and third columns are the sum of changes in ΔTΔS and ΔMeanTrend and the second and fourth columns are the changes in ΔTΔSΔMean minus the sum of changes in ΔTΔS and ΔMeanTrend. The white contours are the temperature trend every 0.5°C and salinity trend every 0.1 PSS-78 for the temperature and salinity plots respectively. The black contours in the temperature plots (first and second columns) are the mean temperature every 8°C (thick lines) and every 4°C (thin lines). The black contours in the salinity plots (third and fourth columns) are the mean salinity every 0.5 PSS-78 (thick lines) and 0.25 PSS-78 (thin lines).

Chapter 5

Conclusion

Our results demonstrate that simple experiments with idealized linearly enhanced surface forcing can reproduce the main observed features of changes in temperature and salinity in the ocean interior. An exception is the effect of the linear wind trends on the ocean temperature outside of the equatorial oceans and Southern Ocean (Section 4.3.1). A combination of surface warming, and surface salinity pattern amplification are needed to reproduce the observed salinity changes on density surfaces in the ocean interior (Section 2.3.2). Both changes in surface temperature and salinity contribute equally to changes in ocean heat content (Section 3.3.4). The ocean warming is overestimated in our idealized experiments by almost double that observed, however, once an estimated correction on the observations is applied (Durack *et al.,* 2014) our experiments overestimate the warming by a factor of 1.5. This overestimate hints at an excessive heat diffusivity in our ocean model (Chapter 3). Additionally, the wind-driven pattern of cooling in the equatorial region of the ocean interior is necessary to reproduce the pattern of temperature change in the ocean interior.

5.1 Linearity

The surface temperature, salinity and momentum changes act quasi-linearly together in their effect on the temperature and salinity field in the ocean interior (Figures 2.6, 3.10 and 4.11). For the rates of perturbation over the past 50 years, the changes they cause in the ocean interior can be added independently to reproduce the pattern of changes induced by their combined effect in this model. This suggests that regardless of the turbulent and sensitive response of the ocean to each of these forcings, the current rates of change can be assessed as linearly additive. The impact on the properties in the ocean interior from each of these surface forcing can be taken independently in simple experiments and evaluate individually with the range of multi-decadal changes of our experiments. However, as global climate change continues to alter the forcings at the ocean surface, the range in which these act linearly might be exceeded. In particular, as the rate of change increases, non-linear processes in the ocean system might take more importance.

5.2 Salinity

The salinity changes on pressure surfaces in the ocean are led by the surface salinity pattern amplification. An amplification of the surface salinity pattern by 8% reproduces the observed pattern of salinity changes in the ocean interior with similar amplitude to observations (Figure 2.5). However, on isopycnals, a combination of the effect of the subducted surface salinity changes and isopycnal migration induced by surface warming is necessary to reproduce observed subsurface salinity changes (Figure 2.7). These results give a pathway to infer the surface forcing based on the interior changes. Earlier work (Bindoff and McDougall, 1994; 2000) using a kinematic approach to infer the surface changes from changes in the ocean interior showed that, in the case of the salinity minimum, could be explained by surface freshening alone. However, in these results both surface warming and surface salinity changes is required to explain salinity changes in the interior. This result is a significant change in the earlier conceptualisation of the inferred changes in the ocean. The isopycnal migration and the surface salinity pattern amplification contribute equally to the pattern of salinity changes in density space. The largest salinity changes on isopycnals induced by the surface warming are in regions of high salinity gradient. As the isopycnals move across the mean salinity field, the regions of high horizontal gradient are where this displacement causes the strongest apparent salinity change. We can extend this conclusion to passive tracers as the effect of isopycnal migration would have similar consequences when assessing their changes in density space in the ocean interior. Therefore, the effect of isopycnal migration due to ocean warming has to be taken into consideration when interpreting changes of a passive tracer on density surfaces.

Changes in surface wind also produce strong changes in the mid-latitudes salinity field of the ocean interior, although these are unrealistic (Figures 4.9 and 4.10). The wind changes alone cannot alter the total salinity balance of the ocean, but rather displace the salinity field regionally. The strong salinity changes, especially within the subtropical gyres, indicate that the model is very sensitive to long term changes in the surface wind stress. We also find that the multidecadal wind trends from the atmospheric reanalyses that we examined are inconsistent with each other

on their effect on the subsurface properties and the observed changes in most of the global ocean.

5.3 Temperature

Changes in surface temperature, salinity and momentum all induce change in ocean interior temperature of similar amplitude, but differ in the induced patterns of changes. They are all required to reproduce the observed field of temperature changes as the individual effects from each surface forcing complements each other. The temperature changes in the top 100 m are led by the surface temperature increase through mixed layer processes and shallow subduction. Between 100 m and about 1000 m, the temperature changes are due to a combination of the effects due to the surface warming, salinity pattern amplification and wind changes. Below 1000 m, the main changes in temperature are produced by a combination of the changes in surface salinity and surface wind stress. The surface warming does not penetrate as much below 1000 m through the subduction in the ventilated gyres whilst the surface salinity pattern amplification and wind trends induces dynamical changes that leads to temperature changes at depth.

The surface warming is subducted into the ocean interior in the ventilated gyres. The surface salinity pattern amplification also induces warming in the ventilated gyres due to decreased upwelling and agrees with previous studies of the impact of the simulated increase of CO_2 in model simulations (Gregory, 2000; Banks and Gregory, 2006; Kuhlbrodt *et al.*, 2015). The subpolar North Pacific below 100 m warms when the surface salinity pattern is amplified due to increased heat advection between the subtropical and subpolar gyres. In the case of the Southern Ocean and North Atlantic Deep Water (NADW) warming, when the surface salinity pattern is amplified, there is increased stratification of the water column and thus reduced convection (Dickson *et al.*, 1996; Curry and McCartney, 2001; Häkkinen and Rhines, 2004). In the Southern Ocean, stronger westerlies drive an increase in Ekman transport (Oke and England, 2004; Meredith and Hogg, 2006; Hogg *et al.*, 2007; Abernathey *et al.*, 2011). This effect causes a warming of the Southern Ocean and cooling in the South Indian and South Pacific. NADW cools when the surface is warmed and the surface salinity is fixed, which is consistent with

observations. This cooling is induced by increased sub-polar convection led by the increased surface temperature gradient (Thorpe *et al.*, 2001; Straneo, 2006; Hurrel and Deser, 2010).

The changes in heat content reflect this combination of the effects of the different forcings on regional changes in temperature. Globally, the Southern Ocean accumulates the most heat due to the changes in surface salinity and wind. The surface freshening reduces the cooling effect from high latitude convection (Marsland and Wolff, 2001), and the strengthened westerlies increase the exchange with warmer waters and the penetration of the surface signal into the ocean interior through enhanced Ekman pumping (Oke and England, 2004; Meredith and Hogg, 2006; Hogg *et al.*, 2007; Abernathey *et al.*, 2011). The North Atlantic also accumulates more heat than the global average. The presence of deep convection sites in the North Atlantic allow rapid warming of the deep water masses with the weakened convection which occurs with the freshened surface at high latitudes.

As the ocean surface temperature keeps rising, it might reach temperatures that are sufficient to also impact on the properties in the ocean interior at high latitudes along with the effects due to changes in surface salinity. Especially as the effect of multi-year sea ice melting due to warming provides an additional source of surface freshwater. Warming at high latitudes could also hinder convection along with the freshening and amplify the warming effect thus induced. (Dickson *et al.*, 1996).

5.4 Winds

In the western (eastern) equatorial Pacific and Atlantic, strengthened trade winds drive an increased downwelling (upwelling). The strengthened trade winds induce heaving due to lifting and depressing of the isopycnals (Qiu and Chen, 2012; England *et al.*, 2014). This causes warming on the western side and cooling on the eastern side of the ocean basins and compares well with the observed temperature changes for that time period.

In the North Indian Ocean, the strengthened eastward wind stress in the reanalysis datasets results in warming in the east and cooling in the west. However, the observations exhibit

warming on the western side and cooling on the eastern side, which is reproduced through a weakening of the eastward wind in the CMIP5 wind. This suggests that the wind data reanalyses over the equatorial Indian Ocean are of the wrong sign for this time period and region whilst the long term trend in CMIP5 in this region is more accurate (Section 4.3.1.2 and Figure 4.7). It brings into question some of the assumptions about the accuracy of the long-term trends in the wind reanalyses especially in the equatorial region where internal variability is high. Another possibility is that the idealized surface temperature and salinity changes in our experiments are too simple and should include regional variations, which might affect the temperature changes in this region.

In the tropics and subtropics, the wind changes from reanalyses induce temperature changes of ~0.5 to 1 ^{o}C and salinity changes of ~0.05 to 0.15 PSS-78 in the upper 2000 m that are not consistent across the different forcing datasets and do not compare well with the observed patterns of changes. The salinity and temperature changes in the tropics and subtropics are smaller with the CMIP5 wind trends, with amplitudes of ~0.5 ^{o}C and 0.05 PSS-78 due to its smaller surface wind changes. Although small, the patterns of change are more accurately simulated. The CMIP5 wind do induces mainly cooling in the upper 2000 m with warming north of the ACC. Changes in the salinity pattern include freshening under the ventilated gyre and increased salinity in the upper 200 m and high latitudes. The changes in salinity pattern with CMIP5 do improve the comparison with the observation from the salinity changes induced from the surface salinity pattern amplification and warming. Although, the changes in the ocean interior suggests the trends in CMIP5 are more accurate, the equatorial strengthening of the trade wind is missing to reproduce the cooling features observed and accurately simulated with the wind data reanalyses.

The inconsistencies between the changes induced by the wind data reanalyses outside of the equatorial region and Southern Ocean and with the observed ocean changes suggest that the wind reanalyses likely overestimate the changes in wind speed. The trends in the salinity and temperature fields under the subtropical gyres induced by the changes imposed in the wind speed at the surface are an indication that the intensified wind stress shifts the circulation in a way that isn't seen in the observations (Sections 4.3.1 and 4.3.2). The wind speed trends drive

changes in the wind stress curl over the subtropical gyres that results in unrealistic shifts of the Sverdrup transport. This likely points to the great challenge in deducing the long term wind changes over the sparsely observed oceans, particularly in the Southern Hemisphere. It also indicates that the ocean is sensitive to the small differences in the long term trends between the different wind reanalyses.

5.5 Conclusion

We were able to reproduce many of the observed changes in temperature and salinity using simple experiments, showing that the effects of surface temperature, salinity and wind stress can be used to understand the drivers of the changes in physical properties of the ocean interior. In our experiments, we show that long-term changes in the ocean interior are driven by the long term changes in temperature, salinity and momentum at the surface. The pattern of change in temperature in the ocean interior is the result of the subducted surface warming, reduced convection, reduced upwelling and changes in advection due to surface salinity pattern amplification coincident to an increase in transport due to strengthened trade winds and westerlies. The changes in salinity at depth are predominantly a consequence of subducted amplification of the surface salinity pattern. When analysed on density surfaces, however, ocean temperature change moves the isopycnals, this movement needs to be taken into account within the mean salinity field, resulting in a change to the apparent salinity trends (Bindoff and McDougall, 1994; 2000; Durack and Wijffels, 2010). The effect of isopycnal migration due to temperature change would also impact analyses of changes of other tracers within the ocean and should be taken into account in analyses on density surfaces.

A quantifiable relative contribution from each driver of heat content change in the ocean interior is difficult to establish due to the overestimated warming in our experiments. Our result suggests excessive heat diffusivity within the model. This issue hinders evaluation of changes within the oceans by enhancing the heat update due to the surface warming and salinity pattern amplification. Furthermore, the changes in heat content from shifts in the wind pattern are not accurately depicted through either forcing from the wind data reanalyses or CMIP5. This limits

the evaluation of their contribution to the heat budget within the ocean. However, our experiments suggest a cooling effect in the equatorial ocean induced by a strengthening of the trade winds. The long-term trend in surface wind speeds is likely a combination of the pattern in the wind data reanalyses and CMIP5 long-term trend. Although, because none of our wind experiments alone produces patterns of temperature changes that are realistic in the ocean interior, it limits the quantification of their role on the total heat budget. The inconsistent and unrealistic impacts of changes in the wind pattern points to the need of improving our knowledge of the nature of the long-term trends in the surface wind field. For the correlation analyses in chapter 4, it is clear that the observed changes in the ocean interior provides more information about the changes in surface temperature and salinity than it does for the long-term trends in the wind field (Tables 4.3 and 4.4).

These results provide insight in the drivers of properties changes in the ocean interior. Alternately, these results can help understand changes in surface properties such as hydrological cycle amplification and changes in surface wind. The changes in temperature and salinity in the ocean interior are driven from variability at the ocean surface and thus the later could be derived from the variations inside the ocean. Additionally, with improved observations of the ocean interior, comparison with these results would become easier as uncertainties due to sparse observations will be reduced, especially in the Southern Hemisphere.

With continuous warming of the atmosphere, the sea surface temperature is expected to keep rising and the hydrological cycle to keep amplifying, which will only enhance the effects described in this study. As per the scenarios described in the IPCC report (Kirtman *et al*., 2013; Collins *et al*., 2013), these surface trends could be 8 to 12 times stronger for surface warming alone. However, as the surface conditions keep on changing, non-linear effects could be enhanced and the combined effect from the different forcings might not be additive anymore. Furthermore, in this work the high latitudes were kept at constant temperature and as surface warming could play a more important role on changes in the high latitudes, especially as it reaches a point where it can hinder on convection along with the changes in salinity and melt more sea ice which would amplify the role of freshening in the high latitudes.

The results from the idealized experiments presented here could be compared to similar experiments that would include the regional variations in the ocean surface temperature and salinity changes to estimate the role of these spatial variations. Likewise, experiments including the non-linear trends within the surface temperature, salinity and winds forcings could be compared to the results of these idealized experiments to estimate the impact of the non-linear changes of the surface forcings.

Understanding the drivers of the observed trends in the ocean help evaluate future changes. We expect that under continued global warming and an amplified hydrological cycle, these experiments help us better understand the processes driving ocean heat uptake and water mass transformation in the climate models that provide the predictions of future changes in the ocean.

References

Abernathey R., J. Marshall and D. Ferreira, 2011: The Dependence of Southern Ocean meridional overturning on wind stress. *Journal of Physical Oceanography*, **41**, pp.2261-2278. doi:10.1175/JPO-D-11-0.23.1

Banks, H.T., J.M. Gregory, 2006: Mechanisms of ocean heat uptake in a coupled climate model and the implications for tracer based predictions of ocean heat uptake. *Geophysical Research Letters*, **33**, L07608. doi:10.1029/2005GL025352

Bindoff, N.L., and T.J. McDougall, 1994: Diagnosing climate change and ocean ventilation using hydrographic data. *Journal of Physical Oceanography*, **24**, pp. 1137–1152.

Bindoff, N.L., and T.J. McDougall, 2000: Decadal Changes along an Indian Ocean Section at 32^{o}S and Their Interpretation. *Journal of Physical Oceanography*, **30**, pp. 1207-1222.

Collins, M., R. Knutti, J. Arblaster, J.-L. Dufresne, T. Fichefet, P. Friedlingstein, X. Gao, W.J. Gutowski, T. Johns, G. Krinner, M. Shongwe, C. Tebaldi, A.J. Weaver and M. Wehner, 2013: Long-term Climate Change: Projections, Commitments and Irreversibility. In: Climate Change 2013: The Physical Science Basis. Contribution of Working Group I to the Fifth Assessment Report of the Intergovernmental Panel on Climate Change [Stocker, T.F., D. Qin, G.-K. Plattner, M. Tignor, S.K. Allen, J. Boschung, A. Nauels, Y. Xia, V. Bex and P.M. Midgley (eds.)]. Cambridge University Press, Cambridge, United Kingdom and New York, NY, USA.

Curry, R.G. and M.S. McCartney, 2001: Ocean Gyre Circulation Changes Associated with the North Atlantic Oscillation. *Journal of Physical Oceanography*, **31**, pp. 3374–3400. doi:10.1175/1520-0485(2001)031<3374:OGCCAW>2.0.CO;2

Dickson, R., J. Lazier, J. Meincke, P. Rhines, and J. Swift, 1996: Long-term coordinated changes in the convective activity of the North Atlantic. *Progress in Oceanogr*aphy, **38**, pp. 241-295.

Durack, P.J. and S. E. Wijffels, 2010: Fifty-year trends in the global ocean salinities and their relationship to broad-scale warming. *Journal of Climate*, **23**, pp. 4342-4362.

Durack, P.J., P.J. Gleckler, F.W. Landerer and K. E. Taylor, 2014: Quantifying underestimates of long-term upper-ocean warming. *Nature Climate Change*, **4**, pp. 999-1005. doi:10.1038/NCLIMATE2389

England M.H., S. McGregor, P. Spence, G.A. Meehl, A. Timmermann, W. Cai, A.S. Gupta, M.J. McPhaden, A. Purich and A. Santoso, 2014: Recent intensification of wind-driven circulation in the Pacific and the ingoing warming hiatus. *Nature Climate Change*, **4**, pp. 222-227. doi:10.1038/NClimate2106

Gregory, J.M., 2000: Vertical heat transports in the ocean and their effect on time-dependant climate change. *Climate Dynamics*, **16**, pp. 501-515.

Häkkinen, S. and P.B. Rhines, 2004: Decline of Subpolar North Atlantic Circulation During the 1990s. *Science*, **304**, pp. 555-559. doi:10.1126/science.1094917

Hogg, A.M., M.P. Meredith, J.R. Blundell and C. Wilson, 2007: Eddy Heat Flux in the Southern Ocean: Response to Variable Wind Forcing. *Journal of Climate*, **21**, pp. 608-620.

Hurrell J.W. and C. Deser, 2010: North Atlantic climate variability: The role of the North Atlantic Oscillation. *Journal of Marine Systems*, **79**, pp. 231-244.

Kirtman, B., S.B. Power, J.A. Adedoyin, G.J. Boer, R. Bojariu, I. Camilloni, F.J. Doblas-Reyes, A.M. Fiore, M. Kimoto, G.A. Meehl, M. Prather, A. Sarr, C. Schär, R. Sutton, G.J. van Oldenborgh, G. Vecchi and H.J. Wang, 2013: Near-term Climate Change: Projections and Predictability. In: Climate Change 2013: The Physical Science Basis. Contribution of Working Group I to the Fifth Assessment Report of the Intergovernmental Panel on Climate Change [Stocker, T.F., D. Qin, G.-K. Plattner, M. Tignor, S.K. Allen, J. Boschung, A. Nauels, Y. Xia, V. Bex and P.M. Midgley (eds.)]. Cambridge University Press, Cambridge, United Kingdom and New York, NY, USA.Meredith, M.P.,

A. M. Hogg, 2006: Circumpolar response of Southern Ocean eddy activity to a change in the Southern Annular Mode. *Geophysical Research Letters*, **33**, L16608. doi:10.1029/2006GL026499

Oke, P.R., M.H. England, 2004: Oceanic Response to Changes in the Latitude of the Southern Hemisphere Subpolar Westerly Winds. *Journal of Climate*, **17**, pp. 1040-1054.

Qiu, B. and S. Chen, 2012: Multidecadal Sea Level and Gyre Circulation Variability in the Northwestern Tropical Pacific Ocean. *Journal of Physical Oceanography*, **42**, pp. 193-206, doi:10.1175/JPO-D-11-061.1

Straneo, F., 2006: On the Connection between Dense Water Formation, Overturning, and Poleward Heat Transport in a Convective Basin. *Journal of Physical Oceanography*, **36**, pp. 1822-1840.

Thorpe, R.B., J. M. Gregory, T. C. Johns, R. A. Wood, and J. F. B. Mitchell, 2001: Mechanisms Determining the Atlantic Thermohaline Circulation Response to Greenhouse Gas Forcing in a Non-Flux-Adjusted Coupled Climate Model. *Journal of Climate*, **14**, pp. 3102-3116.